Title
The Development and Application of Fluorescent Protein Reporters to Measure Endoplasmic Reticulum Stress in Single Cells

Author
Merksamer, Philip Ian

Publication Date
2010

The Development and Application of Fluorescent Protein Reporters to Measure Endoplasmic Reticulum Stress in Single Cells

by

Philip I. Merksamer

DISSERTATION

Submitted in partial satisfaction of the requirements for the degree of

DOCTOR OF PHILOSOPHY

in

CELL BIOLOGY

in the

GRADUATE DIVISION

of the

Acknowledgements

I have numerous people to thank for their help and support throughout graduate school. First, I would like to thank Feroz Papa for being a supportive mentor. He was always available to discuss my project and was instrumental in my scientific development. In addition to Feroz, I was fortunate to have an insightful and stimulating thesis committee consisting of Jonathan Weissman, Cynthia Kenyon, and Scott Oakes. My committee was a tremendous source of knowledge and wisdom that helped shape the direction of my thesis.

Next, I must thank Ala Trusina for being an amazing collaborator. Ala introduced me to computer programming and mathematical modeling and spear-headed the effort to apply mathematical tools to my real-time and genomic data. Additionally, I am grateful for Ala's invitation to visit and work at the Niels Bohr Institute in Copenhagen, Denmark. During my stay in Copenhagen, I had the opportunity to learn how to apply mathematical modeling to the biological sciences.

In addition to Ala, I am grateful for the help of several other graduate students and post-doctoral fellows. Victor Chubukov granted me unfettered access to the chemostat system that he had developed. He also provided MATLAB scripts for data analysis and copious amounts of technical support. Martin Jonikas and Maya Schudliner provided various reagents and yeast strains, and they were also a great source of knowledge in regards to working with yeast. Onn Brandman provided a great deal of help with the high-throughput eroGFP screen especially with

construction of the gene library and with data analysis. Jimena Weibezahn assisted with the immunopercipitations of yeast extracts.

I would also like to thank all the members of the Papa lab that I worked with during the past five years including Andrew Hagen, Alana Lerner, Dan Han, Lieselotte Vande Walle, Praveen, Xiaocong Chen, Sarah Shen, Kris Prado, and Rajarshi Ghosh. I am grateful for the cordial atmosphere that they helped to create as well as the thoughtful discussions and technical assistance that they provided.

I would also like to acknowledge James Remington who provided the initial roGFP-2 construct on which eroGFP is derived.

Finally, I'd like to thank my family, Linda, Steve, and Alissa Merksamer for their love and support throughout graduate school. Their enthusiasm and genuine interest in my thesis work has always impressed me and I could not have made it through graduate school without their support.

The contents of chapter 2 were originally published in as "Real-Time Redox Measurements during Endoplasmic Reticulum Stress Reveal Interlinked Protein Folding Functions" Philip I. Merksamer, Ala Trusina, and Feroz R. Papa (2008) *Cell*, 135(5): 933-947. Copyright © 2008, Elsevier. All work was performed by Philip I Merksamer. Ala Trusina assisted with data analysis and some experimental procedures. Feroz R. Papa oversaw the work. Chapter 3 describes unpublished work that is currently being prepared for submission to a peer-reviewed journal. Philip I. Merksamer performed all the work. Ala Trusina and Onn Brandman assisted with data analysis. Feroz R. Papa oversaw the work. Chapter 4 was originally published

as “The UPR and cell fate at a glance” Philip I. Merksamer and Feroz R. Papa (2010) *Journal of Cell Science*, 123: 1003-1006. Copyright © 2010, The Company of Biologists. This chapter consists of a review article that places my work in the broader context and outlines future directions for the development of fluorescent reporters to measure endoplasmic reticulum stress in mammalian cells.

The Development and Application of Fluorescent Protein Reporters to Measure Endoplasmic Reticulum Stress in Single Cells

Philip I. Merksamer

Abstract

In eukaryotic cells, secreted and membrane proteins fold within the endoplasmic reticulum (ER). Various physiological or pathophysiological conditions can disrupt ER protein folding homeostasis and cause unfolded proteins to accumulate within the ER. Unfolded proteins activate a conserved intracellular signaling pathway called the unfolded protein response (UPR) that increases the ER's protein-folding capacity in order to restore protein folding homeostasis. However, because it is infeasible to directly measure the concentration of unfolded proteins within the ER, any UPR-activated cell is generically described as experiencing "ER stress." To address this problem, I utilized an ER-targeted green fluorescent protein whose fluorescent output is responsive to its oxidation state (called eroGFP). I found that many stressors to ER protein folding homeostasis—both experimental and physiological—compromise oxidation of eroGFP in *S. cerevisiae*. By combining eroGFP with an additional fluorescent protein reporter to follow changes in UPR activity I was able to determine conditions in which the UPR is capable of promoting adaptation. Additionally, using high-throughput flow cytometry, I measured eroGFP oxidation in approximately 6000 yeast strains each with a deletion or hypomorphic allele of a single gene. Through this analysis, I was able to identify genes important for maintaining oxidative protein folding during normal growth conditions and during protein folding stress. The

strategy of utilizing eroGFP as a proximal reporter for ER stress proved to be complimentary to UPR-based metrics to provide a more comprehensive understanding of ER protein folding. The tools and concepts developed here should be broadly applicable to other biological processes and should aid investigations of how ER stress affects human disease.

Table of Contents

List of Tables

List of Figures

Chapter 1. Introduction—no tables

Chapter 2. Real-time Redox Measurements during Endoplasmic Reticulum Stress Reveal Interlinked Protein Folding Functions

Chapter 1

Introduction

The endoplasmic reticulum (ER) is the organelle dedicated to the folding, modification, and export of secretory and membrane proteins which together represent nearly one-third of the cellular proteome. In order to efficiently fold these proteins, the ER has evolved a specialized environment containing molecular chaperones, oxidoreductases, and other protein-modification enzymes that aid protein maturation (van Anken and Braakman, 2005). Proteins that cannot fold are retro-translocated out of the ER and targeted for degradation via the 26S proteasome in a process called ER-associated protein degradation (ERAD) (Vembar and Brodsky, 2008). Together, these molecular machines help ensure that only correctly folded proteins transit to the Golgi for further processing.

Despite these mechanisms to correctly fold proteins, various physiological or pathophysiological conditions may cause protein flux through the ER to exceed the ER's protein-folding capacity. To maintain protein folding fidelity, the cell has evolved a signal transduction pathway called the unfolded protein response (UPR) that matches the ER's protein-folding capacity to cellular demand. The UPR was discovered over 20 years ago with the observation that disruption of protein folding in the ER increased gene expression of ER-resident chaperones (Kozutsumi et al., 1988). Since this discovery, many of the molecular details of the UPR have been revealed and are briefly summarized below (for a detailed review see Ron and Walter, 2007 and references therein).

In metazoans, the UPR consists of at least three proximal sensors called inositol-requiring enzyme-1 (IRE1), activating transcription factor-6 (ATF6), and protein kinase RNA (PKR)-like ER kinase, (PERK). The budding yeast, *Saccharomyces cerevisiae*, has a simpler UPR with IRE1 as the sole proximal sensor (Cox et al., 1993). These sensors reside

in the ER membrane and are thought to be activated by the presence of unfolded proteins in the ER (Credle et al., 2005). Upon activation, IRE1 and ATF6 initiate a signaling cascade that increases the transcription rates of genes encoding ER-resident molecular chaperones and other factors that support protein folding in the ER (Yamamoto et al., 2007). PERK signaling transiently inhibits protein translation (Harding et al., 1999). Together, these outputs promote protein-folding homeostasis in the ER by temporarily reducing protein influx and by increasing protein-folding capacity.

The discoveries in the UPR field over the past 20 years have led to the development of a number of tools to measure the activity of the UPR in living cells (Back et al., 2006; Iwawaki et al., 2004; Travers et al., 2000). However, there are no useful methods for monitoring protein folding conditions within the ER independent of UPR signaling, because it is infeasible to measure concentrations of unfolded proteins within an organelle. As a consequence, any cell that has activated the UPR is operationally defined as experiencing a condition called ER stress.

ER stress is associated with a loss of protein folding homeostasis in the ER, a condition that may not always correlate with UPR activity. For example, is a UPR-activated cell experiencing protein misfolding in the ER or has it successfully adapted? This question cannot be definitively addressed using UPR-based metrics because they simply indicate that the UPR is active, but they do not provide information on the UPR's effectiveness. Therefore, reporters that monitor multiple aspects of ER physiologically are required to comprehensively understand ER stress.

For my graduate work, I developed a system of fluorescent protein reporters to study the physiology of ER protein folding in real time and in single living cells. Instead of attempting to measure concentrations of unfolded proteins, I utilized an ER-localized redox-sensitive green fluorescent protein (eroGFP) to measure changes in the ER's redox environment. The ER maintains a more oxidizing redox environment relative to the cytosol in order to facilitate disulfide bond formation in nascent secretory proteins (Tu and Weissman, 2004). I hypothesized that unfolded protein accumulation may perturb the molecular machines that maintain ER redox homeostasis and may cause the ER to become less oxidizing.

In the work described in the following chapters, I demonstrated that redox changes measured by eroGFP occur during ER stress in *S. cerevisiae*, thus validating its utility as a stress metric. By combining eroGFP with a UPR-metric, I was able to identify conditions for which the UPR is capable of successfully promoting adaptation in response to various environmental or genetic perturbations to ER protein folding. Additionally, I used high-throughput genomic studies in *S. cerevisiae* to uncover novel genes that contribute to protein folding homeostasis in the ER.

These studies lay the groundwork for investigating the relationship between ER stress and the UPR in mammals. The mammalian UPR is more complex than the yeast UPR, and dysregulation of the mammalian UPR contributes to myriad human diseases including neurodegeneration, diabetes, and cancer (Kim et al., 2008). Utilizing redox-based reporters in mammalian systems may help define how the UPR contributes to these pathologies which should aid the development of therapeutics to treat ER-stress-related disorders.

REFERENCES

Back, S. H., Lee, K., Vink, E., and Kaufman, R. J. (2006). Cytoplasmic IRE1alpha-mediated XBP1 mRNA splicing in the absence of nuclear processing and endoplasmic reticulum stress. J Biol Chem *281*, 18691-18706.

Cox, J. S., Shamu, C. E., and Walter, P. (1993). Transcriptional induction of genes encoding endoplasmic reticulum resident proteins requires a transmembrane protein kinase. Cell *73*, 1197-1206.

Credle, J. J., Finer-Moore, J. S., Papa, F. R., Stroud, R. M., and Walter, P. (2005). On the mechanism of sensing unfolded protein in the endoplasmic reticulum. Proc Natl Acad Sci U S A *102*, 18773-18784.

Harding, H. P., Zhang, Y., and Ron, D. (1999). Protein translation and folding are coupled by an endoplasmic-reticulum-resident kinase. Nature *397*, 271-274.

Iwawaki, T., Akai, R., Kohno, K., and Miura, M. (2004). A transgenic mouse model for monitoring endoplasmic reticulum stress. Nat Med *10*, 98-102.

Kim, I., Xu, W., and Reed, J. C. (2008). Cell death and endoplasmic reticulum stress: disease relevance and therapeutic opportunities. Nat Rev Drug Discov *7*, 1013-1030.

Kozutsumi, Y., Segal, M., Normington, K., Gething, M. J., and Sambrook, J. (1988). The presence of malfolded proteins in the endoplasmic reticulum signals the induction of glucose-regulated proteins. Nature *332*, 462-464.

Ron, D., and Walter, P. (2007). Signal integration in the endoplasmic reticulum unfolded protein response. Nat Rev Mol Cell Biol *8*, 519-529.

Travers, K. J., Patil, C. K., Wodicka, L., Lockhart, D. J., Weissman, J. S., and Walter, P. (2000). Functional and genomic analyses reveal an essential coordination between the unfolded protein response and ER-associated degradation. Cell *101*, 249-258.

Tu, B. P., and Weissman, J. S. (2004). Oxidative protein folding in eukaryotes: mechanisms and consequences. J Cell Biol *164*, 341-346.

van Anken, E., and Braakman, I. (2005). Versatility of the endoplasmic reticulum protein folding factory. Crit Rev Biochem Mol Biol *40*, 191-228.

Vembar, S. S., and Brodsky, J. L. (2008). One step at a time: endoplasmic reticulum-associated degradation. Nat Rev Mol Cell Biol *9*, 944-957.

Yamamoto, K., Sato, T., Matsui, T., Sato, M., Okada, T., Yoshida, H., Harada, A., and Mori, K. (2007). Transcriptional induction of mammalian ER quality control proteins is mediated by single or combined action of ATF6alpha and XBP1. Dev Cell *13*, 365-376.

Chapter 2

Real-time Redox Measurements during

Endoplasmic Reticulum Stress Reveal

Interlinked Protein Folding Functions

Real-time Redox Measurements during Endoplasmic Reticulum Stress Reveal Interlinked Protein Folding Functions

Philip I. Merksamer[1,2,3], Ala Trusina[1,2,3], Feroz R. Papa[1,2,3,*]

Department of Medicine[1], Diabetes Center[2],

& California Institute for Quantitative Biosciences[3]

University of California, San Francisco

San Francisco, CA 94143-2520. U.S.A.

Tel: 415-476-2117

FAX: 415-514-9656

* Correspondence: frpapa@medicine.ucsf.edu (F.R.P.)

SUMMARY

Disruption of protein folding in the endoplasmic reticulum (ER) causes unfolded proteins to accumulate, triggering the unfolded protein response (UPR). UPR outputs in turn decrease ER unfolded proteins to close a negative feedback loop. However, because it is infeasible to directly measure the concentration of unfolded proteins *in vivo*, cells are generically described as experiencing “ER stress” whenever the UPR is active. Because ER redox potential is optimized for oxidative protein folding, we reasoned that measureable redox changes should accompany unfolded protein accumulation. To test this concept, we employed fluorescent protein reporters to dynamically measure ER redox status and UPR activity in single cells. Using these tools, we show that diverse stressors, both experimental and physiological, compromise ER protein oxidation when UPR-imposed homeostatic control is lost. Using genetic analysis we uncovered redox heterogeneities in isogenic cell populations, and revealed functional interlinks between ER protein folding, modification, and quality control systems.

INTRODUCTION

Aided by chaperones and other activities, secretory proteins fold precisely to their native conformations as they transit through the endoplasmic reticulum (ER). However, cells can encounter conditions during which demand on ER protein-folding activities exceeds capacity. During these instances of "ER stress" unfolded proteins accumulate within the organelle, triggering intracellular signaling pathways collectively called the unfolded protein response (UPR). The UPR transcriptionally upregulates genes encoding chaperones, oxidoreductases, and ER-associated degradation (ERAD) components (Travers et al., 2000). In metazoans, the UPR also transiently inhibits translation (Harding et al., 2002; Zhang and Kaufman, 2006). Thus, UPR outputs are adaptive because they reduce secretory protein load, enhance protein-folding capacity and promote degradation of misfolded proteins (Brodsky and McCracken, 1999; Meusser et al., 2005; Ron and Walter, 2007). In mammalian cells, the UPR can also trigger apoptosis, perhaps when adaptive outputs fail (Zhang and Kaufman, 2006).

Cells are described as experiencing "ER stress" if they have induced downstream UPR components, such as the ER chaperone BiP. But this operational definition is circular, and it is easy to see that the definition breaks down when the UPR machinery is disabled or absent. Cells lacking UPR components are likely to be more stressed than their wild-type counterparts as they are unable to effectively mount a response. Conversely, UPR activation indicates that a response has been initiated, but not whether homeostasis becomes restored. Unfolded proteins are likely to be the UPR's activating input signals (Credle et al., 2005; Kimata et al., 2007; Zhou et al., 2006), but it is difficult to measure unfolded proteins in

organelles even with disruptive techniques, and unfeasible to measure them directly within living cells. However, measuring UPR activity in living cells using transcriptionally-activated fluorescent protein reporters is straightforward (Back et al., 2006; Iwawaki et al., 2004; Travers et al., 2000). If a gauge could be developed to also measure changes in ER protein-folding functions under stress, it should reveal how far such functions drift from homeostasis when perturbed, and indicate whether the UPR successfully promotes adaptation, thereby providing a more comprehensive picture of the physiological state of ER protein folding in living cells.

The ER's molecular environment is specialized to fold secretory proteins. Compared to the cytosol, the ER has greater calcium concentration, a more oxidizing redox potential, and dedicated enzymes for protein glycosylation (van Anken and Braakman, 2005). Distinct stresses ensue when the activities supporting these specialized functions are focally perturbed, either genetically or pharmacologically. But if ER functions are tightly coupled, a focal stress such as ER calcium depletion, for example, could ripple outward to provoke other stresses, such as decreased protein glycosylation. Such ripple effects might occur if glycosylating enzymes function best in a calcium-rich environment. If true, we reasoned that it should be possible to gather global information about changes in ER protein-folding capacity through measuring effects of different stresses on a single ER function. To this end, we decided to measure changes in the ER's redox potential as protein folding is perturbed.

The ER maintains an oxidizing redox potential to promote disulfide bond formation in maturing secretory proteins (Sevier and Kaiser, 2002; Tu and Weissman, 2004). Under "ER

stress" the UPR upregulates catalytic activities to further enhance disulfide bond formation and promote oxidative protein folding (Travers et al., 2000). However, an overwhelming secretory protein load could saturate the ER's oxidative folding machinery, which should impede disulfide bond formation and folding of many ER-localized proteins. So depending on the strength and timing of adaptive responses, the ER's redox environment may deviate from its set point in either direction as unfolded proteins accumulate. An ER redox gauge should therefore report widely on different stresses. To test this concept, we adapted fluorescent proteins to monitor ER redox status and UPR activity dynamically in populations of single cells under stress.

RESULTS

Characterization of an ER-localized redox-sensing GFP

To follow the ER's redox state *in vivo*, we adapted recently described redox-sensitive green fluorescent proteins (GFP) as oxidation reporters for the ER (Dooley et al., 2004; Hanson et al., 2004). These GFPs have an engineered cysteine pair on adjacent surface-exposed β-strands that become disulfide-linked under oxidizing conditions. Disulfide formation reorients GFP's chromophore, altering fluorescence excitability from two maxima: 400 and 490 nm. When oxidized, excitation from 400 nm increases, while excitation from 490 nm decreases; when reduced the opposite trend occurs. Therefore, the ratio of fluorescence excitation from these two wavelengths provides an internally-controlled readout of this GFP's redox state, while canceling out factors affecting absolute optical sensitivity (e.g. varying fluorescence output due to photobleaching, changes in reporter levels, etc.).

We appended the ER retrieval signal, HDEL, to the C-terminus of a variant called roGFP2 for ER expression. The recombinant tagged protein called eroGFP (ER-targeted redox-sensitive GFP) displayed distinct excitation spectra in the fully oxidized and reduced species, with maxima at 400 and 490 nm (Figure 1A). Titration with increasing concentrations of reduced to oxidized lipoic acid caused fluorescence emission from 400 nm excitation to incrementally decrease and emission from 490 nm excitation to increase. The curves intersected at an isosbestic point indicating two equilibrating species (Figure 1B). The ratio of fluorescence from these two excitation maxima could be related back to the fraction of reduced eroGFP. Fitting a curve to the reduced eroGFP fraction gave a midpoint value of -282 +/- 3mV (Figure 1C).

DNA sequences encoding the cleavable signal peptide of the ER chaperone Kar2p were N-terminally fused to eroGFP's coding sequence, and the reporter was expressed in *S. cerevisiae*. eroGFP co-localized with the ER marker Sec61p, indicating proper ER targeting (Figure 1D). To monitor eroGFP *in vivo*, we used flow cytometry to measure the ratio of fluorescence from excitation at 488 nm versus 405 nm. This ratio—expressed in log_2 space and normalized to wild-type untreated cells—is called the "eroGFP ratio". Cells treated with increasing dithiothreitol (DTT), a cell-permeable reductant, displayed progressively increasing eroGFP ratios that saturated when the reporter was completely reduced (Figure 1E). The eroGFP ratio of a cysteine mutant (C147S) unable to form the surface disulfide did not increase with DTT (Figure S1A). The oxidant H_2O_2 caused only a slight decrease in the eroGFP ratio, allowing us to estimate that eroGFP is 96.9% oxidized (+/-0.3% SD) *in vivo* (Figure 1E).

To use eroGFP as an ER stress reporter, we first needed to ensure that it did not affect UPR signaling. Expression of eroGFP did not provoke *HAC1* mRNA splicing (Figure 1F, lanes 1 vs. 3), which occurs under ER stress (Cox and Walter, 1996; Kawahara et al., 1997). Cells treated with the ER stress-inducing agent tunicamycin (Tm) displayed comparable *HAC1* splicing with or without eroGFP expression (Figure 1F, lanes 2 vs. 4). Therefore eroGFP neither perturbs ER function to activate the UPR, nor does it compromise the UPR's ability to signal when unfolded proteins accumulate.

Dynamic monitoring of ER redox changes and UPR activity during pharmacologically-induced ER stress

To monitor the UPR, we constructed a second reporter gene encoding the red fluorescent protein, mCherry, driven by a minimal CYC1 promoter and four tandem unfolded protein response elements that the UPR transcription factor Hac1p binds—we call this UPR-RFP. eroGFP and UPR-RFP genes were combined onto a single construct that was chromosomally integrated (Figure 2A). For dynamic monitoring, we employed an automated setup recently developed by Chin and colleagues to inject 10^4-10^5 cells growing in bioreactors into a flow cytometer every 3-10 minutes over 3-14 hours (Chin et al., 2008). A combination of 3 laser lines allowed measurement of the eroGFP ratio and UPR-RFP level of individual cells as they passed through the flow cytometer (Figure 2B). Through the automated setup, single cells within large populations could be interrogated in these two metrics, and the populations represented as time-lapse histograms as ER-stress agents were added or removed (Figures 2C-F).

DTT unfolds ER proteins by reducing disulfides, thereby activating the UPR. In wild-type cells, DTT caused a rapid increase in the eroGFP ratio, apparent on the histogram as a deflection of the entire population (Figure 2C). Resolved on a finer time scale, the median eroGFP ratio deflected within 3 minutes, peaking to 1.5 by 12 minutes (Figure S2). The upward spike was followed by a steady decline over many hours (Figure 2C). Media exchange experiments showed that this decline was due in part to cellular adaptation, rather than just DTT oxidation (Figure S3). Changes in eroGFP ratio were not

due to re-localization, since the reporter remained co-localized with Sec61p during DTT treatment (Figure S4).

The UPR-RFP metric (defined as fluorescence from 532nm excitation, expressed in log_2 space, and normalized to wild-type untreated cells) started to deflect 40 minutes after DTT addition, and steadily increased from 0 to 5 over ten hours (Figure 2D). During this time course, we witnessed induction and accumulation of UPR target activities promoting ER protein oxidation, such as the protein-disulfide isomerase, Pdi1p, which increased within two hours and remained elevated over eight hours (Figure S5).

ER protein folding can be perturbed through a different mechanism using Tm, which inhibits protein glycosylation. If glycosylation and disulfide bond formation in the ER are interlinked, Tm could cause under-oxidation of ER proteins. Alternatively, UPR activation by Tm could cause ER hyperoxidation as oxidoreductases become upregulated. eroGFP ratios in the entire population of cells treated with Tm steadily increased, clearly indicating reduction of the reporter (Figure 2E). Unlike rapid changes from DTT, the eroGFP ratio of Tm-treated cells started to deflect 60 minutes after treatment, progressively increasing over four more hours up to 0.75. As with DTT, eroGFP remained ER-localized after Tm treatment (Figure S4). As with DTT, Tm caused UPR-RFP to increase from 0 to 5, albeit with a 70 minute lag time because Tm affects folding of newly synthesized ER proteins, while DTT also unfolds existing ones (Figure 2F). Movies S1 and S2 show that while dynamic changes in the UPR-RFP metric were remarkably similar for both treatments, dynamic eroGFP ratio changes were very distinct.

To confirm that changes in the eroGFP ratio reflected changes in its oxidation state *in vivo*, we incubated extracts from cells treated with DTT or Tm with the thiol-alkylating agent AMS. Non-reducing gels showed only one slower migrating form of eroGFP after DTT treatment, suggesting that its disulfide had been completely reduced, and thereafter AMS modified (Figure 2G, lanes 1 and 2). Tm treatment produced both oxidized (disulfide-protected) and reduced (AMS-modified) species, consistent with its intermediate eroGFP ratio (lane 3). The control eroGFP (C147S) could be AMS-modified with or without ER stress-inducing agents (Figure S1B).

The lag time needed to change the eroGFP ratio under Tm suggested that eroGFP oxidation changes were secondary to glycosylation inhibition of proteins promoting disulfide bond formation. To test this notion, we incubated yeast extracts with AMS after treatment with DTT or Tm, and immunoblotted for the ER oxidase, Ero1p (Frand and Kaiser, 1998; Pollard et al., 1998). Ero1p is a glycoprotein and Tm treatment caused complete underglycosylation *in vivo*. DTT treatment produced a single AMS-modified (slower migrating) species, indicating complete reduction of Ero1p. Tm caused intermediately-migrating AMS-modified Ero1p species, indicating incomplete oxidation (Figure S6). As Ero1p is the proximal generator of oxidizing equivalents necessary for forming disulfide bonds in the ER, its incomplete oxidation could be expected to impair its ability to oxidize other ER proteins such as eroGFP.

Another possibility could explain the lag time for eroGFP reduction under Tm treatment: reduced eroGFPs may represent newly-synthesized proteins unable to form disulfides during glycosylation inhibition. To address this, we positioned eroGFP under the inducible GAL1 promoter, so we could rapidly terminate its expression with glucose. Pulse-chase analysis confirmed that eroGFP synthesis ceased after glucose addition (Figure S7A). Since eroGFP decayed with a 4 hr half-life (Figure S7B), it provided a long time window to monitor its fluorescence. As with cells continually synthesizing eroGFP (SGal), cells switched to glucose (SD) experienced similar increases in eroGFP ratio with DTT or Tm (Figure S7C-F). These results indicated that eroGFP oxidation changes under stress do not result merely from an inability to form disulfides in newly imported eroGFP, but must also include reduction of pre-existing eroGFP.

ER redox changes are affected by genetic background

Since the eroGFP ratio of cells exposed to DTT declined while UPR-RFP rose (Figures 2C and D), UPR activity may have been re-oxidizing ER proteins after DTT treatment. To test this genetically, we integrated our composite reporter into deletion mutants of two UPR genes—*IRE1* and *HAC1*—needed to sense and respond to unfolded proteins (Cox et al., 1993; Cox and Walter, 1996). As with wild-type cells (Figures 2C-F), the UPR mutants displayed unimodal distributions in both eroGFP ratio and UPR-RFP metric under treatment (not shown); therefore their medians were informative of the whole population, and are henceforth presented as overlaid trajectories instead of histograms (Figure 3). Unexpectedly, the resting median eroGFP ratio of both UPR mutants was

identical to wild-type (i.e at 0), indicating that protein oxidation was preserved under unstressed conditions to the extent that eroGFP could be fully oxidized.

However, when challenged with DTT, both UPR mutants exhibited greater eroGFP ratio increases than wild-type, peaking to 2 by twenty minutes (Figures 3C and E), and remaining elevated throughout the time course in contrast to the steady decay seen in wild-type cells (Figure 3A). Tm also caused greater eroGFP ratio changes in the UPR mutants than in wild-type, peaking to 1.5 (Figures 3B, D, F). The UPR-RFP metric was initially -3 for *ire1*Δ and -2 for *hac1*Δ, and exhibited only a slight upward drift under DTT or Tm, which may have occurred due to RFP accumulation in the cells as they became growth arrested (see analysis below).

To ask whether re-oxidation occurs after glycosylation stress is relieved, we diluted wild-type cells treated with Tm for four hours into fresh media lacking Tm, and found that the eroGFP ratio steadily decreased over eight more hours. The UPR-RFP metric remained elevated for three hours after dilution, after which it also descended back towards its initial state as the population resumed growth (Figure S8). In contrast, the eroGFP ratio in both UPR mutants remained elevated upon Tm washout, and the mutants did not resume growth (Figure S8). Taken together, these results implied that the UPR is needed to both buffer the ER against acute challenges to oxidative folding, and to re-establish homeostasis after stress is encountered.

Since UPR transcriptional targets include enzymes mediating ER protein oxidation, we next measured the behavior of mutants in two ER oxidation genes—*ERO1* and *PDI1*—to DTT and Tm. These genes encode enzymes that generate disulfide bonds in secretory proteins through a relay of dithiol-disulfide exchange reactions (Sevier and Kaiser, 2002; Tu and Weissman, 2004). As both genes are essential, we expressed our composite reporter in DAmP alleles for *PDI1* and *ERO1*, which are hypomorphic due to reduced mRNA abundance (Schuldiner et al., 2005). Unexpectedly, both mutants had a resting eroGFP ratio similar to wild-type (i.e. near 0). Compensation from elevated UPR activity may have allowed complete oxidation of eroGFP in these hypomorphs as the initial UPR-RFP metric was 2 and 1 for *pdi1*-DAmP and *ero1*-DAmP respectively (Figures 3G, H, I, and J). However, DTT treatment of these mutants caused rapid increases in the eroGFP ratio to 1.5 by 20 minutes (Figures 3G and 3I). After its initial spike, the eroGFP ratio modestly decreased, but not to the same extent as in wild-type cells. Moreover, the UPR-RFP metric only increased by 3 and 4 for *pdi1*-DAmP and *ero1*-DAmP respectively, compared to an absolute increase of 5 in wild-type (Figures 3A, G, and I).

Surprisingly, Tm treatment of these mutants caused a smaller eroGFP ratio change than in wild-type cells (Figures 3H and J). In both mutants, eroGFP displayed a maximal increase of 0.70 compared to 0.75 for wild-type cells, and remained slightly below that of wild-type throughout the time courses. However, for both mutants changes in the UPR-RFP metric from DTT or Tm treatment were indistinguishable (Figures 3H and J).

Another critical ER function is to identify and remove misfolded secretory proteins for degradation by the 26S proteasome, a process called ERAD (Meusser et al., 2005; Romisch, 2005). To study ER oxidation changes when ERAD function is compromised, we expressed our composite reporter in a strain deleted for *HRD1,* which encodes an E3 ubiquitin ligase needed to degrade ER luminal misfolded proteins (Bays et al., 2001; Deak and Wolf, 2001). Like the protein oxidation mutants, *hrd1*Δ's initial eroGFP ratio was 0. Its initial UPR metric was also elevated at 2 (Figures 3K and L). In *hrd1*Δ, DTT caused the eroGFP ratio to increase to 1.3 over the first 20 minutes, after which it leveled off to 0.75 with a slower decay than in wild-type (Figure 3K). Under Tm, the eroGFP ratio rose to 0.8—also slightly greater than wild-type (Figure 3L). Rises in the UPR-RFP metric of *hrd1*Δ cells were indistinguishable under DTT or Tm treatment (Figure 3L).

Redox deviations occur under conditions of physiological ER stress

Until now, we have only employed chemical agents to induce extreme and non-physiological ER protein misfolding. We next inquired whether ER oxidation changes occur during physiologically-relevant challenges such as inositol starvation, a stress known to activate the UPR (Cox et al., 1997; Nikawa and Yamashita, 1992). To this end, we removed inositol from the media of dividing wild-type cells. The UPR-RFP metric began to rise 140 minutes after inositol starvation, increasing to 2 before slightly decreasing, then leveling off (Figure 4B). This decline to a lower sustained level could be due to a slight overshoot in UPR signaling, or could indicate a fine tuning of the response as it established homeostasis. However, the eroGFP ratio remained unchanged at zero over the ten hour starvation (Figure 4A). This suggested that UPR induction may have

consequently protected the ER from under-oxidation. To test this idea, we repeated the inositol starvation experiment in *ire1*Δ and *hac1*Δ mutants. As expected, the UPR-RFP metric was initially -3 for *ire1*Δ and -2 for *hac1*Δ, and drifted upward due to RFP accumulation (Figures 4D and 4F). Strikingly, two subpopulations with different eroGFP ratios emerged at 4.5 hours after inositol starvation: a deflected population and a static population (Figures 4C, E and Movie S3). The deflected subpopulations had eroGFP increases of 1.3 and 1.4 and represented 51% and 69% of cells for *ire1*Δ and *hac1*Δ respectively.

As UPR mutant cells continue to grow and divide for several generations after inositol deprivation (albeit at slower rates than wild-type) (Figure 4G), we hypothesized that the distinct eroGFP populations could represent mother and daughter cells. To investigate this, we subjected eroGFP-expressing *hac1*Δ cells to a lineage-tracing strategy that fluorescently labels mother cell walls with a Cy5 dye (Chin et al., 2008). When deprived of inositol, the sub-population with the increased eroGFP ratio was clearly overrepresented as Cy5-surface stained cells (mothers), and the sub-population that maintained eroGFP in an oxidized state was underrepresented as Cy5-surface stained cells (daughters) (Figures 4H-L and Movie S4).

We next simulated another common physiological ER challenge: increased expression of secretory proteins. For this purpose, we employed different versions of the well-studied secretory protein carboxypeptidase Y (CPY). We first generated constructs expressing CPY, or the misfolded ERAD substrate (CPY*), under conditional control of the CUP1

promoter. Cells expressing P_{CUP1}-CPY or P_{CUP1}-CPY* could be induced to produce protein by adding copper sulfate ($CuSO_4$) (Figure S9B). $CuSO_4$ addition to cells harboring empty vector caused neither eroGFP nor UPR-RFP to deflect (Figure S9A). Induction of CPY with 200μM $CuSO_4$ changed neither eroGFP ratio nor UPR-RFP metric (Figures 5A and B), but escalation of $CuSO_4$ to 500μM (which produced greater amounts of CPY protein—Figure S9C) revealed a small sub-population (3.7% of the total during the entire time course) displaying eroGFP ratios above a threshold of 1 (Figure 5I). This indicates that overexpression of an endogenous secretory protein can cause ER oxidation changes in some cells. Induction of misfolded CPY* with 200μM $CuSO_4$ caused 5.7% of the total population to have eroGFP ratios greater than 1 (Figure 5C). This population emerged two hours after $CuSO_4$ addition, when there was 18-fold increased CPY* over baseline (Figure S9D). Dose escalation of $CuSO_4$ to 500μM further increased CPY* expression (Figure S9C), and increased the population of cells with eroGFP ratios above 1 to 12% (Figure 5K). Remarkably, the populations with increased eroGFP ratios declined near the end of the time course despite continued CPY* expression, suggesting adaptation (Figure S9D). UPR-RFP increases also became evident in these populations, and cells with greater eroGFP ratios tended to have higher UPR-RFP levels (Movie S5).

Since CPY* is efficiently degraded through ERAD, we performed two experiments to study the effects of a misfolded protein that is not efficiently degraded. First, we expressed CPY and CPY* in *hrd1*Δ cells which are compromised for CPY* degradation (Friedlander et al., 2000). Addition of 200μM $CuSO_4$ to *hrd1*Δ cells expressing CPY and

CPY* caused 4.2% and 10% of the populations to have eroGFP ratios above 1 respectively (Figures 5E and G). Like wild-type, *hrd1*Δ cells that had the greatest eroGFP deflection also had the greatest increase in UPR-RFP (Figure 5H and Movie S6). Second, we expressed a non-glycosylated version of CPY*, called CPY*0000, in wild-type cells which is not efficiently degraded (Kostova and Wolf, 2005; Spear and Ng, 2005). In these cells, the percentage of cells with eroGFP ratios above 1 climbed to 16%, and deflections occurred more rapidly after $CuSO_4$ addition than with CPY* (Figure 5M). The deflected population eventually decayed, again suggesting adaptation, albeit slower than the CPY*-expressing population. (Movie S7).

Because CPY* contains 11 cysteines, we next studied the effects of eliminating the cysteines in CPY* on eroGFP changes. We generated two CUP1-inducible CPY* variants containing either 1 cysteine or no cysteines (Haynes et al., 2004). Expression of CPY*-1Cys caused similar changes as observed for CPY*, however, expression of CPY*-Cysless caused only 4.3% of cells to have eroGFP ratios above 1 (Figures 5O and Q). Thus the "potency" of CPY variants in their ability to cause eroGFP deflection was CPY*0000 > CPY* > CPY*-1Cys > CPY*-Cysless > CPY (Figure S9G).

eroGFP and UPR-RFP changes under stress reveal interlinked protein folding functions orchestrated by the UPR

While cells undergoing the relatively milder stresses of inositol deprivation or overexpression of CPY variants displayed heterogeneity in their populations, cells subjected to the strong stressors DTT and Tm deflected across both metrics as

homogeneous populations. To further analyze the behavior of wild-type and mutants under these strong stresses, we displayed their eroGFP and UPR-RFP changes using trajectories in two dimensional space to illustrate two major points (Figures 6A and B). First, in the absence of stress, mutants varied in their UPR-RFP metric, yet their eroGFP ratio was the same, indicating that these mutants can sustain near complete oxidation (at least of eroGFP). Second, the two different stressors caused distinct trajectories for each strain. Only wild-type cells were capable of near complete re-oxidization of eroGFP after DTT treatment. UPR mutants displayed the greatest eroGFP deflections under both stresses, indicating their pivotal roles in countering diverse protein folding challenges. Most surprisingly, the oxidative folding mutants showed greater deflections than wild-type cells after DTT treatment, but slightly smaller changes after Tm treatment.

In all cases, UPR-RFP never decreased over the time courses. Since RFP has a long half-life and because both DTT and Tm caused growth arrest in wild-type and all mutants examined leading to its further accumulation (Figures 6C and D and data not shown), the rate of change of UPR-RFP was a better indicator of UPR activity for any given time point. To this end, we calculated the first derivative of median UPR-RFP (d(UPR-RFP)/dt) for wild-type and mutants. For wild-type cells, d(UPR-RFP)/dt was positive throughout the time course of DTT treatment, although it declined 4 hours after treatment as eroGFP became re-oxidized (Figure 6E). For Tm treatment, d(UPR-RFP)/dt also remained positive throughout the time course, also declining before leveling off (Figure 6F). As expected, d(UPR-RFP)/dt was fixed at zero for the UPR mutants (Figures 6E and F). Surprisingly, d(UPR-RFP)/dt displayed larger maximal values in both the oxidative

folding and ERAD mutants than wild-type, in Tm but not DTT (Figures 6E and F). Increased basal UPR activation in these mutants may allow for faster UPR induction under stress. Indeed, *pdi1*-DAmP displayed 28% greater *HAC1* mRNA splicing than wild-type in the absence of Tm, suggesting that it was "pre-conditioned" due to low level UPR activation. (Figure S10). As DTT unfolds existing ER proteins rapidly, while Tm affects folding of newly synthesized proteins (and therefore more slowly), differences in UPR activation kinetics may be less apparent in the former treatment than in the latter.

To quantify the stressed state further, we integrated the area under each eroGFP ratio curve (AUC) over the time course of stress for each mutant, and normalized the AUCs by subtracting from wild-type's AUC (Figure S11). Normalized this way, a positive AUC denotes greater cumulative eroGFP change over the time course than wild-type, while negative values indicated less change. A heat map of the analysis (Figure 6G) showed that ERAD and UPR mutants were uniformly more stressed than wild-type under Tm or DTT. Unexpectedly oxidative folding mutants were less stressed than wild-type during Tm, but more stressed under DTT. We therefore predicted that *ero1*-DAmP cells would grow under Tm but not DTT, and confirmed this notion (Figure S12). Interestingly, *ero1*-DAmP cells grew slightly better than wild-type in Tm, consistent with their negative AUC.

Taken together, our results show that the UPR is necessary to orchestrate readjustment of ER protein oxidation under distinct stresses. We therefore asked whether UPR activity is also sufficient to buffer ERs from under-oxidation during stress. To this end, we applied a

chemical-genetic approach we previously developed to activate the UPR in the absence of stress. Through rational protein engineering, Ire1p—a bi-functional ER transmembrane kinase/RNase responsible for UPR signaling—can be sensitized to a cell-permeable nucleotide analog called 1NM-PP1. In *ire1*Δ cells harboring this Ire1 allele, 1NM-PP1 activates the UPR independent of stress (Papa et al., 2003). Treatment with 1NM-PP1 caused a slight decrease in the eroGFP ratio, suggesting hyperoxidation of the ER. Adding 1NM-PP1 and Tm together caused a smaller increase in the eroGFP ratio compared to Tm alone, suggesting a buffering effect against protein under-oxidation (Figure 6H). UPR output therefore is both necessary and sufficient to mitigate under-oxidation of ER proteins during stress.

DISCUSSION

This is the first study of "ER stress" using real-time analysis to interrogate the stressed state of single cells within large populations. We utilized separate reporters to measure two independent variables: UPR-RFP for UPR activity, and a redox-sensitive reporter—eroGFP—to follow oxidation of cysteine sulfhydryls to disulfides. Thus eroGFP was positioned as a "proximal" reporter for the critical ER function of disulfide formation. eroGFP is internally controlled because it is ratiometric by excitation, obviating the need to consider and correct for confounding factors affecting absolute reporter levels. Although an individual eroGFP molecule is either reduced or oxidized (binary), cumulative fluorescence from many eroGFP molecules provided a continuous (analog) readout of eroGFP's average oxidation state within single cells. Adding UPR-RFP as a "distal" reporter for UPR signaling provided complementary information that could not have been gathered using either reporter alone. Our design strategy of positioning proximal and distal reporters may be useful for studying other intracellular signaling pathways where input signals are not easily quantifiable.

We propose a model that accounts for our observations and analyses, and provides conceptual advances (Figure 7). Using our systems, we found (as expected) that chemical reduction is a "primary" stress causing under-oxidation of eroGFP and other ER proteins—we refer to this as ER oxidative folding stress. Unexpectedly, other challenges to protein folding—including under-glycosylation, inositol deprivation, and increased protein secretion—"secondarily" caused varying degrees of ER oxidative folding stress. Based on these results, we propose that the ER's protein folding, modification, and

quality control systems are functionally interlinked with the oxidative folding machinery—and by extension perhaps with each other. Thus, eroGFP can measure many discrete challenges to ER function that have historically been grouped and studied under the rubric of “ER stress”.

Our model highlights four extreme states of ER oxidation state and UPR activity. Consistent with previous estimates of a highly oxidizing ER redox potential obtained through disruptive methods (Hwang et al., 1992), eroGFP was almost completely oxidized in wild-type cells without imposed stress. Unexpectedly, eroGFP remained similarly oxidized in all mutants tested in this study. This unexpected result points to a remarkable plasticity in ER oxidative folding. Only through actively perturbing ER functions are eroGFP differences between mutants revealed. Unstressed UPR mutants can still support ER oxidation, perhaps because the UPR is only required to increase expression of ER oxidoreductases during stress. ER oxidation, however, is essential, and hypomorphs in oxidative folding activities exhibit an adapted state through low-level UPR activation.

The ER-stressed (UPR-activated) state can be achieved in any cell competent for UPR signaling. Here the combination of eroGFP and UPR-RFP revealed subtle differences between mutants under distinct stresses. Both *ero1*-DAmP and *pdi1*-DAmP resisted challenges to glycosylation better than oxidation. This difference may occur because UPR activation resets ER oxidation to minimum levels for viability, but in the process augments other ER folding activities such as those supporting glycosylation. Thus these mutants come “pre-conditioned” against challenge to other functions. We predict that

many such pre-conditioned states could exist, and dynamic monitoring with eroGFP should delineate these at the genomic level, allowing assignment of primary functions to uncharacterized genes. Pre-conditioning could also be achieved through chemical-genetic activation of Ire1, which revealed slight hyperoxidation in the absence of stress. Future versions of eroGFPs exhibiting more oxidizing midpoint potentials may allow more accurate quantification of these changes under both resting and stressed states.

The ER-stressed (decompensated) state of UPR mutants was revealed through larger and sustained eroGFP deflections than wild-type under stress, and could not have been described using the distal UPR-RFP reporter alone. Therefore measuring eroGFP oxidation changes provides information on drift from ER homeostasis, while measuring UPR activity provides information on compensation.

How can eroGFP become reduced during myriad ER stresses? Like any ER protein containing cysteines, eroGFP must be oxidized through dithiol-disulfide exchange reactions through specific protein-protein interactions mediated by oxidoreductases. These activities may become compromised during stress. Indeed, oxidation of Ero1p decreased when under-glycosylated. Additionally, as the vast majority of secretory proteins contain cysteines, their accumulation in unfolded form may saturate the ER's oxidative machinery due to futile cycling attempts to form disulfide bonds (Haynes et al., 2004). This effect may occur in some cells during overexpression of the cysteine-containing protein, CPY and its misfolded variants. Interestingly, overexpression of a cysteine-less CPY* variant still caused eroGFP deflection in some cells (although to a

lesser degree than a variant containing one cysteine) indicating that a saturation mechanism cannot be the sole explanation for eroGFP changes.

Because we also observed reduction of pre-existing eroGFP, its disulfide bond must be labile and may become reduced by enzymatic activities or ER permeable reductants such as glutathione. PDI has been shown to have reductase activity, facilitating removal of unfolded proteins from the ER (Tsai et al., 2001). More recently a mammalian ER reductase, ERdj5, was described (Ushioda et al., 2008). Interestingly, a conserved disulfide in the ER-luminal domain of the UPR sensor ATF6 is reduced during ER stress, allowing ATF6 to traffic to the Golgi for processing and activation (Nadanaka et al., 2006). When protein oxidation becomes generally compromised during ER stress as we have shown, ATF6's labile disulfide bond may become reduced, raising the exciting prospect that ER homeostasis is maintained through sensing both redox state as well as unfolded proteins.

While we observed eroGFP co-localized with the ER (i.e. in reticular structures containing Sec61) during stresses we imposed, it is conceivable that dynamic remodeling of ER to terminal or salvage organelles may expose eroGFP to less oxidizing milieus, also contributing to its reduction.

Finally, eroGFP revealed unanticipated heterogeneities between individual cells in a number of our experiments. During inositol starvation, the eroGFP ratio rose in UPR-deficient mother cells, but not in daughters. We speculate that asymmetric segregation of

ER tubules containing under-oxidized proteins may occur under stress. This observation adds to reports that oxidatively damaged cytosolic and mitochondrial proteins are retained in mothers (Aguilaniu et al., 2003). The heterogeneity observed for CPY* expression—which could represent a stress to which cells can successfully adapt—also suggests that some individuals escape homeostatic control. Such differences may account for different cell fate outcomes in metazoans, which eliminate highly stressed cells through apoptosis. The metazoan UPR can alternatively transmit survival or apoptotic signals though it is unclear how the UPR separates and relegates some cells to an apoptotic fate, while allowing others to successfully adapt. The tools and concepts we have developed may be applicable to the study and understanding of such questions.

EXPERIMENTAL PROCEDURES

Plasmid Construction

See Supplemental Experimental Procedures

Determination of redox midpoint potentials

1μM recombinant eroGFP was diluted into buffer containing 75mM HEPES (pH 7.0), 140mM NaCl, 1mM EDTA, and 10mM total lipoic acid in an anaerobic glove box for one hour at 21.5 C. The lipoic acid consisted of a mixture of oxidized and reduced species that ranged from 10mM reduced to 10mM oxidized in 1mM increments. Fluorescence spectra were measured on a Spectramax M2 microplate reader (Molecular Devices) with excitation wavelengths from 350nm to 500nm with a 2nm step and emission wavelength at 520nm. Midpoint determination was performed as described (Hanson et al., 2004) and plots were made with Origin software.

Media and strains

Strains were from the Yeast Consortium Deletion Library (Giaever et al., 2002) or from the DAmP library (Schuldiner et al., 2005) (Table S1). Sec61-mCherry yeast were a gift from Bernales, S and Walter, P (Bernales et al., 2006). Cultures were grown in SD or SGal complete media supplemented with myo-inositol (Sigma) at 100μg/ml. For flow cytometry time courses, DTT (Roche) was 2mM and Tm (CalBiochem) was 1ug/ml. For inositol starvation experiments, cells were washed twice with pre-warmed sterile water and resuspended into pre-warmed SD complete media lacking inositol. Cell surface Cy5 labeling was previously described (Chin et al., 2008). All CPY* experiments used SD-leucine+inositol media to maintain plasmid selection.

Light Microscopy

Exponentially growing cells were imaged with a Yokogawa CSU-22 spinning disc confocal on a NikonTE2000 microscope. The images were recorded with a 100x / 1.4 NA Plan Apo objective on a Cascade II EMCCD with a sample magnification of 60nm/pixel. eroGFP was excited with the 488nm Ar-ion laser line and Sec61-mCherry was excited with the 568 nm Ar-Kr laser line.

Micro-Manager and ImageJ were used to control the microscope and process the images.

Northern Blot Analysis

Northern blots were previously described (Papa et al., 2003).

Flow Cytometry Analysis

Fluorescence was measured with a flow cytometer (LSRII, BD) with a setup described in Figure 2B. Cell delivery to the cytometer was automated as described (Chin et al., 2008). Data analysis was performed using MATLAB (The Mathworks). eroGFP and UPR-RFP values for each mutant were normalized to wild-type and corrected based on their baseline values (data not shown). The first derivative of UPR-RFP at time t, $\frac{d(UPR-RFP)}{dt} = \frac{UPR-RFP(t+\Delta t)-UPR-RFP(\Delta t)}{\Delta t}$ was calculated as the difference in UPR-RFP form two consecutive time points t and t+Δt, divided by the time interval, Δt = 7 minutes.

Determination of oxidation state of eroGFP and Ero1p

Oxidation state determination was performed as described (Frand and Kaiser, 1999). See supplemental experimental procedures for details.

Immunoblots

Immunoblots were performed as described (Papa et al., 2003). See supplemental experimental procedures for details.

ACKNOWLEDGEMENTS

We thank S. James Remington for providing the roGFP2 construct, Victor Chubukov for assistance with automated flow cytometry and for data analysis software, Maya Schuldiner, Martin Jonikas, Erin Quan, Davis Ng, and Antony Cooper for reagents, and Kurt Thorn for imaging assistance. We thank Mark Hochstrasser, Scott Oakes, Chris Patil, Jonathan Weissman, and members of the Papa lab for comments on the manuscript. Microscopy images were collected at the Nikon Imaging Center at UCSF/QB3. F.R.P. is funded through an NIH Director's New Innovator Award (DP2OD001925), a Burroughs Wellcome Fund Career Award in Biomedical Sciences, a Culpeper Scholarship from the Partnership for Cures, and startup awards from the Sandler Foundation and the Hillblom Foundation. P.I.M. is supported through a National Science Foundation Pre-doctoral Fellowship.

REFERENCES

Aguilaniu, H., Gustafsson, L., Rigoulet, M., and Nystrom, T. (2003). Asymmetric inheritance of oxidatively damaged proteins during cytokinesis. Science *299*, 1751-1753.

Back, S.H., Lee, K., Vink, E., and Kaufman, R.J. (2006). Cytoplasmic IRE1alpha-mediated XBP1 mRNA splicing in the absence of nuclear processing and endoplasmic reticulum stress. J Biol Chem *281*, 18691-18706.

Bays, N.W., Gardner, R.G., Seelig, L.P., Joazeiro, C.A., and Hampton, R.Y. (2001). Hrd1p/Der3p is a membrane-anchored ubiquitin ligase required for ER-associated degradation. Nat Cell Biol *3*, 24-29.

Bernales, S., McDonald, K.L., and Walter, P. (2006). Autophagy counterbalances endoplasmic reticulum expansion during the unfolded protein response. PLoS Biol *4*, e423.

Brodsky, J.L., and McCracken, A.A. (1999). ER protein quality control and proteasome-mediated protein degradation. Seminars in Cell and Developmental Biology *10*, 507-513.

Chin, C.S., Chubukov, V., Jolly, E.R., DeRisi, J., and Li, H. (2008). Dynamics and design principles of a basic regulatory architecture controlling metabolic pathways. PLoS Biol *6*, e146.

Cox, J.S., Chapman, R.E., and Walter, P. (1997). The unfolded protein response coordinates the production of endoplasmic reticulum protein and endoplasmic reticulum membrane. Mol Biol Cell *8*, 1805-1814.

Cox, J.S., Shamu, C.E., and Walter, P. (1993). Transcriptional induction of genes encoding endoplasmic reticulum resident proteins requires a transmembrane protein kinase. Cell *73*, 1197-1206.

Cox, J.S., and Walter, P. (1996). A novel mechanism for regulating activity of a transcription factor that controls the unfolded protein response. Cell *87*, 391-404.

Credle, J.J., Finer-Moore, J.S., Papa, F.R., Stroud, R.M., and Walter, P. (2005). On the mechanism of sensing unfolded protein in the endoplasmic reticulum. Proc Natl Acad Sci U S A *102*, 18773-18784.

Deak, P.M., and Wolf, D.H. (2001). Membrane topology and function of Der3/Hrd1p as a ubiquitin-protein ligase (E3) involved in endoplasmic reticulum degradation. J Biol Chem *276*, 10663-10669.

Dooley, C.T., Dore, T.M., Hanson, G.T., Jackson, W.C., Remington, S.J., and Tsien, R.Y. (2004). Imaging dynamic redox changes in mammalian cells with green fluorescent protein indicators. J Biol Chem *279*, 22284-22293.

Frand, A.R., and Kaiser, C.A. (1998). The ERO1 gene of yeast is required for oxidation of protein dithiols in the endoplasmic reticulum. Mol Cell *1*, 161-170.

Frand, A.R., and Kaiser, C.A. (1999). Ero1p oxidizes protein disulfide isomerase in a pathway for disulfide bond formation in the endoplasmic reticulum. Mol Cell *4*, 469-477.

Friedlander, R., Jarosch, E., Urban, J., Volkwein, C., and Sommer, T. (2000). A regulatory link between ER-associated protein degradation and the unfolded-protein response. Nat Cell Biol *2*, 379-384.

Giaever, G., Chu, A.M., Ni, L., Connelly, C., Riles, L., Veronneau, S., Dow, S., Lucau-Danila, A., Anderson, K., Andre, B., *et al.* (2002). Functional profiling of the Saccharomyces cerevisiae genome. Nature *418*, 387-391.

Hanson, G.T., Aggeler, R., Oglesbee, D., Cannon, M., Capaldi, R.A., Tsien, R.Y., and Remington, S.J. (2004). Investigating mitochondrial redox potential with redox-sensitive green fluorescent protein indicators. J Biol Chem *279*, 13044-13053.

Harding, H.P., Calfon, M., Urano, F., Novoa, I., and Ron, D. (2002). Transcriptional and translational control in the Mammalian unfolded protein response. Annu Rev Cell Dev Biol *18*, 575-599.

Haynes, C.M., Titus, E.A., and Cooper, A.A. (2004). Degradation of misfolded proteins prevents ER-derived oxidative stress and cell death. Mol Cell *15*, 767-776.

Hwang, C., Sinskey, A.J., and Lodish, H.F. (1992). Oxidized redox state of glutathione in the endoplasmic reticulum. Science *257*, 1496-1502.

Iwawaki, T., Akai, R., Kohno, K., and Miura, M. (2004). A transgenic mouse model for monitoring endoplasmic reticulum stress. Nat Med *10*, 98-102.

Kawahara, T., Yanagi, H., Yura, T., and Mori, K. (1997). Endoplasmic reticulum stress-induced mRNA splicing permits synthesis of transcription factor Hac1p/Ern4p that activates the unfolded protein response. Mol Biol Cell *8*, 1845-1862.

Kimata, Y., Ishiwata-Kimata, Y., Ito, T., Hirata, A., Suzuki, T., Oikawa, D., Takeuchi, M., and Kohno, K. (2007). Two regulatory steps of ER-stress sensor Ire1 involving its cluster formation and interaction with unfolded proteins. J Cell Biol *179*, 75-86.

Kostova, Z., and Wolf, D.H. (2005). Importance of carbohydrate positioning in the recognition of mutated CPY for ER-associated degradation. J Cell Sci *118*, 1485-1492.

Meusser, B., Hirsch, C., Jarosch, E., and Sommer, T. (2005). ERAD: the long road to destruction. Nat Cell Biol *7*, 766-772.

Nadanaka, S., Okada, T., Yoshida, H., and Mori, K. (2006). A Role of Disulfide Bridges Formed in the Lumenal Domain of ATF6 in Sensing Endoplasmic Reticulum Stress. Mol Cell Biol.

Nikawa, J., and Yamashita, S. (1992). IRE1 encodes a putative protein kinase containing a membrane-spanning domain and is required for inositol phototrophy in Saccharomyces cerevisiae. Mol Microbiol *6*, 1441-1446.

Papa, F.R., Zhang, C., Shokat, K., and Walter, P. (2003). Bypassing a kinase activity with an ATP-competitive drug. Science *302*, 1533-1537.

Pollard, M.G., Travers, K.J., and Weissman, J.S. (1998). Ero1p: a novel and ubiquitous protein with an essential role in oxidative protein folding in the endoplasmic reticulum. Mol Cell *1*, 171-182.

Romisch, K. (2005). Endoplasmic reticulum-associated degradation. Annu Rev Cell Dev Biol *21*, 435-456.

Ron, D., and Walter, P. (2007). Signal integration in the endoplasmic reticulum unfolded protein response. Nat Rev Mol Cell Biol *8*, 519-529.

Schuldiner, M., Collins, S.R., Thompson, N.J., Denic, V., Bhamidipati, A., Punna, T., Ihmels, J., Andrews, B., Boone, C., Greenblatt, J.F., *et al.* (2005). Exploration of the function and organization of the yeast early secretory pathway through an epistatic miniarray profile. Cell *123*, 507-519.

Sevier, C.S., and Kaiser, C.A. (2002). Formation and transfer of disulphide bonds in living cells. Nat Rev Mol Cell Biol *3*, 836-847.

Spear, E.D., and Ng, D.T. (2005). Single, context-specific glycans can target misfolded glycoproteins for ER-associated degradation. J Cell Biol *169*, 73-82.

Travers, K.J., Patil, C.K., Wodicka, L., Lockhart, D.J., Weissman, J.S., and Walter, P. (2000). Functional and genomic analyses reveal an essential coordination between the unfolded protein response and ER-associated degradation. Cell *101*, 249-258.

Tsai, B., Rodighiero, C., Lencer, W.I., and Rapoport, T.A. (2001). Protein disulfide isomerase acts as a redox-dependent chaperone to unfold cholera toxin. Cell *104*, 937-948.

Tu, B.P., and Weissman, J.S. (2004). Oxidative protein folding in eukaryotes: mechanisms and consequences. J Cell Biol *164*, 341-346.

Ushioda, R., Hoseki, J., Araki, K., Jansen, G., Thomas, D.Y., and Nagata, K. (2008). ERdj5 is required as a disulfide reductase for degradation of misfolded proteins in the ER. Science *321*, 569-572.

van Anken, E., and Braakman, I. (2005). Versatility of the endoplasmic reticulum protein folding factory. Crit Rev Biochem Mol Biol *40*, 191-228.

Zhang, K., and Kaufman, R.J. (2006). The unfolded protein response: a stress signaling pathway critical for health and disease. Neurology *66*, S102-109.

Zhou, J., Liu, C.Y., Back, S.H., Clark, R.L., Peisach, D., Xu, Z., and Kaufman, R.J. (2006). The crystal structure of human IRE1 luminal domain reveals a conserved dimerization interface required for activation of the unfolded protein response. Proc Natl Acad Sci U S A *103*, 14343-14348.

FIGURE LEGENDS

Figure 1. Characterization of an ER-localized redox-sensitive GFP (eroGFP)

(A) Fluorescence excitation spectra of recombinant fully reduced (red triangles) and oxidized (blue circles) eroGFP. Emission was measured at 520 nm. (B) Excitation spectra of recombinant eroGFP through titration of reduced to oxidized lipoic acid (ratios in inset—total 10 mM). (C) Fraction-reduced eroGFP—data from (B)—as a function of ratios of reduced to oxidized lipoic acid expressed as redox potential values. (D) Representative confocal image of cells expressing eroGFP and Sec61-mCherry. (E) eroGFP ratio (defined as the ratio of fluorescence from excitation at 488 nm vs. 405 nm expressed in $\log_2$ space and normalized to the untreated case—UT) in cells treated with the indicated concentration of DTT or H_2O_2. Data represent means +/- SD from three independent experiments. (F) Northern blot for *HAC1* mRNA in cells expressing vector or eroGFP, treated with or without tunicamycin, Tm, (1μg/ml) for 1 hr. $HAC1^{u}$ denotes unspliced and $HAC1^{i}$ spliced mRNA respectively. An asterisk signifies the *HAC1* 5' exon.

Figure 2. Dynamic monitoring of ER redox status and UPR activity during pharmacologically-induced ER stress

(A) Schematic of composite reporter gene. (B) Schematic showing configuration of flow cytometer laser lines and filters. A syringe-pump periodically (~10 minutes) injected 25μl of sample from cultures growing in bioreactors into a flow cytometer. (C-F) Time courses of eroGFP ratio or UPR-RFP metric histograms in wild-type cells during treatment with DTT (2mM) or Tm (1μg/ml). The eroGFP ratio and UPR-RFP metrics are normalized to

wild-type unstressed cells. Color represents percentage of cells at a given metric value and time point. Dashed gray line signifies time of DTT or Tm addition. (G) Non-reducing SDS-PAGE and immunoblot (anti-GFP) of AMS-treated protein extracts from untreated cells (lane 1), cells treated with 10mM DTT for 30 min (lane 2), or 2μg/ml Tm for 3 hrs (lane 3).

Figure 3. Dynamic monitoring of ER redox status and UPR activity in ER oxidative folding, quality control, and UPR signaling mutants during pharmacologically-induced ER stress

(A-L) Median eroGFP ratio (green circles) and UPR-RFP metric (red x-marks) during treatment with DTT (2mM) or Tm (1μg/ml) for wild-type and indicated mutants. Values are normalized to wild-type unstressed cells. Dashed gray line signifies time at which stressor was added.

Figure 4. Dynamic monitoring of ER redox status and UPR activity during inositol starvation

(A-F) Time courses of eroGFP ratio or UPR-RFP metric histograms in wild-type, *ire1*Δ, or *hac1*Δ cells starved for inositol at time, t=0. (G) Growth curves for the time courses of (A-F). (H-J) Snapshots of *hac1*Δ cell populations for eroGFP ratio vs. Cy5 signal at three time points. Mothers (m) have a high Cy5 signal ($\log_2$ Cy5 > 10.5) while daughters (d) have a low Cy5 signal ($\log_2$ Cy5 < 10.5). Time courses of eroGFP histograms for *hac1Δ* mothers (K) and daughters (L). The three time points of (H-J) are indicated in (L). Color represents percentage of cells at a given metric value and time point.

Figure 5. Dynamic monitoring of ER redox status and UPR activity during overexpression of secretory proteins

(A-R) Time courses of eroGFP ratio or UPR-RFP metric histograms in wild-type (WT) or *hrd1*Δ cells expressing CPY, CPY*, CPY*-0000, CPY*-1cys, or CPY*-Cysless under control of the copper-inducible CUP1 promoter. Color represents percentage of cells at a given metric value and time point. The dashed gray line signifies time of $CuSO_4$ (200μM or 500μM) addition.

Figure 6. Analysis of ER oxidative folding, quality control, and UPR signaling mutants under stress

(A, B) Median trajectories of wild-type or mutant cells (treated with DTT or Tm) through UPR-RFP metric and eroGFP ratio two-dimensional space. The trajectories begin at the last data point before stress addition, and conclude when the time course ends (signified by the arrow). Consecutive white circles within each trajectory line are separated by 30 minutes. Color denotes each mutant. (C, D) Growth curves for wild-type cells treated with DTT (2mM) or Tm (1μg/ml). (E, F) The first derivative of median UPR-RFP with respect to time, d(UPR-RFP)/dt, vs. time for wild-type and mutants treated with DTT or Tm. (G) Integrated eroGFP ratios over the time courses for each mutant normalized to wild-type and represented as heat maps ranging from blue (negative values) to yellow (positive values). Data for (A-G) are from Figure 3. (H) Histogram of *ire1*Δ cells expressing eroGFP, reconstituted with a 1NM-PP1-sensitized IRE1 allele, and treated with DMSO (black line), 30μM 1NM-PP1 (green line), DMSO and 1μg/ml Tm (red line), and 30μM 1NM-PP1 and 1μg/ml Tm (yellow line). Inset shows median eroGFP ratio change for each treatment. Error bars are SD of three independent experiments.

Figure 7. Conceptual model of ER stress and UPR-mediated compensation

ER oxidative folding stress, as measured by increased eroGFP ratios, can be provoked by various perturbations to ER protein folding, modification, and quality control systems. In addition, increased protein secretion and nutrient (inositol) deprivation cause ER oxidative folding stress in some cells. UPR activity, as measured by UPR-RFP, provides information on the strength of compensatory mechanisms. Triangles indicate that each variable is a continuum. Four cell states are depicted at extremes of each continuum, with positions of mutants indicated across the two variables. See text for further details.

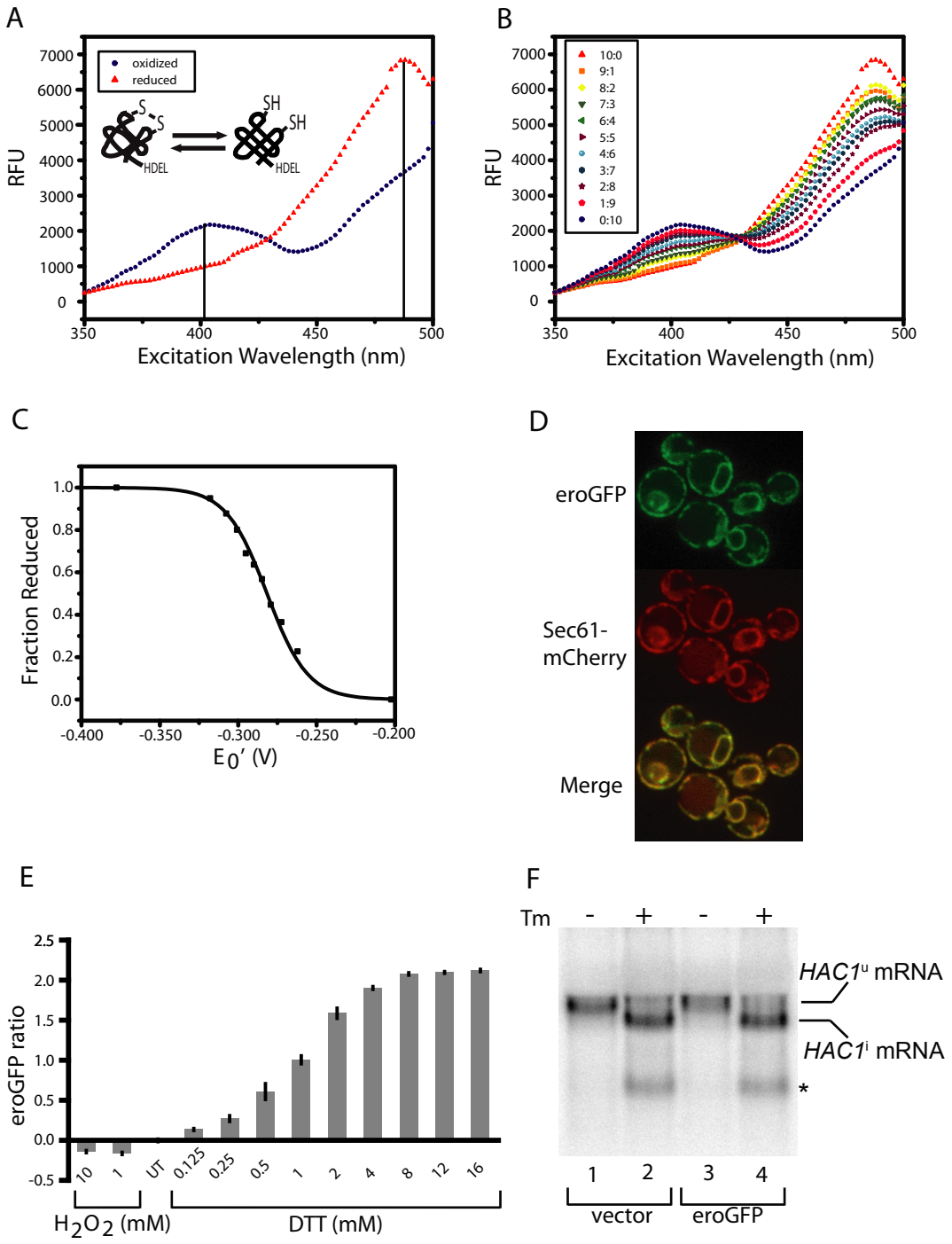

Merksamer et al Figure 1

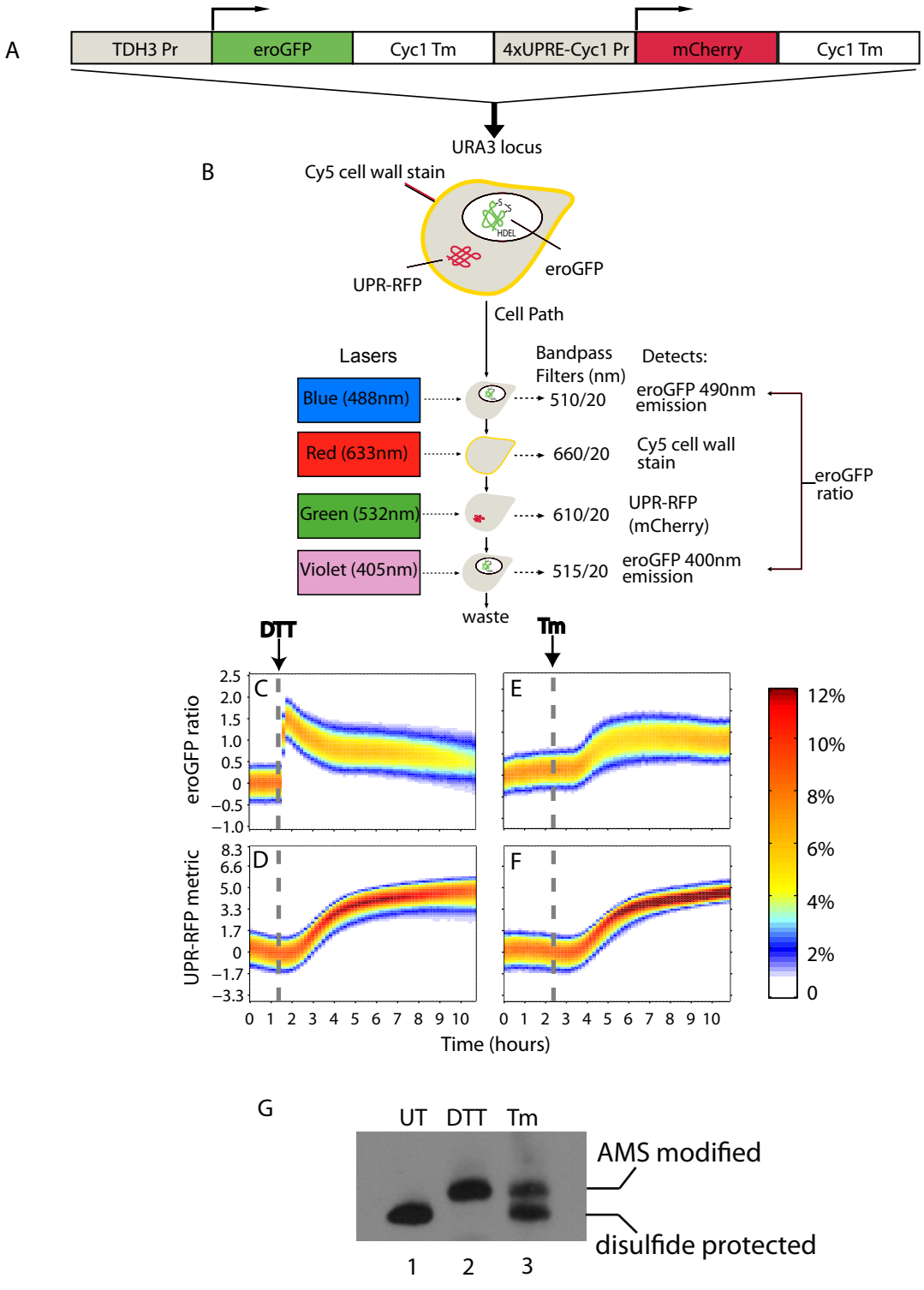

Merksamer et al Figure 2

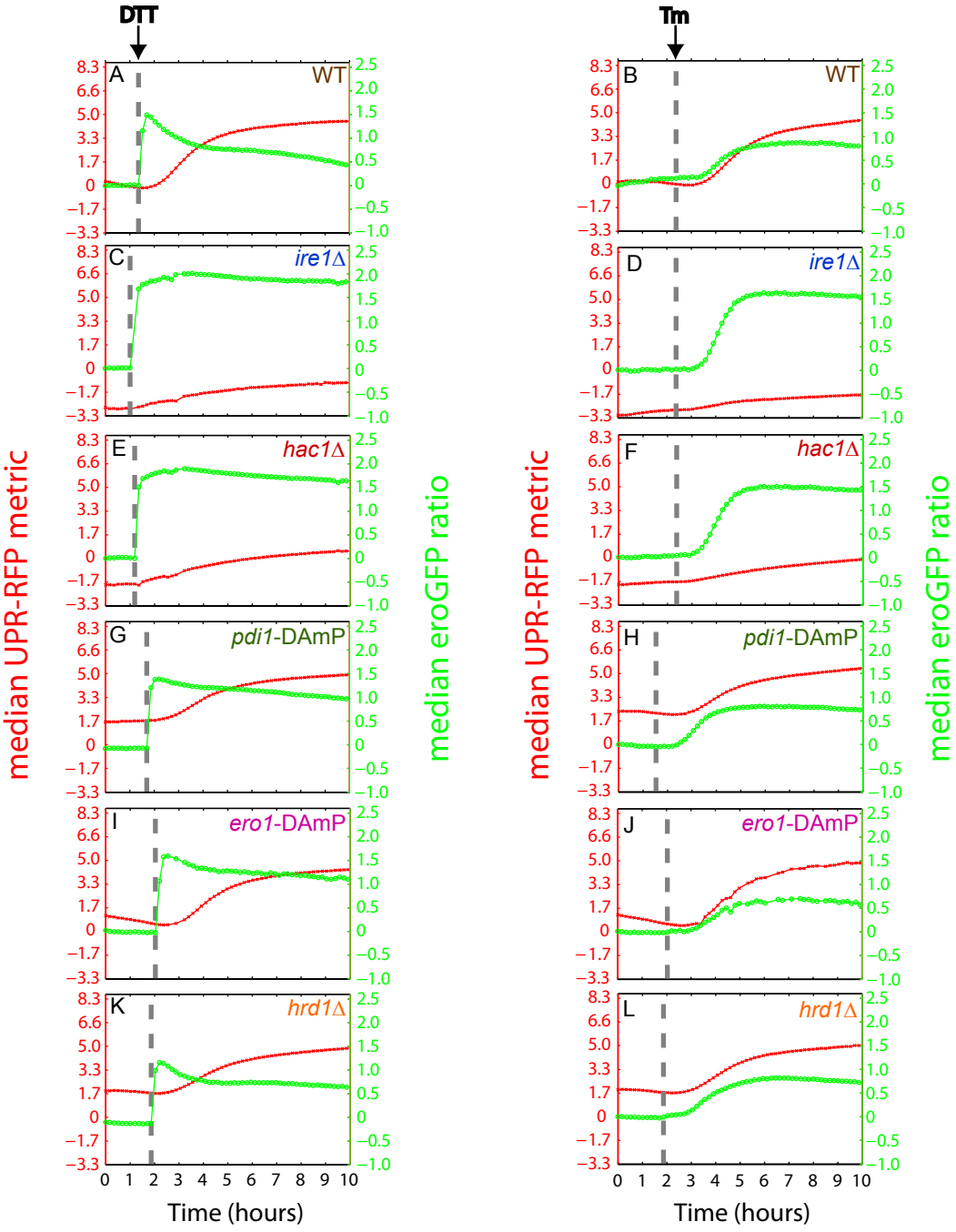

Merksamer et al Figure 3

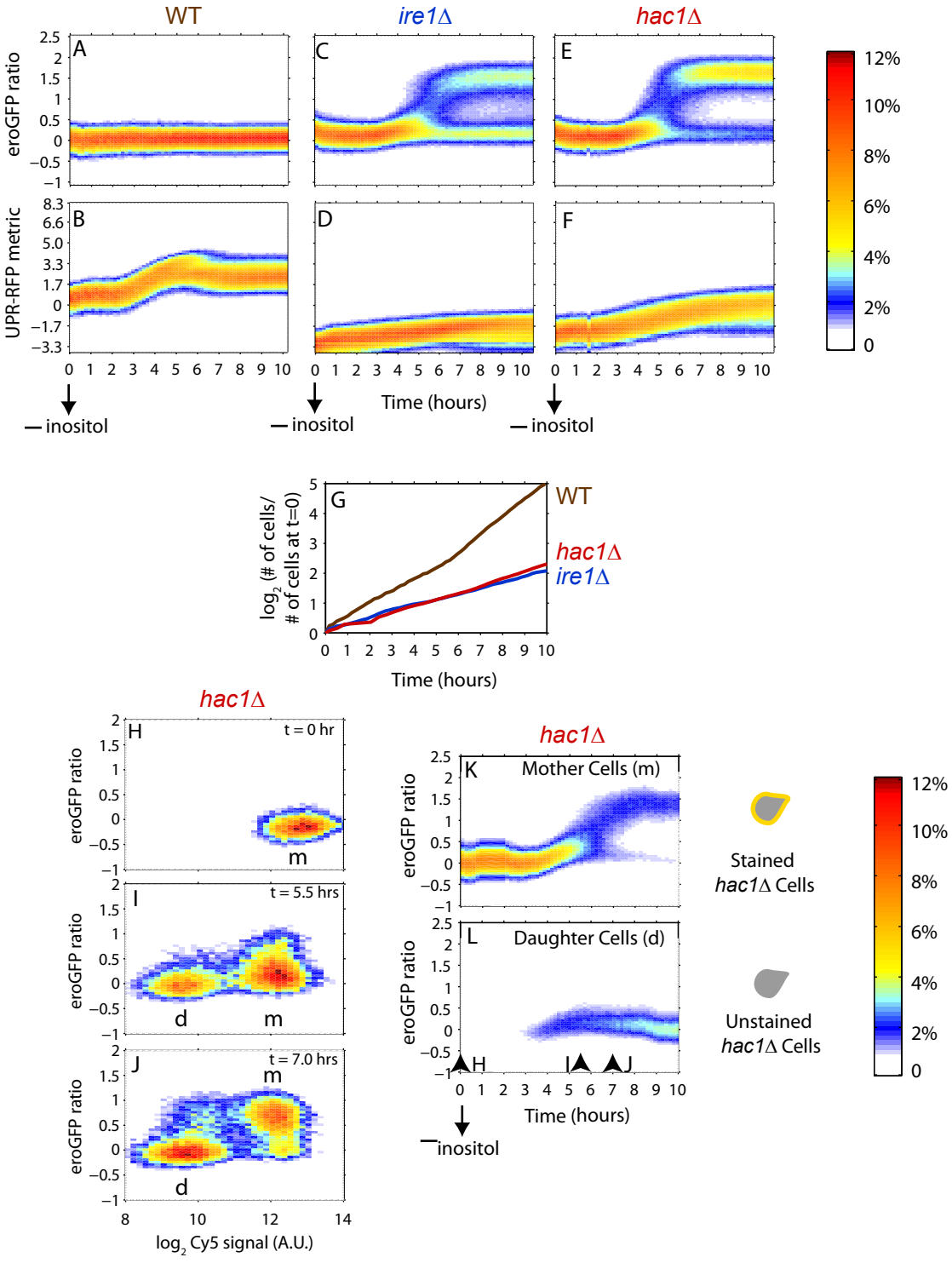

Merksamer et al Figure 4

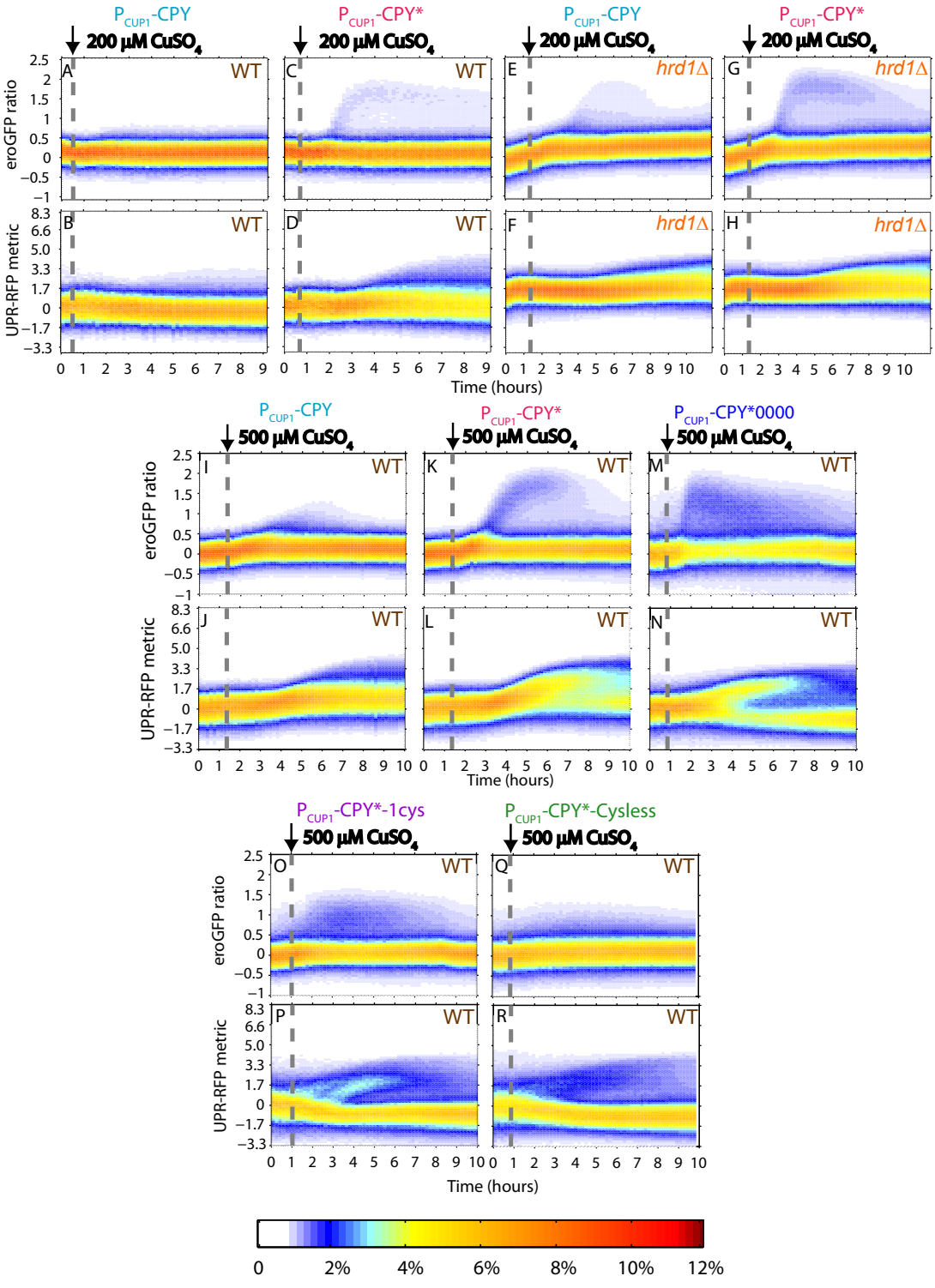

Merksamer et al Figure 5

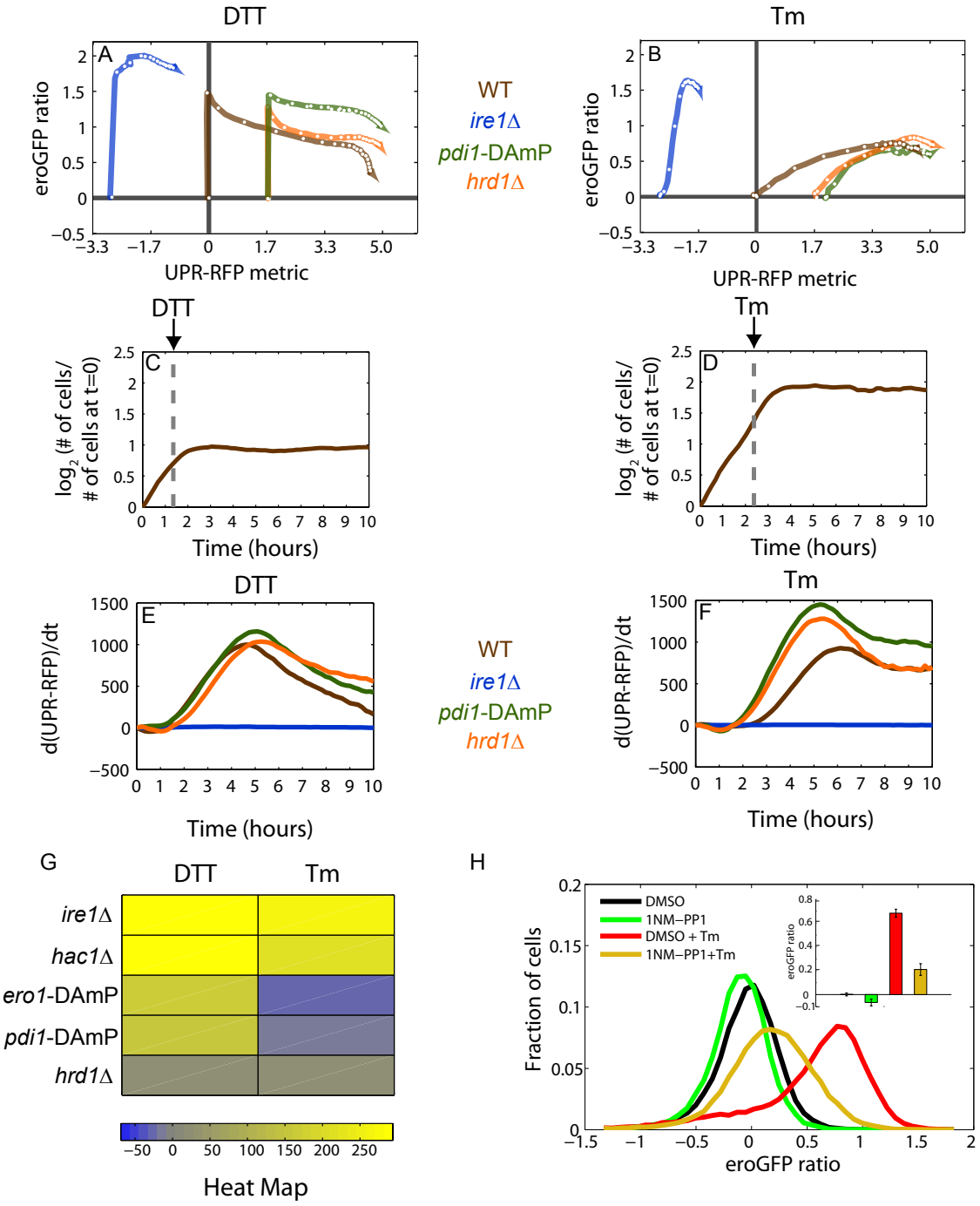

Merksamer et al Figure 6

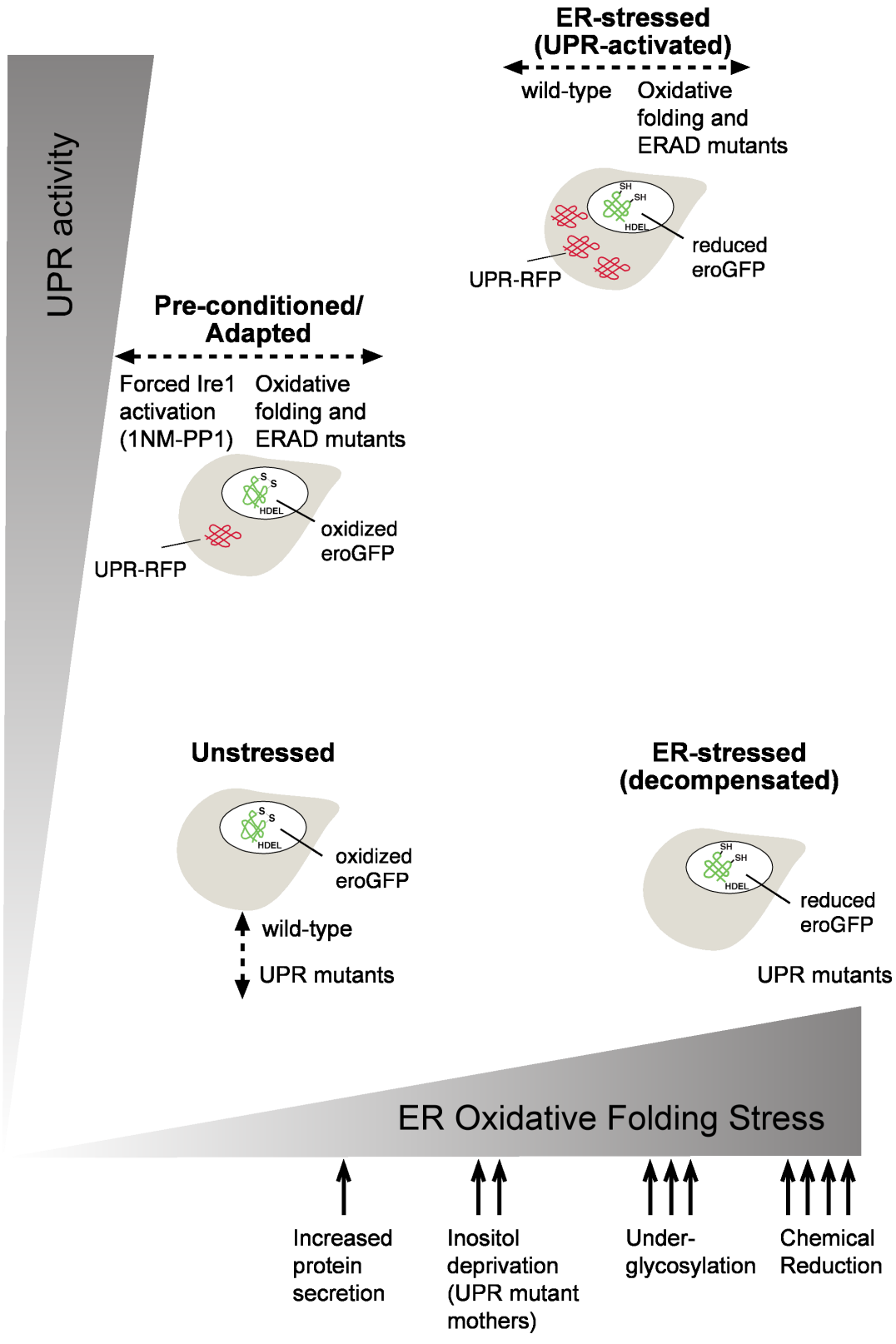

Merksamer et al Figure 7

***Cell*, Volume 135**

Supplemental Data

Real-Time Redox Measurements during Endoplasmic Reticulum Stress Reveal Interlinked Protein Folding Functions

Philip I. Merksamer, Ala Trusina, and Feroz R. Papa

SUPPLEMENTARY EXPERIMENTAL PROCEDURES

Plasmid Construction

The eroGFP gene was generated by ligating the first 135 nucleotides of the *KAR2* ORF to the N-terminus of the ro2GFP ORF (Dooley et al., 2004; Hanson et al., 2004) using Nhe1 and BamH1 restriction sites, and by fusing an HDEL retention sequence to its C-terminus using overlap extension PCR. This gene was then positioned under control of the constitutive TDH3 promoter and the CYC1 terminator. This construct is on pPM28 [*CEN URA3 eroGFP*] used for light microscopy and pPM44 [*integrating NAT eroGFP*] used for flow cytometry in Figure 1. Recombinant eroGFP was made by ligating ro2GFP-HDEL into the pRSETb bacterial expression vector (Invitrogen) (pPM35) using BamH1 and HindIII sites. pPM57 containing eroGFP(C147S) was made by QuickChange site-directed mutagenesis (Stratagene) of pPM44. GAL-eroGFP (pPM60) was made by replacing the TDH3 promoter in pPM44 with the GAL1 promoter using *in vivo* DNA gap repair (Papa et al., 1999). UPR-RFP (pPM47) was made by fusing a tandem 4xUPRE containing *CYC1* promoter upstream of the coding sequence for mCherry by overlap extension PCR. 4xUPRE-Cyc1pr and mCherry containing plasmids were gifts from JS Weissman. pPM48

[*integrating NAT eroGFP-UPR-RFP*] and pPM56 [*integrating KAN eroGFP-UPR-RFP*] were made by overlap extension PCR. The Ero1-3HA construct was a gift from J.S. Weissman (Pollard et al., 1998). CPY-3HA and CPY*-3HA constructs were derived from plasmids from J.S. Weissman (Bhamidipati et al., 2005) and made by fusing the CUP1 promoter to the coding sequences of pcr1 and pcr1-1 (encoding the CPY or CPY* proteins respectively) on *2μ* shuttle *LEU2* vectors using *in vivo* DNA gap repair—pPM17 [*2μ LEU2 CPY-HA*] and pPM18 [*2μ LEU2 CPY*-HA*]. The non-glycosylated CPY* construct—CPY*0000—(pPM65) was derived from a CPY*0000 containing plasmid from D.T. Ng (Spear and Ng, 2005) and placed under the CUP1 promoter as described above. The single cysteine (pPM66) and cysteine-less CPY* (pPM67) constructs were derived from a CUP1-CPY* construct containing three cysteines from A.A. Cooper (Haynes et al., 2004) and modified by QuickChange site-directed mutagenesis (Stratagene) and cloned into *2μ* shuttle *LEU2* vectors using SacI and XhoI restriction sites. The single cysteine in pPM66 is located at position 167. The constitutive-ON, kinase-dead, 1NM-PP1-sensitized Ire1 plasmid was previously described (Papa et al., 2003). All plasmids were sequenced on both DNA strands.

Pulse Chase of eroGFP

Wild-type cells expressing GAL-eroGFP were grown to mid-log phase in SGal media at which point 2% glucose was added. An equal volume of galactose was added to the control group. After 2.5 hrs cells were washed two times in 1 ml of either SD or SGal without amino acids and resuspended in 150 μl of SD or SGal without amino acids. Cells were pulsed with 20μCi of Tran^{35}S-label (MP Biomedicals) for 15 minutes and chased

with SD or SGal supplemented with 10mM methionine for 5 min. Cells were lysed in Triton lysis buffer (150 mM NaCl, 50 mM HEPES pH 7.5, 5mM EDTA, and 1% Triton-X100) with glass bead vortexing. eroGFP was immunoprecipitated with 8 µg/ml of anti-GFP (Invitrogen/Molecular Probes) and anti-rabbit magnetic beads (Invitrogen) following the manufacture's protocol, with the exception that we only used one instead of the three recommended washes in 5% Normal Goat Serum (NGS) 1%Triton, 3% BSA wash buffer. Equal amounts of supernatant recovered from magnetic beads were loaded in two SDS-PAGE protein gels: one was analyzed by immunoblotting and the other was exposed to Kodak autoradiography film for 5 days after being fixed in 65% Isopropanol, 10% Acetic acid, 25 % water, incubated in Enhance solution (Amersham) for 30 min, and dried at 55^{o}C for 2 hours.

Determination of the Oxidation State of eroGFP and Ero1p

Oxidation state determination was performed as previously described (Frand and Kaiser, 1999). In brief, mid-log phase growing yeast cultures were harvested by centrifugation and resuspended in 15% TCA to precipitate proteins and prevent disulfide exchange. Vortexing with glass beads was used to disrupt the cell wall and membranes. Protein pellets were washed with acetone and were solubilized in 50µl of non-reducing sample buffer containing 80mM Tris-HCl (pH 6.8), 2% SDS, 1mM PMSF, and bromophenol blue. This buffer contained 25mM 4-acetamido-4′-maleimidylstilbene-2,2′-disulfonic acid (AMS, Molecular Probes) when indicated. For analysis of Ero1p-3HA this buffer also contained 6M urea. Samples were incubated on ice for 15 minutes, at 37^{o}C for 10 minutes (for Ero1p only), and boiled for 5 minutes. To deglycosylate Ero1p-3HA, samples were diluted 4-fold into 50 mM sodium citrate (pH 5.5) containing 5 mU of

Endoglycosidase H (Roche Diagnostics) and incubated at 37°C for 2.5 hr. Samples were resolved by non-reducing SDS-PAGE and immunoblotted with anti-GFP (1:1000, Invitrogen/Molecular Probes) or anti-HA (1:2000, Rockland) when indicated.

Immunoblots

Yeast protein extracts and immunoblots were performed as previously described (Leber et al., 2004). The following primary antibodies were used: anti-Pdi1p (1:2000, a gift from JS Weissman), anti-Pgk1p (1:5000, Invitrogen/Molecular Probes), anti-HA (1:2000, Rockland), and anti-CPY (1:5000, Abcam).

SUPPLEMENTARY REFERENCES

Bhamidipati, A., Denic, V., Quan, E.M., and Weissman, J.S. (2005). Exploration of the topological requirements of ERAD identifies Yos9p as a lectin sensor of misfolded glycoproteins in the ER lumen. Mol Cell *19*, 741-751.

Dooley, C.T., Dore, T.M., Hanson, G.T., Jackson, W.C., Remington, S.J., and Tsien, R.Y. (2004). Imaging dynamic redox changes in mammalian cells with green fluorescent protein indicators. J Biol Chem *279*, 22284-22293.

Frand, A.R., and Kaiser, C.A. (1999). Ero1p oxidizes protein disulfide isomerase in a pathway for disulfide bond formation in the endoplasmic reticulum. Mol Cell *4*, 469-477.

Hanson, G.T., Aggeler, R., Oglesbee, D., Cannon, M., Capaldi, R.A., Tsien, R.Y., and Remington, S.J. (2004). Investigating mitochondrial redox potential with redox-sensitive green fluorescent protein indicators. J Biol Chem *279*, 13044-13053.

Haynes, C.M., Titus, E.A., and Cooper, A.A. (2004). Degradation of misfolded proteins prevents ER-derived oxidative stress and cell death. Mol Cell *15*, 767-776.

Leber, J.H., Bernales, S., and Walter, P. (2004). IRE1-independent gain control of the unfolded protein response. PLoS Biol *2*, E235.

Papa, F.R., Amerik, A.Y., and Hochstrasser, M. (1999). Interaction of the Doa4 deubiquitinating enzyme with the yeast 26S proteasome. Mol Biol Cell *10*, 741-756.

Papa, F.R., Zhang, C., Shokat, K., and Walter, P. (2003). Bypassing a kinase activity with an ATP-competitive drug. Science *302*, 1533-1537.

Pollard, M.G., Travers, K.J., and Weissman, J.S. (1998). Ero1p: a novel and ubiquitous protein with an essential role in oxidative protein folding in the endoplasmic reticulum. Mol Cell *1*, 171-182.

Spear, E.D., and Ng, D.T. (2005). Single, context-specific glycans can target misfolded glycoproteins for ER-associated degradation. J Cell Biol *169*, 73-82.

Supplementary Figure S1

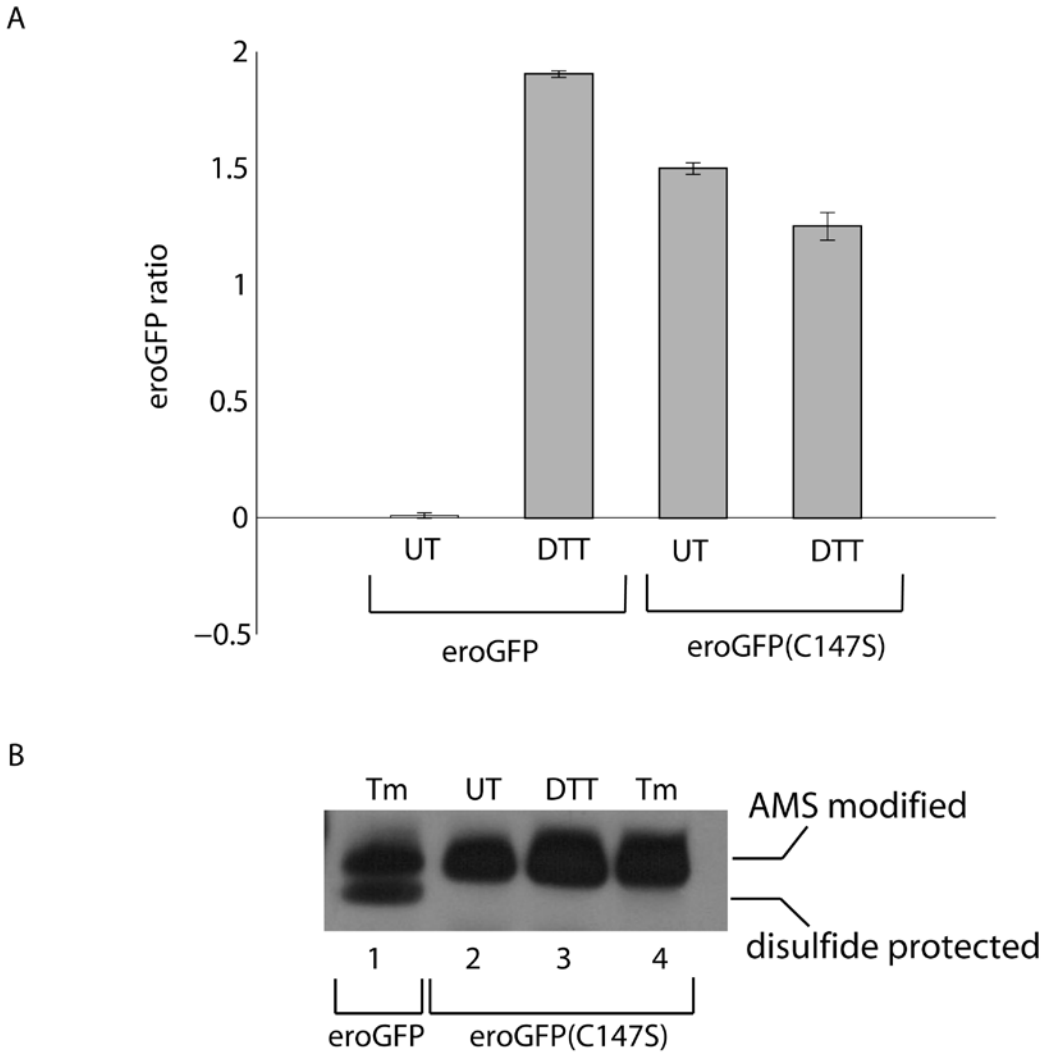

Figure S1. Oxidation changes in eroGFP require a disulfide pair

(A) Wild-type cells expressing eroGFP or eroGFP(C147S) were treated with 4mM DTT for 10 minutes and fluorescence measured by flow cytometery as described in Figure 1. UT indicates untreated. The eroGFP ratio was normalized to the untreated case for wild-type eroGFP. Data represent means +/- SD of three independent experiments. (B) Protein extracts from cells expressing eroGFP treated with 2μg/ml Tm for 3 hours (lane 1) and from cells expressing eroGFP(C147S) untreated (lane 2), treated with 10mM DTT for 10

minutes (lane 3), or treated with 2μg/ml Tm for 3 hours (lane 4). Extracts were treated with AMS, resolved on non-reducing SDS-PAGE, and immunoblotted against GFP.

Supplementary Figure S2

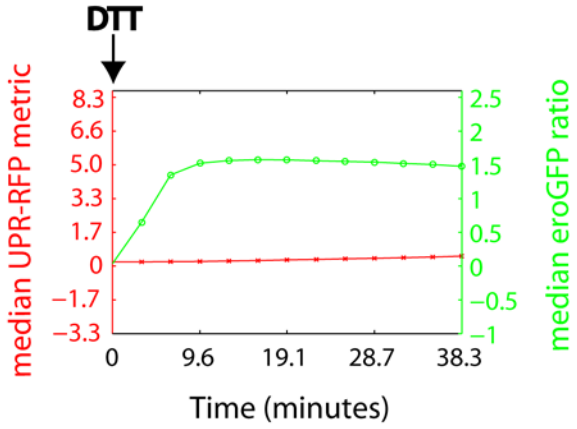

Figure S2. Finer resolution time course of ER redox status and UPR activity for early time points during inhibition of protein oxidation

Time-course of wild-type cells expressing the composite reporter treated with 2mM DTT at time, t=0. Automated sampling was performed every ~3 min for ~40 min. The median eroGFP ratio is represented by green circles and the median UPR-RFP metric is represented by red x-marks.

Supplementary Figure S3

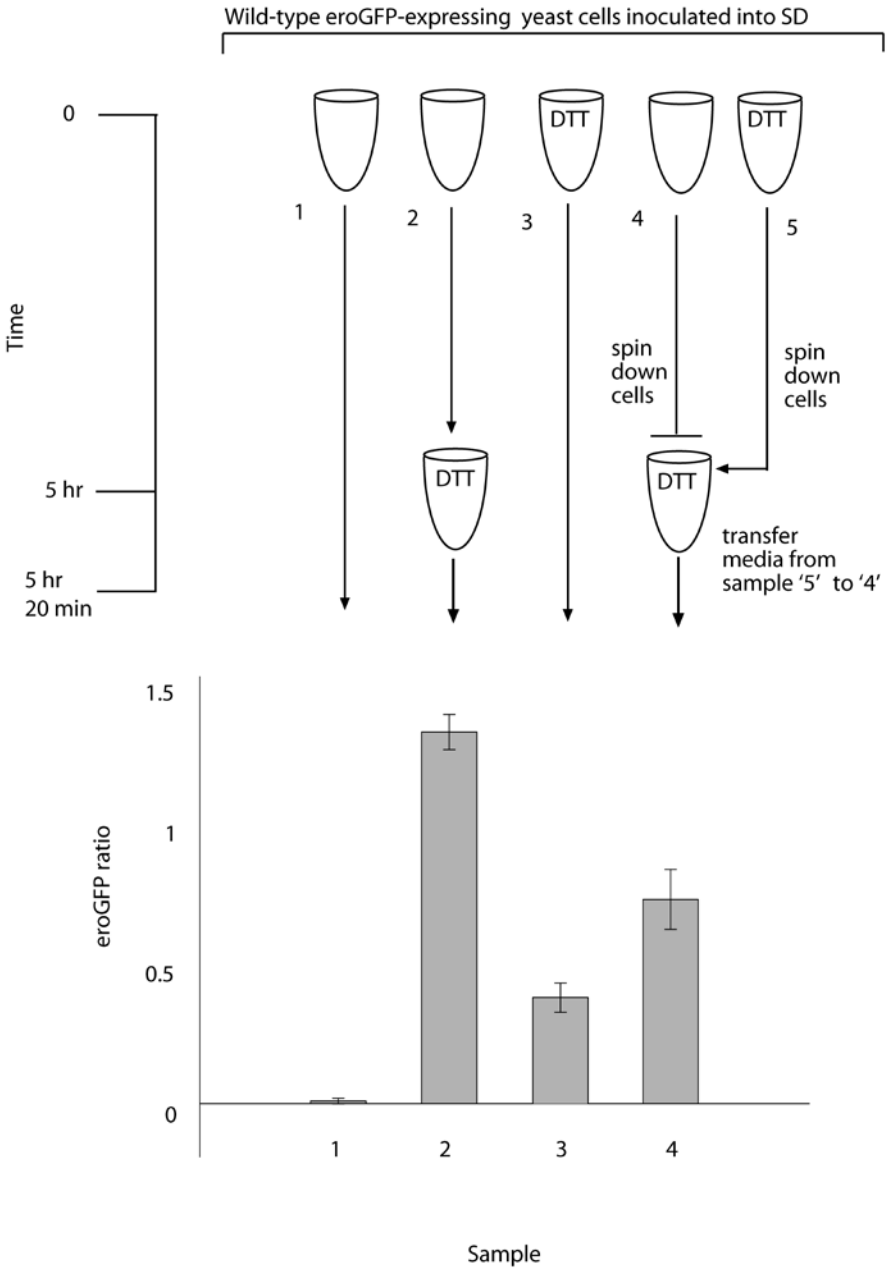

Figure S3. Adaptation to prolonged exposure to DTT

Upper panel: Schematic of experimental design. Wild-type cells expressing eroGFP were inoculated into SD media. At time t=0, samples 3 and 5 were treated with 2mM DTT. At t=5 hrs, sample 2 was treated with 2mM DTT. At t=5 hrs, samples 4 and 5 were centrifuged, media was discarded from sample 4, and cells were resuspended in the media from sample 5. At t=5 hrs 20min, the eroGFP ratio was measured. Lower panel: Bar graph of eroGFP ratio for samples 1-4. The eroGFP ratio was normalized to sample 1. Data represent means +/- SD of two independent experiments.

Supplementary Figure S4

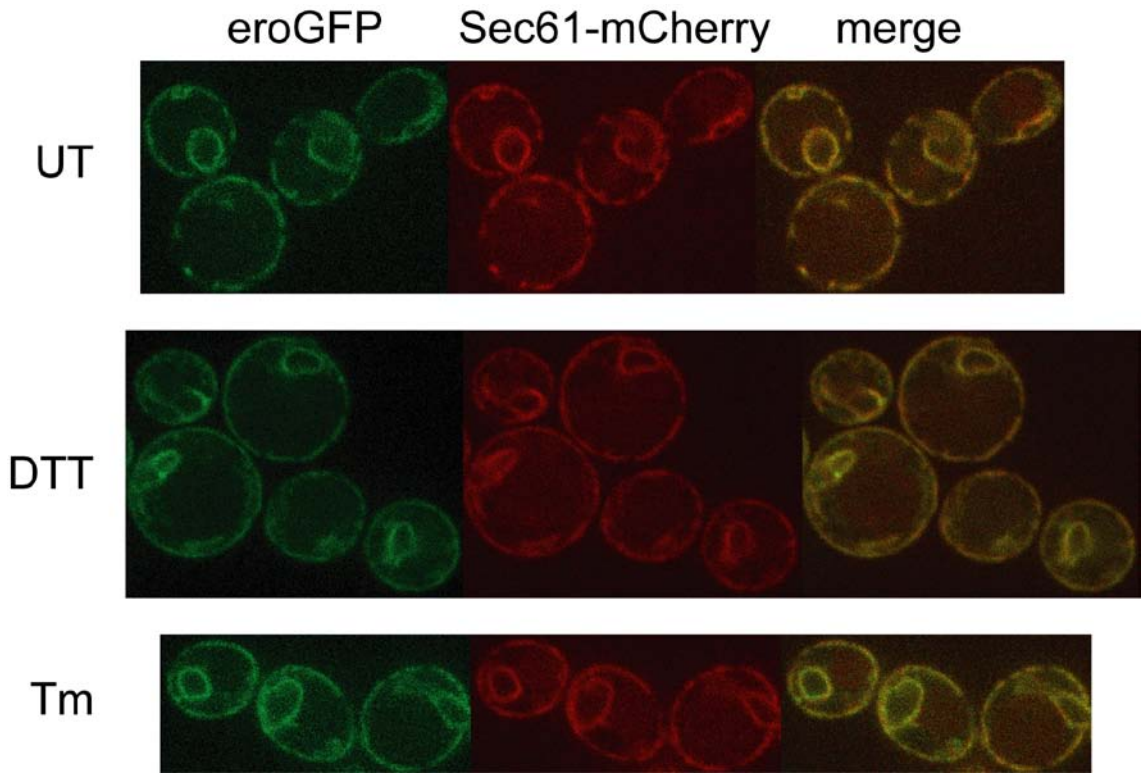

Figure S4. Localization of eroGFP during ER stress

Representative images of cells expressing eroGFP and Sec61-mCherry taken by spinning disk confocal microscopy. UT: untreated. DTT: 2mM DTT for 1 hour. Tm: 1μg/ml Tm for 2 hours.

Supplementary Figure S5

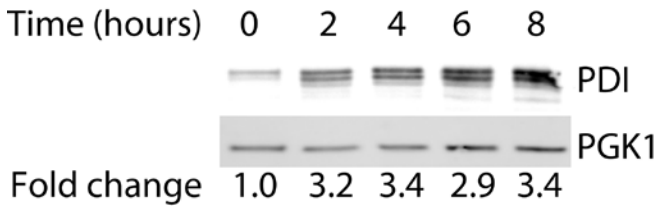

Figure S5. Induction of the ER chaperone and oxidoreductase, PDI, after ER stress

Wild-type cells expressing the composite reporter were treated with 2mM DTT for eight hours. Samples were taken every two hours for SDS-PAGE and immunoblotted against PDI and PGK1, a loading control.

Supplementary Figure S6

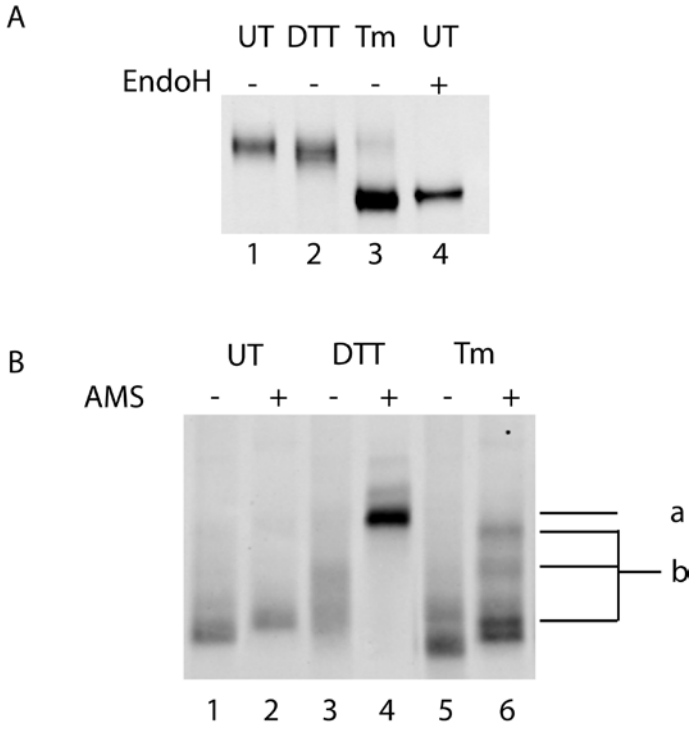

Figure S6. Changes in oxidation state of Ero1p during ER stress

(A) Protein extracts from wild-type cells expressing the composite reporter and Ero1p-3HA were treated with 10mM DTT for 30 min (lane 2), treated with 2µg/ml Tm for 3 hours (lane 3), or untreated (lanes 1 and 4). Extracts in lane 4 were deglycosylated with EndoH. Extracts were resolved on reducing SDS-page and immunoblotted against HA. Note that deglycosylation from Tm treatment produced the same faster migrating species from *in vitro* EndoH treatment of the untreated sample indicating its complete under-glycosylation *in vivo* (lanes 3 and 4). (B) Protein extracts from cells described above were treated with AMS as indicated, followed by treatment with EndoH to deduce mobility shifts due to AMS modification of available sulfhydryls in the different

treatments. Samples were then resolved on non-reducing SDS-PAGE, and immunoblotted against HA. Note the appearance of the AMS modified band due to DTT treatment in lane 4 (marked a), and the three AMS modified bands due to Tm treatment in lane 6 (marked b).

Supplementary Figure S7

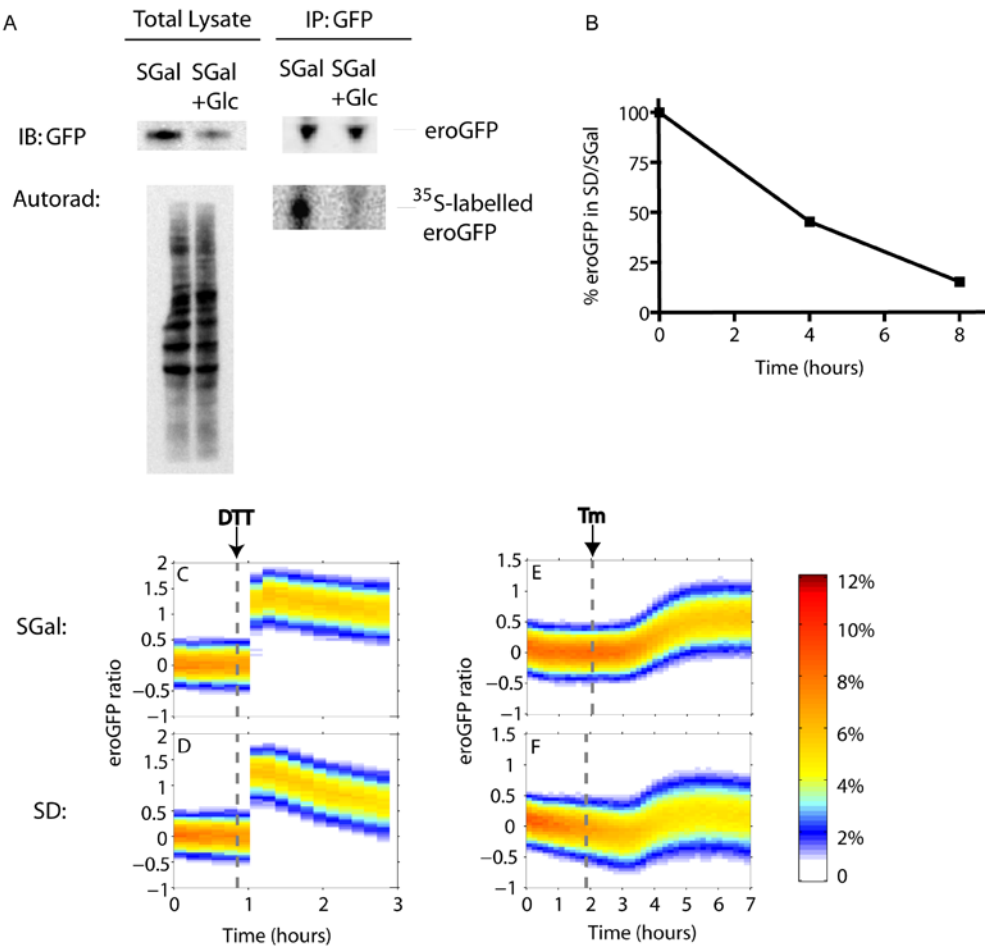

Figure S7. Dynamic monitoring of pre-existing eroGFP redox status during ER stress

(A) Pulse-chase of wild-type cells expressing GAL-eroGFP. See supplementary experimental procedures for details. (B) Quantification of eroGFP protein levels normalized to PGK1 for wild-type cells expressing GAL-eroGFP in SD vs. SGal media. (C-F) Time courses of the eroGFP ratio histograms in wild-type cells expressing GAL-eroGFP during treatment with DTT (2mM) or Tm (1µg/ml). The eroGFP ratio is normalized to unstressed cells. Color represents percentage of cells at a given metric value and time point. Dashed gray line signifies time of stressor addition. Thirty minutes

prior to sampling cells growing exponentially in SGal media were diluted 1/30 into SGal media (C) and (E) or SD media (D) and (F). We noted a slightly faster decay after DTT treatment in (D) vs. (C), possibly due to the lack of newly-synthesized eroGFP requiring oxidation in (D).

Supplementary Figure S8

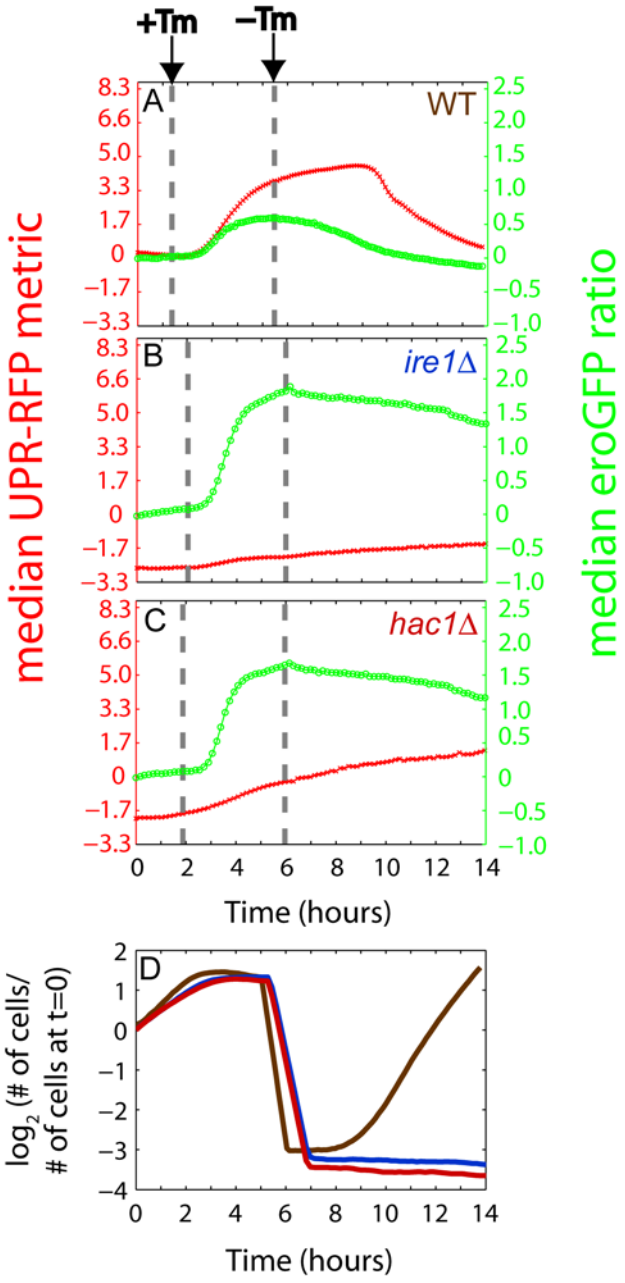

Figure S8. Dynamic monitoring of ER redox status and UPR activity during recovery from glycosylation inhibition

Median values for the eroGFP ratio and the UPR-RFP metric in wild-type (A), *ire1*Δ (B), and *hac1*Δ (C) cells expressing the composite reporter during treatment with Tm

(1μg/ml) and during recovery. The eroGFP ratio is represented by green circles the UPR-RFP metric is represented by red x-marks. The first dashed gray line denotes time of Tm addition and the second dashed gray line denotes time of dilution (1:25) into fresh media. The upward drift of UPR-RFP in the UPR mutants may be due to RFP accumulation in the growth-arrested cells. (D) Growth curves for WT (brown), *ire1*Δ (blue), and *hac1*Δ (red) cells are plotted as the $\log_2$ number of cells normalized to the number of cells at time, t=0. Note that only wild-type cells resume growth upon Tm removal.

Supplementary Figure S9

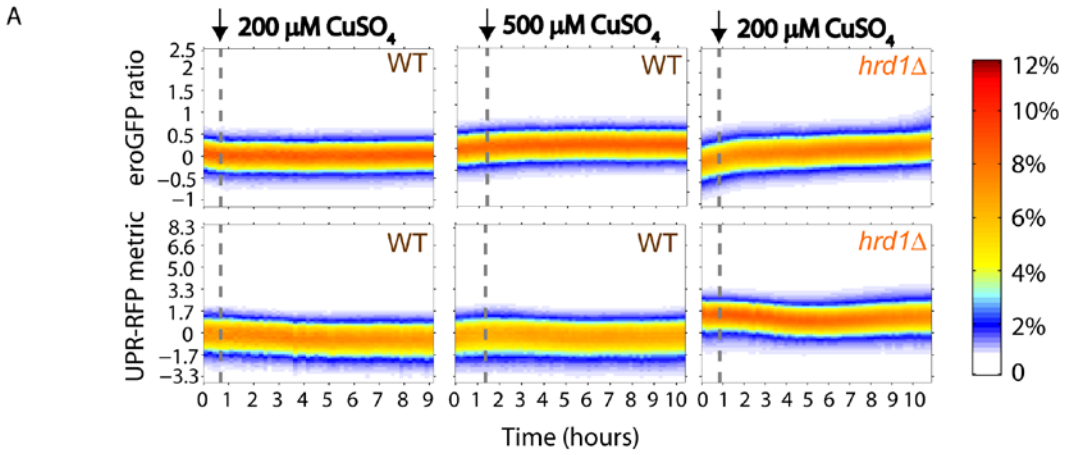

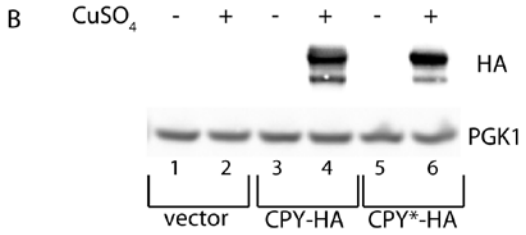

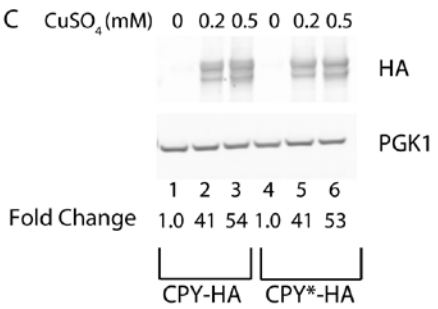

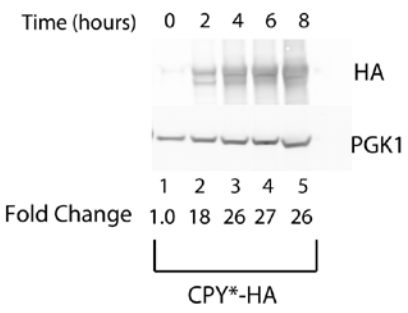

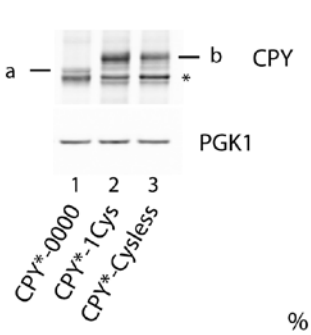

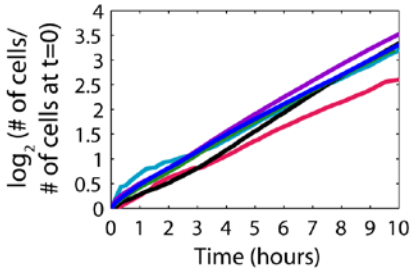

G

Construct	Strain	[$CuSO_4$]	% cells with eroGFP ratio>1 Median	Mean
Empty	WT	200	0.078	0.082
CPY			0.39	0.33
CPY*			5.9	5.7
Empty	*hrd1Δ*		0.40	0.63
CPY			4.1	4.2
CPY*			11	10
Empty	WT	500	0.55	0.51
CPY			3.4	3.7
CPY*			11	12
CPY*0000			15	16
CPY*-1cys			10	11
CPY*-Cysless			4.6	4.3

Figure S9. Characterization of copper-inducible CPY and CPY* variants

(A) Time courses of the eroGFP ratio and UPR-RFP histograms for wild-type and *hrd1*Δ cells expressing the composite reporter and empty vector treated with 200μM or 500μM copper sulfate. Color represents percentage of cells at a given metric value and time point. The dashed gray line signifies time of copper addition. (B) Immunoblot against HA and PGK1 of protein extracts from cells harboring empty vector, P_{CUP1}-CPY-HA, or P_{CUP1}-CPY*-HA in the presence and absence of 200μM copper sulfate. (C) Immunoblot against HA and PGK1 of protein extracts from cells treated with 200μM or 500μM copper sulfate. (D) Cells expressing P_{CUP1}-CPY*-HA were treated with 200μM copper sulfate at time, t=0 and samples were taken for immunoblot every 2 hours for 8 hours. (E) Immunoblot against CPY from cells expressing P_{CUP1}-CPY*0000, P_{CUP1}-CPY*-1cys, or P_{CUP1}-CPY*Cys-less treated with 200μM copper sulfate. The band marked "a" denotes unglycosylated CPY*, while "b" denotes glycoyslated CPY*. An * signifies a non-specific band. (F) Growth curves from experiments described in Figure 5 for wild-type cells treated with 500μM copper sulfate expressing the indicated CPY construct or empty vector. The color of the line denotes which construct was expressed (see G). (G) Summary of the percentage of cells in the deflected population from Figure 5 defined as cells with an eroGFP ratio greater than 1.

Supplementary Figure S10

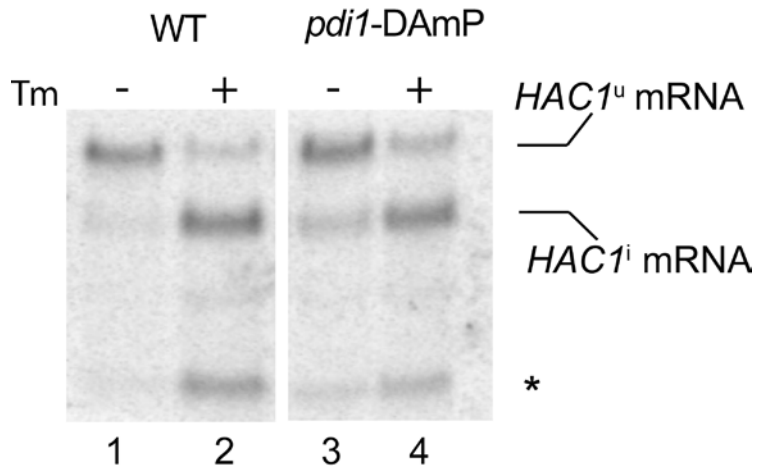

Figure S10. Increased UPR activity in a protein oxidation mutant in the absence of ER stress

Northern blot for *HAC1* mRNA for wild-type or *pdi1*-DAmP cells treated with or without tunicamycin (1μg/ml) for 1 hour. *HAC1*^{u} denotes unspliced and *HAC1*^{i} spliced mRNA respectively. An asterisk signifies the *HAC1* 5' exon. Percent spliced *HAC1* mRNA was calculated as *HAC1*^{i} mRNA over *HAC1*^{i} + *HAC1*^{u} mRNA. 28% greater splicing was evident in lane 3 vs. 1 (unstressed).

Supplementary Figure S11

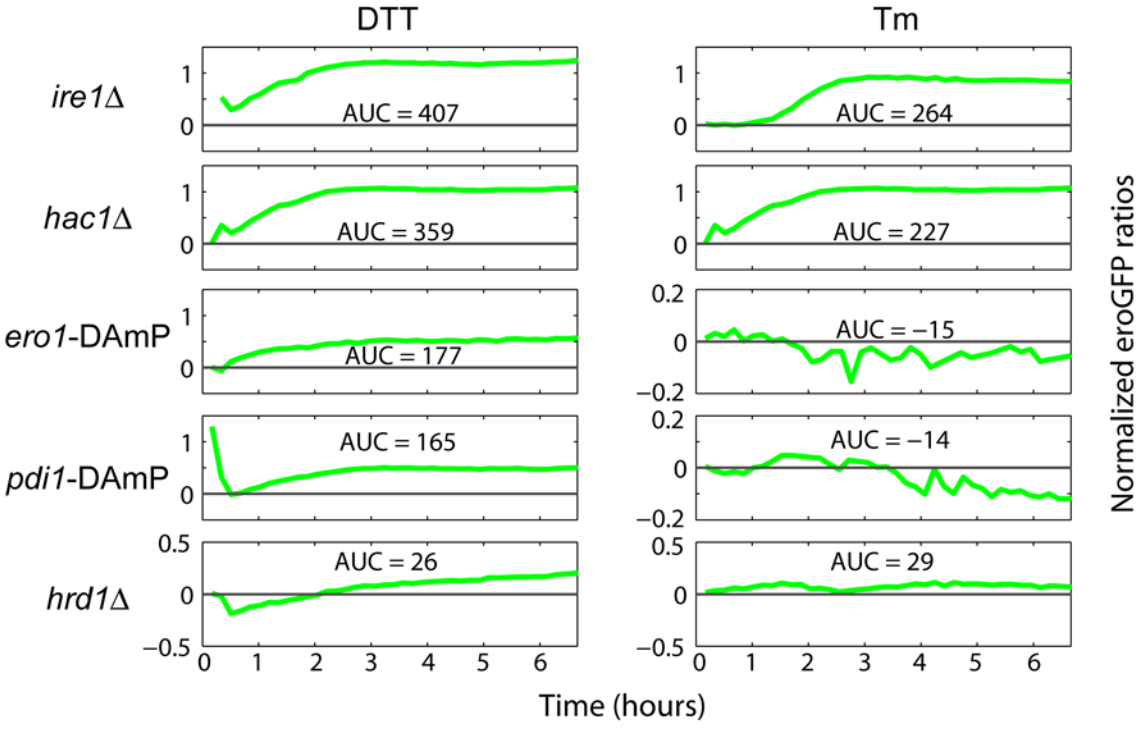

Figure S11. Normalized eroGFP ratios for ER oxidative folding, quality control, and UPR signaling mutants during pharmacologically-induced ER stress

Median values of the eroGFP ratio time courses for each mutant were normalized to wild-type. These normalized curves were then integrated over the time course with time, t= 0 denoting time of stressor addition, and reported as areas under the curves (AUC)

Supplementary Figure S12

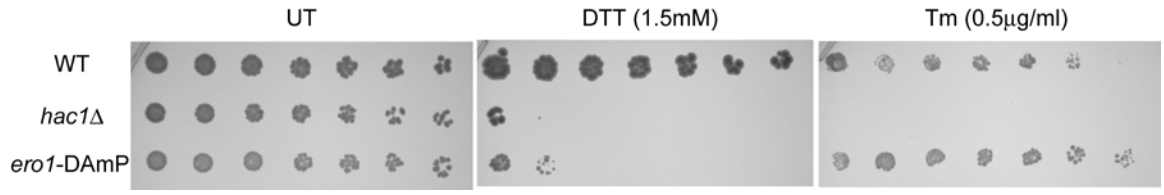

Figure S12. Differential growth for *ero1*-DAmP during protein oxidation and protein glycosylation stresses

Serial dilutions for wild-type, *hac1*Δ, and *ero1*-DAmP cells "frogged" onto synthetic-media plates without drug (UT), or with DTT (1.5mM) or Tm (0.5µg/ml). Image was taken 3 days after plating.

Supplementary Table S1

Strain	**Genotype**
YPM46	MAT**a**, *his3Δ1*, *leu2Δ0*, *met15Δ0*, *ura3Δ0*, eroGFP::NAT
YPM51	MAT**a**, *his3Δ1*, *leu2Δ0*, *met15Δ0*, *ura3Δ0*, eroGFP-UPR-RFP::NAT
YPM59	MAT**a**, *his3Δ1*, *leu2Δ0*, *met15Δ0*, *ura3Δ0*, *hrd1*Δ::KAN, eroGFP-UPR-RFP::NAT
YPM66	MAT**a**, *his3Δ1*, *leu2Δ0*, *met15Δ0*, *ura3Δ0*, *ire1*Δ::KAN, eroGFP-UPR-RFP::NAT
YPM67	MAT**a**, *his3Δ1*, *leu2Δ0*, *met15Δ0*, *ura3Δ0*, *hac1*Δ::KAN, eroGFP-UPR-RFP::NAT
YPM68	MAT**a**, *his3Δ1*, *leu2Δ0*, *met15Δ0*, *ura3Δ0*, *pdi1*-DAmP::NAT, eroGFP-UPR-RFP::KAN
YPM69	MAT**a**, *his3Δ1*, *leu2Δ0*, *met15Δ0*, *ura3Δ0*, *ero1*-DAmP::NAT, eroGFP-UPR-RFP::KAN
YPM70	MAT**a**, *his3Δ1*, *leu2Δ0*, *met15Δ0*, *ura3Δ0*, eroGFP(C147S)::NAT
YPM72	MAT**a**, *his3Δ1*, *leu2Δ0*, *met15Δ0*, *ura3Δ0*, GAL1-eroGFP::NAT

Chapter 3

Global Analysis of Genes Required for Maintaining Oxidative Folding of an ER-targeted Protein

Global Analysis of Genes Required for Maintaining Oxidative Folding of an ER-targeted Protein

Philip I. Merksamer[1,2,3,6], Ala Trusina[6], Onn Brandman,[3,4,5], Isabel Nocedal[1,2,3], Jonathan S. Weissman[3,4,5], Feroz R. Papa[1,2,3,*]

[1]Department of Medicine

[2]Diabetes Center

[3]California Institute for Quantitative Biosciences

[4]Department of Cellular and Molecular Pharmacology

[5]Howard Hughes Medical Institute

University of California, San Francisco, San Francisco, CA 94158, USA.

[6]Center for Models of Life,

Niels Bohr Institute, Copenhagen, Denmark

* Correspondence: frpapa@medicine.ucsf.edu

SUMMARY

The endoplasmic reticulum (ER) is dedicated to the folding of secretory and membrane proteins, however the mechanisms that maintain protein folding homeostasis remain poorly understood. Here, we use an ER-targeted redox sensitive fluorescent protein to identify several hundred yeast genes that affect ER protein folding during normal growth and ER stress conditions. We find that the ER is largely robust to genetic perturbation during normal growth conditions. However, under acute ER stress, multiple conserved complexes and pathways that contribute to ER protein folding are revealed. Our strategy of leveraging a physiological reporter in a whole genomic screen should be easily extended to investigate other complex cellular processes in yeast and mammals.

INTRODUCTION

In eukaryotic cells, proteins enter the secretory pathway by translocating though the Sec61 channel into the endoplasmic reticulum (ER) (Rapoport, 2007). Within the ER, these proteins fold to their native conformations as an obligatory step in their biogenesis. The ER is crowded with molecular chaperones, glycosylating enzymes, and oxidoreductases that together promote protein folding (van Anken and Braakman, 2005). The ER imposes stringent quality control over its products by ensuring that misfolded proteins are removed and degraded in the cytosol by the ubiquitin-dependent 26S proteasome (a process called ERAD) (Vembar and Brodsky, 2008). A homeostatic intracellular signaling pathway called the unfolded protein response (UPR) ensures that many components of these protein folding and quality control systems are present in sufficient amounts (Ron and Walter, 2007).

Despite these robust systems, cells often experience conditions that overwhelm ER protein folding, modification, and assembly in myriad ways. During these departures from homeostasis cells are considered to be experiencing "ER stress" as they trigger the UPR. Upon activation, the UPR transcriptionally up-regulates genes encoding chaperones, protein modification factors, lipid biosynthetic enzymes and ERAD components (Travers et al., 2000). In metazoans, the UPR also imposes a transient translational block (Harding et al., 1999). When they are successful, these adaptive UPR outputs decrease levels of unfolded proteins in the ER, thereby closing a negative feedback loop to restore homeostasis (Rutkowski et al., 2006). In multicellular organisms, irremediable ER stress triggers apoptosis when the adaptive UPR outputs

become exhausted and pro-apoptotic programs are activated instead (Zhang and Kaufman, 2006).

Since the UPR's activating inputs—unfolded proteins—are difficult to monitor directly in vivo, it is often unclear whether the UPR has succeeded in restoring homeostasis. To address this question, we previously developed single cell systems to quantify ER oxidative protein folding (an essential ER physiological function) during stress, while simultaneously measuring the level of UPR activation (Merksamer et al., 2008). For this purpose, we utilized an engineered green fluorescent protein (GFP) that responds to changes in its reduction-oxidation (redox) state through changes in its fluorescence properties. When expressed in the ER of *S. cerevisiae*, this fluorescent protein reporter—which we called eroGFP—could report quantitatively on loss of protein folding homeostasis from myriad causes with high precision. In combination with a UPR reporter, eroGFP provided quantitative information at the single cell level of the general physiological state of ER protein folding, both during the adapted state and during acute stress.

We previously explored these concepts in a select group of mutants in genes known to mediate ERAD, the UPR, and oxidative protein folding. Here, we have extended this analysis comprehensively to the entire yeast genome to query nearly all essential and non-essential genes that support oxidation of eroGFP in vivo. Through this analysis, we learned that many components of the secretory pathway supporting targeting and structural maturation are needed to maintain eroGFP in its properly oxidized state.

RESULTS

Comprehensive Identification of Genes Maintaining Oxidation of an ER-Localized Redox-Sensitive GFP

Due to reversible disulfide formation between two engineered cysteine residues, fluorescence excitation of eroGFP varies from its two maxima of 490 and 400nm such that reduction increases excitation from 490nm, at the expense of that from 400nm (Dooley et al., 2004; Hanson et al., 2004). Thus, eroGFP is ratiometric by excitation, which facilitates internally-controlled measurement of the redox state of its environment. Using flow cytometry, we measure the eroGFP ratio—defined as fluorescence from excitation at 488 versus 405 nm expressed in log_2 space—in populations of individual yeast cells (Figure 1A). In wild-type yeast, eroGFP is nearly completely oxidized under basal conditions, since treatment with hydrogen peroxide (H_2O_2) causes only a further small decrease in the eroGFP ratio (Figure 1B). In contrast, titration with increasing amounts of DTT causes the eroGFP ratio in the populations to progressively increase, until the reporter becomes fully reduced (Figure 1B).

To identify genes that perturb the oxidation state of eroGFP, we stably expressed the reporter in the *S. cerevisiae* non-essential gene deletion collection (Giaever et al., 2002) and the essential gene DAmP library (Breslow et al., 2008) using synthetic genetic array techniques (Figure S1; (Tong et al., 2001). Using high-throughput flow cytometry, we measured the eroGFP ratio in each mutant during vegetative growth (Newman et al., 2006). Through this process we were able to comprehensively query eroGFP's oxidation state in approximately 6000 yeast mutant strains (Figure 1C).

To define hits, we fitted a curve to the difference between replicate measurements and obtained threshold eroGFP ratio values corresponding to $P<0.001$ (Figure S2 and methods). In the majority of mutant strains, mean eroGFP ratios are not dramatically altered compared to wild-type (Figure 1C). This is consistent with our previous observations that oxidative protein folding in the ER, an essential cellular function, is largely robust to mutation (Merksamer et al., 2008). Since eroGFP is nearly completely oxidized under basal conditions, we focused our initial attention on genes whose deletion or down-regulation caused eroGFP to become more reduced. Among these genes, there was a clear enrichment for the 26S proteasome (Figures 1D and 1E). The 26S proteasome is a mega-dalton complex containing more than 30 proteins required for the degradation of damaged and misfolded proteins, including those that become extracted from the ER for disposal (Hanna and Finley, 2007). All subcomplexes of the proteasome were enriched, including the 'α' and 'β' subunits of the 20S core particle, and the lid and base subunits of the 19S regulatory particle (Figure 1E). In addition, a chaperone that assembles the 20S core of the proteasome, UMP1, was identified as a hit (See Table S1 for eroGFP ratios for all gene deletions).

The paucity of mutants exhibiting large deviations in their eroGFP ratios indicates that oxidative folding of the reporter in the ER is highly robust, at least during normal vegetative growth. Therefore, we acutely stressed the mutant libraries with tunicamcyin (Tm), a drug which inhibits N-linked glyscoyslation and thereby causes ER protein misfolding. Previously we found that Tm treatment resulted in stable reduction of eroGFP, allowing for reliable high-throughput sampling. Additionally, we found that some mutants—whose eroGFP ratios were identical to wild-type during normal growth

conditions—displayed dramatically different ratios under Tm-induced stress validating its use to uncover genes that affect oxidation of the reporter (Merksamer et al., 2008). After treating the mutant libraries with Tm, eroGFP ratios increased to a mean value of 0.57, normalized to the untreated case (Figure 2B). Because Tm caused reduction of eroGFP, we were able to investigate genes that caused eroGFP to become further reduced than average (sensitive strains; Figure 2C), or less reduced than average (resistant strains; Figure 2D).

As compared with vegetative growth, Tm treatment revealed significantly more hits (both sensitive and resistant) in genes whose functions support the folding, maturation and quality control of proteins utilizing the secretory pathway (Table S2). For instance, in addition to proteasome-encoding genes, we observed enrichments for genes mediating the unfolded protein response (UPR), the ER membrane complex (EMC), ER associated degradation (ERAD), and trafficking between the ER and Golgi (Figure 2E). Unexpectedly, among the resistant strains, we found enrichments for ER-resident molecular chaperones and N-linked glycosylation genes. While the significance of these findings are incompletely understood at this moment, it is clear that pharmacologically perturbing N-linked glycosylation causes additional deviations in eroGFP oxidation when genes affecting myriad processes of ER protein folding and modification are mutated.

Quantitative Relationships among Genes Affecting eroGFP Oxidation, UPR Signaling, and the Early Secretory Pathway

Previously, we employed a UPR-responsive fluorescent reporter to measure changes in UPR activity along with eroGFP in the same cells. Measuring these two

metrics together provided complementary information at the single cell level of the compensated state of ER protein folding during stress. Here we have extended this analysis to the genomic scale using the genome-wide UPR data set (Jonikas et al., 2009). In this data set, a GFP driven by a promoter containing four tandem unfolded protein response elements (4xUPRE) and an RFP expressed from a constitutive promoter was used to ratiometrically measure basal UPR activity in the yeast non-essential deletion library. For each of the non-essential gene mutant strains, we made a two-dimensional plot of the UPR activity level, and the eroGFP ratio under Tm stress (Figure 3). The analysis shows that there is very limited overlap between gene deletions that constitutively induce the UPR and those that perturb eroGFP oxidation during Tm treatment (Figure S3). However, in the overlapping set there are clearly groups of genes that affect ER protein maturation, and these gene sets cluster into three of the four possible quadrants. In quadrant I, which represents mutant strains that display both increased UPR activity and increased eroGFP ratio, we identified genes mediating the EMC, ERAD, and trafficking throughout the secretory pathway. Strains that lack UPR genes are unable to activate the UPR, but experience more protein misfolding stress during Tm treatment than the wildtype; thus these genes cluster in quadrant II. Quadrant IV contained many genes supporting N-linked glycosylation, and the ER co-chaperones LHS1, SCJ1, and HLJ1.

Next, we compared the Tm-stressed eroGFP data set to the epistatic map (e-map) of the early secretory pathway (ESP; Schuldiner et al., 2005). The e-map captures functional relationships of many genes based on growth phenotypes of double mutants. Thus, the e-map presents an alternative and complementary approach to GO functional

annotation. We focused on pairs of genes in the early secretory pathway that are highly correlated and lack aggravating interactions. Such interactions are characteristic of genes that act in a concerted manner, typically as part of the same complex or pathway.

We constructed a network representation of ESP genes, in which the genes are represented by nodes and are connected to other genes based on their epistatic interaction. The distance between nodes reflects the "functional distance" between gene pairs, such that densely connected topological clusters emerge from the network map. Several topological clusters from this ESP network have previously been assigned to GO functional categories (Figure 4A). These include ERAD, the UPR, the EMC, and genes mediating N-linked glycosylation. Under Tm stress, mutants in genes that show eroGFP deflections that are greater than wildtype (sensitive) are shown in orange, and those that deflect less than wildtype (resistant) are shown in blue; non-hits are colored grey. Unexpectedly, eroGFP hits tend to fall in clusters, and given clusters show eroGFP deflections that are either sensitive or resistant, but rarely both (Figures 4B,D,E). In contrast, a similar overlay of gene deletion hits from the UPR reporter onto the ESP network shows greater interdispersion (Figure S4). Remarkably, chaperones and glycosylating enzymes which had similar eroGFP changes also clustered together on the ESP network, suggesting a tight functional relationship between these two ER functions (Figure 4C).

DISCUSSION

Here, we use high-throughput screening of the yeast deletion libraries to identify genes that perturb the oxidation state of eroGFP. We find that oxidative folding of eroGFP is largely robust to genetic manipulation because the majority of deletion strains do not affect eroGFP oxidation. However, some genes including those encoding components of the 26S proteasome cause eroGFP to accumulate in its reduced form. During Tm-induced ER stress, many additional functional groups of genes emerge that affect eroGFP oxidation. Interestingly, many of these gene groups affect other ER processes besides N-linked glycosylation suggesting that eroGFP is a useful probe for monitoring all aspects of the ER biology. Importantly, gene deletions that perturbed eroGFP oxidation under stress showed minimal overlap with genes deletions that induce the UPR demonstrating that eroGFP and UPR metrics provide different and complimentary information. The tools we have developed here should be broadly applicable to other biological processes and should be useful for dissecting how ER protein folding affects human disease such as diabetes and cancer.

METHODS

Generation of eroGFP Gene Libraries

A SGA MATα strain with eroGFP integrated at the URA3 locus, was mated to the MATa deletion library and MATa DAmP library as previously describe (Jonikas et al., 2009).

High-Throughput Flow Cytometry

For all growth conditions described below, yeast strains were grown in 80 ul of SD complete media supplemented with myo-inositol (Sigma). For tunicamycin (Tm) experiments, Tm was added to the media at 6ug/ml. Strains were inoculated from 384-colony agar plates to 384-well liquid cultures using a RoToR HDA robot (Singer Instrument Company Limited). The cultures were grown for 36 hours to saturation in a DTS-4 microplate thermoshaker (Appropriate Technical Resources). They were then diluted 1:400 using a BioMek liquid-handling robot (Beckman Coulter, Inc.) and grown to mid-log phase for 10 hours after which they were diluted 1:10 into media with or without Tm. After 5 hours of growth, cultures were loaded on Becton Dickinson High Throughput Sampler (BD) which injected cells from each well into a LSRII flow cytometer (BD). eroGFP was fluorescence was measured according to Merksamer et al.

Data analysis was performed using MATLAB (The Mathworks) as follows. The eroGFP ratio for each well was calculated according to Merksamer et al., 2008 as the log2 transformed ratio of median fluorescence from 488nm to 405nm. Wells that had cell

counts below 100 were removed. The eroGFP ratio for each well was normalized to the mean eroGFP ratio of the two untreated sample plates that were run on the same day. To estimate error, a histogram of the difference between replicate measurements divided by two was generated (Figure S2). This curve was modeled as the sum of two Guassian distributions using a non-linear regression fit. Threshold values corresponding to $P<0.001$ were obtained from the fitted curve. The threshold eroGFP ratios for untreated and tunicamycin-treated samples were 0.02 and 0.10 respectively. Hits were defined as absolute eroGFP ratios that were greater than the threshold values. GO term enrichments were calculated using a student's t-test with a threshold of $P<0.001$ (Ashburner et al., 2000). For the network analysis, the predicted interacting gene pairs with a complex and pathway (COP) score >15 corresponding to all the entries from Table S4 from (Schuldiner et al., 2005) were visualized using Cytoscape (Shannon et al., 2003).

FIGURE LEGENDS

Figure 1. Quantitative screen for genes whose deletion or down regulation affect eroGFP oxidation

(A) Schematic showing configuration of flow cytometer laser lines and filters used to measure eroGFP fluorescence excitation and emission.

(B) eroGFP ratios for populations of wild-type cells treated with the indicated concentration of DTT or H_2O_2.

(C) Median eroGFP ratios for each mutant in the yeast deletion and DAmP libraries. Dashed grey lines indicate threshold values. Orange dots indicate proteasome genes. Red dots indicate genes that are analyzed further in Figures 5-7.

(D) Zoomed in median eroGFP ratios of the gene libraries. Orange dots indicate proteasome genes with gene names labeled next to each dot.

(E) Fold enrichments ($P<0.001$) for proteasome genes based on gene ontology groups.

Figure 2. Quantitative screen for genes that affect eroGFP oxidation during Tunicamycin-induced ER stress

(A) eroGFP ratios for populations of wild-type cells treated with or without tunicamycin (Tm, 6ug/ml for 5 hours).

(B) Median eroGFP ratios of the deletion and DAmP libraries with and without Tm (6ug/ml for 5 hours).

(C and D) Zoomed in median eroGFP ratios of the gene libraries with representative sensitive (C) or resistant (D) genes indicated.

(E) Fold enrichments ($P<0.001$) for sensitive and resistant genes during Tm-induced stress.

Figure 3. Comparison of UPR activity and eroGFP oxidation for non-essential yeast deletion mutants

Scatter plot of median eroGFP ratios after Tm-treatment vs UPR reporter levels (Jonikas et al) for the non-essential yeast deletion library. The following gene categories are indicated by color: cyan (ERAD), orange (trafficking), magenta (EMC), red (N-linked glycosylation), blue (ER-resident chaperones), green (UPR), and purple (proteasome).

Figure 4. Relationship between eroGFP and a functional genetic map of the early secretory pathway

(A) Network map of the early secretory pathway based on predicted interacting gene pairs with a complex and pathway (COP) score>15 according to data from (Schuldiner et al., 2005). Each node is colored based on its eroGFP ratio during Tm-induced stress. Orange nodes denote sensitive strains while blue nodes denote resistant strains.

(B,C,D,E) Zoomed in map of the each cluster with gene names

Figure S1. Schematic of screen design

Schematic of mating strategy used to generate the eroGFP expressing gene libraries.

Figure S2. Error estimation for the eroGFP screens

(A,B) Histograms of the differences between replicate measurements for untreated and tunicamycin treated samples respectively

(C,D) Fit of the histograms from A and B modeled as the sum of two Gaussian distributions. The fitted lines are in orange overlaid over the histograms from A and B.

(E,F) Histograms of the mean data in green for untreated and tunicamycin treated samples respectively in green overlaid over the histograms described in A-D.

Figure S3. Venn diagrams of UPR activity and eroGFP oxidation for the non-essential yeast deletion mutants

Venn Diagrams showing overlap for each quadrant between hits from the UPR data set and from the eroGFP data set treated with Tm

Figure S4. Relationship between UPR activity and a functional genetic map of the early secretory pathway

Network representation where nodes are colored orange if they are UPR upregulators and blue if they are UPR downregulators

REFERENCES

Ashburner, M., Ball, C. A., Blake, J. A., Botstein, D., Butler, H., Cherry, J. M., Davis, A. P., Dolinski, K., Dwight, S. S., Eppig, J. T.*, et al.* (2000). Gene ontology: tool for the unification of biology. The Gene Ontology Consortium. Nat Genet *25*, 25-29.

Breslow, D. K., Cameron, D. M., Collins, S. R., Schuldiner, M., Stewart-Ornstein, J., Newman, H. W., Braun, S., Madhani, H. D., Krogan, N. J., and Weissman, J. S. (2008). A comprehensive strategy enabling high-resolution functional analysis of the yeast genome. Nat Methods *5*, 711-718.

Dooley, C. T., Dore, T. M., Hanson, G. T., Jackson, W. C., Remington, S. J., and Tsien, R. Y. (2004). Imaging dynamic redox changes in mammalian cells with green fluorescent protein indicators. J Biol Chem *279*, 22284-22293.

Giaever, G., Chu, A. M., Ni, L., Connelly, C., Riles, L., Veronneau, S., Dow, S., Lucau-Danila, A., Anderson, K., Andre, B.*, et al.* (2002). Functional profiling of the Saccharomyces cerevisiae genome. Nature *418*, 387-391.

Hanna, J., and Finley, D. (2007). A proteasome for all occasions. FEBS Lett *581*, 2854-2861.

Hanson, G. T., Aggeler, R., Oglesbee, D., Cannon, M., Capaldi, R. A., Tsien, R. Y., and Remington, S. J. (2004). Investigating mitochondrial redox potential with redox-sensitive green fluorescent protein indicators. J Biol Chem *279*, 13044-13053.

Harding, H. P., Zhang, Y., and Ron, D. (1999). Protein translation and folding are coupled by an endoplasmic-reticulum-resident kinase. Nature *397*, 271-274.

Jonikas, M. C., Collins, S. R., Denic, V., Oh, E., Quan, E. M., Schmid, V., Weibezahn, J., Schwappach, B., Walter, P., Weissman, J. S., and Schuldiner, M. (2009). Comprehensive

characterization of genes required for protein folding in the endoplasmic reticulum. Science *323*, 1693-1697.

Merksamer, P. I., Trusina, A., and Papa, F. R. (2008). Real-time redox measurements during endoplasmic reticulum stress reveal interlinked protein folding functions. Cell *135*, 933-947.

Newman, J. R., Ghaemmaghami, S., Ihmels, J., Breslow, D. K., Noble, M., DeRisi, J. L., and Weissman, J. S. (2006). Single-cell proteomic analysis of S. cerevisiae reveals the architecture of biological noise. Nature *441*, 840-846.

Rapoport, T. A. (2007). Protein translocation across the eukaryotic endoplasmic reticulum and bacterial plasma membranes. Nature *450*, 663-669.

Ron, D., and Walter, P. (2007). Signal integration in the endoplasmic reticulum unfolded protein response. Nat Rev Mol Cell Biol *8*, 519-529.

Rutkowski, D. T., Arnold, S. M., Miller, C. N., Wu, J., Li, J., Gunnison, K. M., Mori, K., Sadighi Akha, A. A., Raden, D., and Kaufman, R. J. (2006). Adaptation to ER stress is mediated by differential stabilities of pro-survival and pro-apoptotic mRNAs and proteins. PLoS Biol *4*, e374.

Schuldiner, M., Collins, S. R., Thompson, N. J., Denic, V., Bhamidipati, A., Punna, T., Ihmels, J., Andrews, B., Boone, C., Greenblatt, J. F.*, et al.* (2005). Exploration of the function and organization of the yeast early secretory pathway through an epistatic miniarray profile. Cell *123*, 507-519.

Shannon, P., Markiel, A., Ozier, O., Baliga, N. S., Wang, J. T., Ramage, D., Amin, N., Schwikowski, B., and Ideker, T. (2003). Cytoscape: a software environment for integrated models of biomolecular interaction networks. Genome Res *13*, 2498-2504.

Tong, A. H., Evangelista, M., Parsons, A. B., Xu, H., Bader, G. D., Page, N., Robinson, M., Raghibizadeh, S., Hogue, C. W., Bussey, H.*, et al.* (2001). Systematic genetic analysis with ordered arrays of yeast deletion mutants. Science *294*, 2364-2368.

Travers, K. J., Patil, C. K., Wodicka, L., Lockhart, D. J., Weissman, J. S., and Walter, P. (2000). Functional and genomic analyses reveal an essential coordination between the unfolded protein response and ER-associated degradation. Cell *101*, 249-258.

van Anken, E., and Braakman, I. (2005). Versatility of the endoplasmic reticulum protein folding factory. Crit Rev Biochem Mol Biol *40*, 191-228.

Vembar, S. S., and Brodsky, J. L. (2008). One step at a time: endoplasmic reticulum-associated degradation. Nat Rev Mol Cell Biol *9*, 944-957.

Zhang, K., and Kaufman, R. J. (2006). The unfolded protein response: a stress signaling pathway critical for health and disease. Neurology *66*, S102-109.

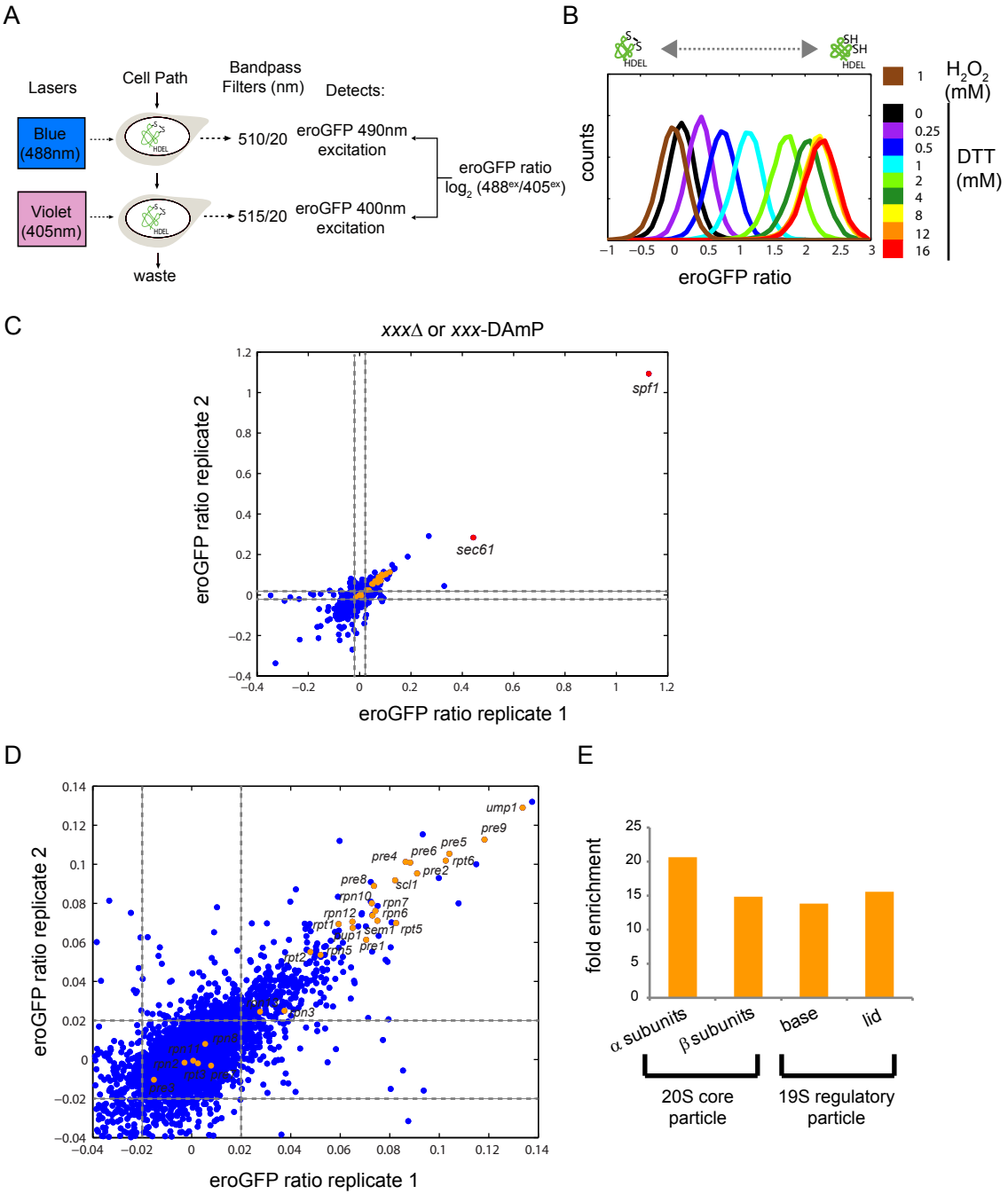

Merksamer et al Figure 1

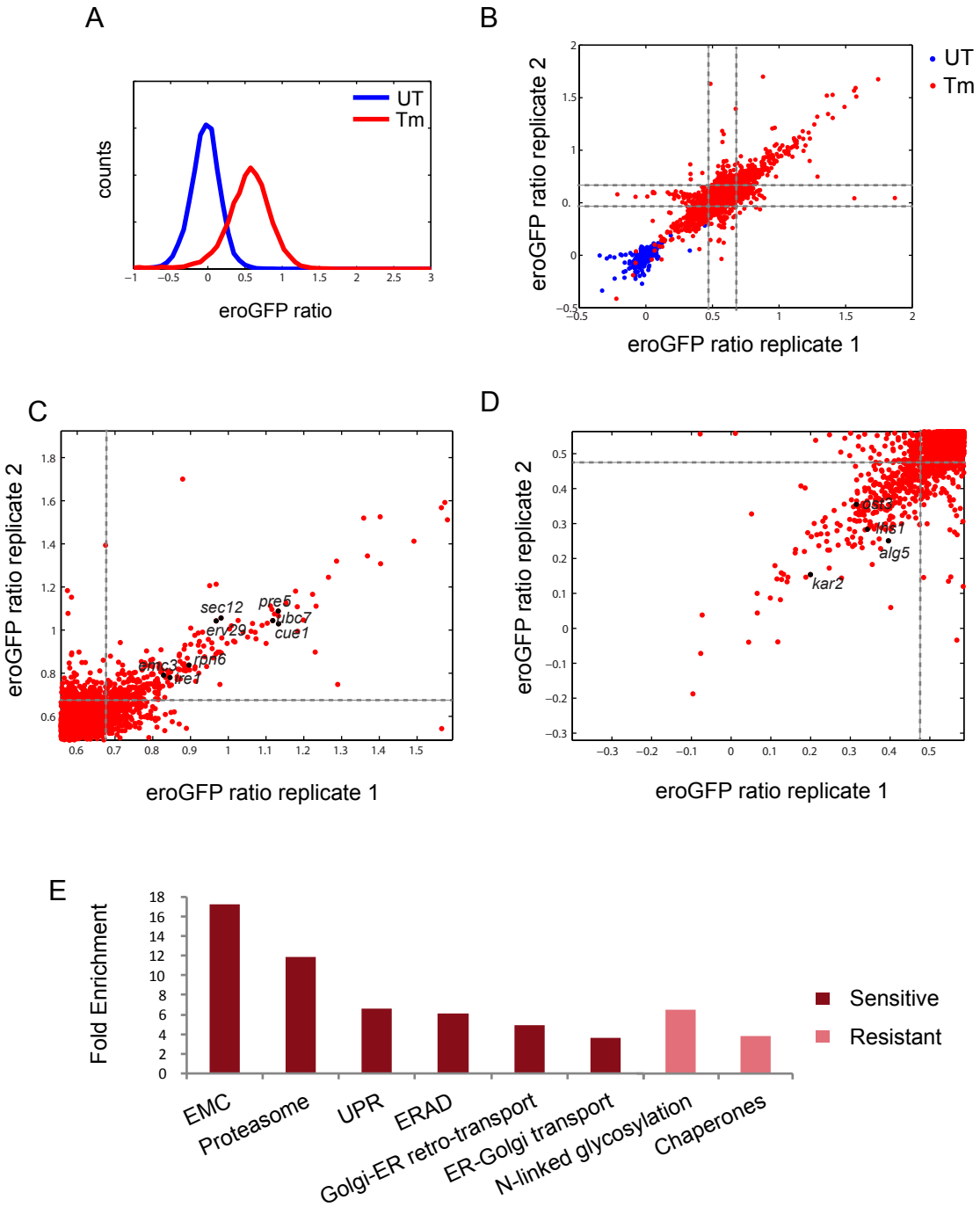

Merksamer et al Figure 2

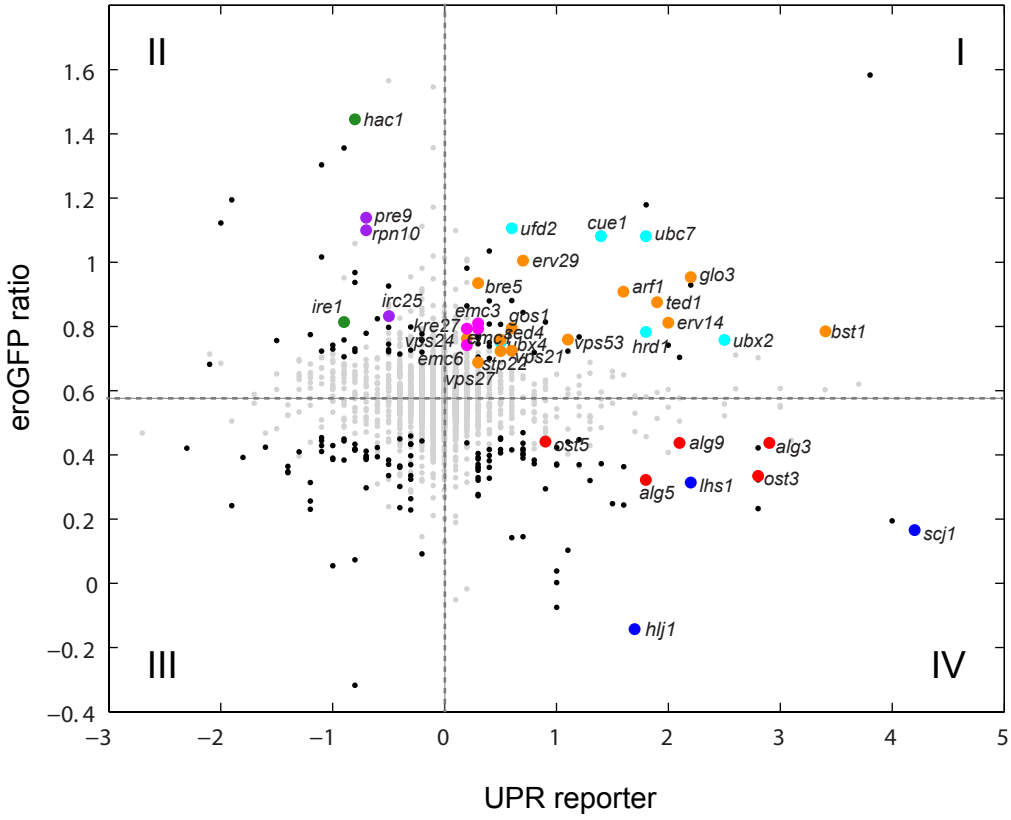

Merksamer et al Figure 3

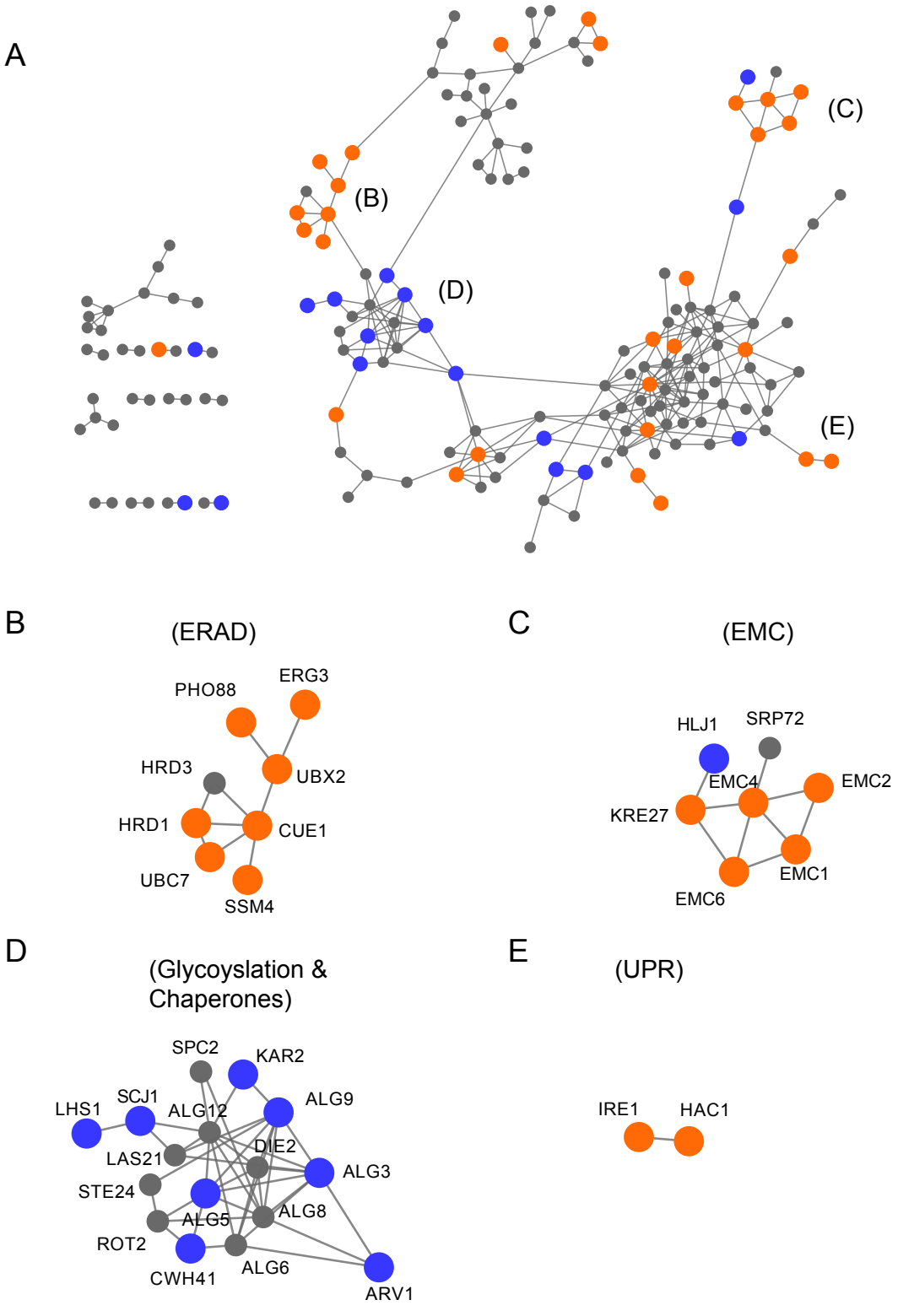

Merksamer et al Figure 4

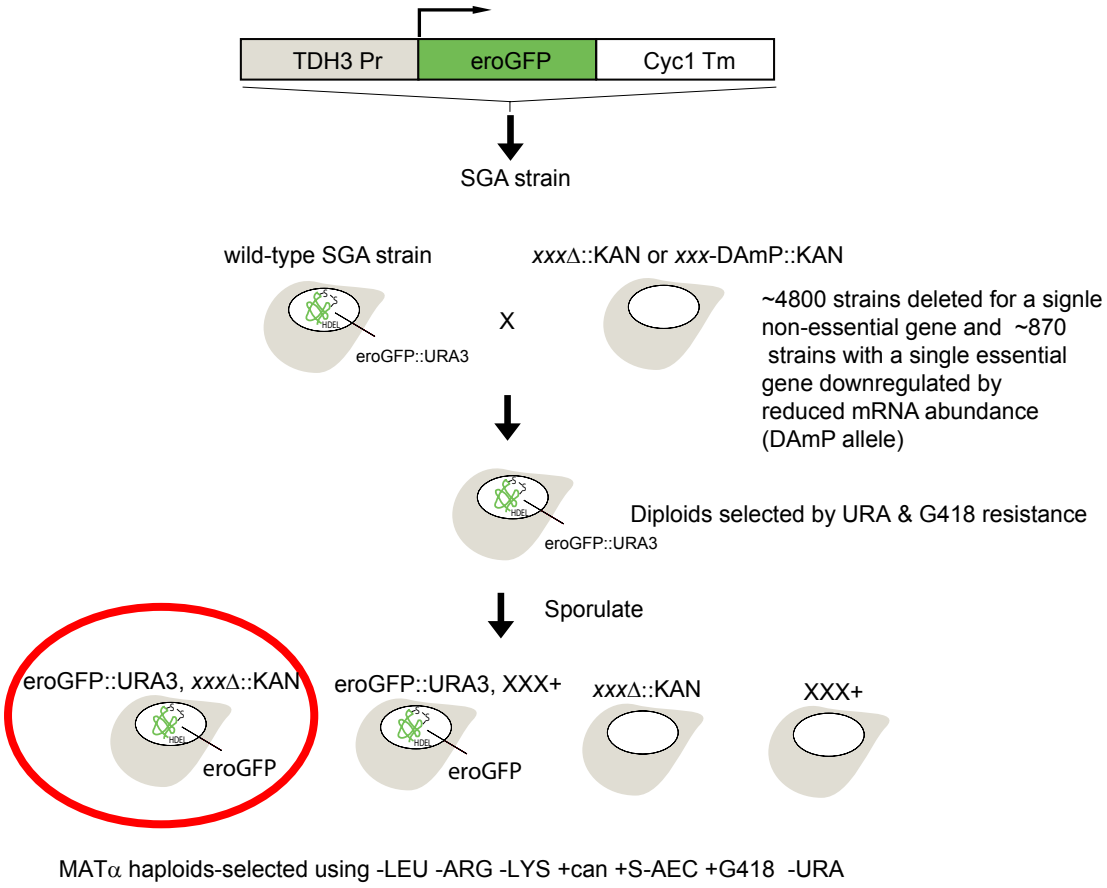

Merksamer et al Figure S1

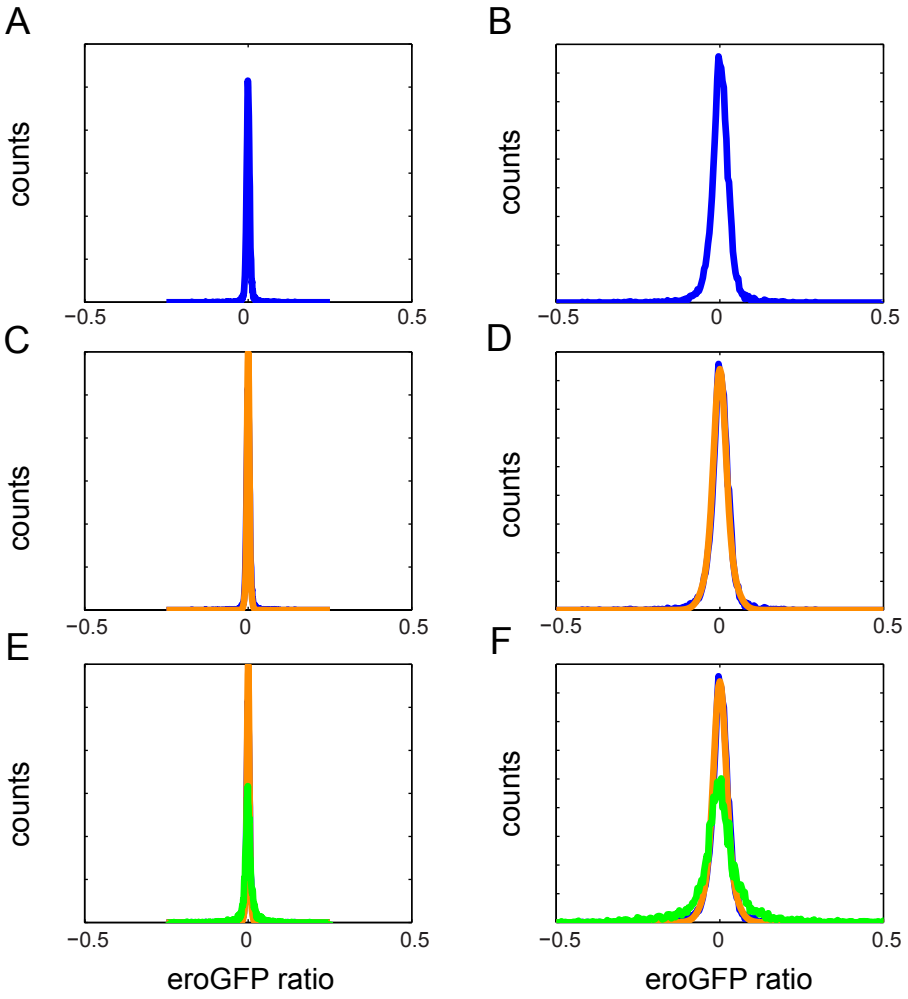

Merksamer Figure S2

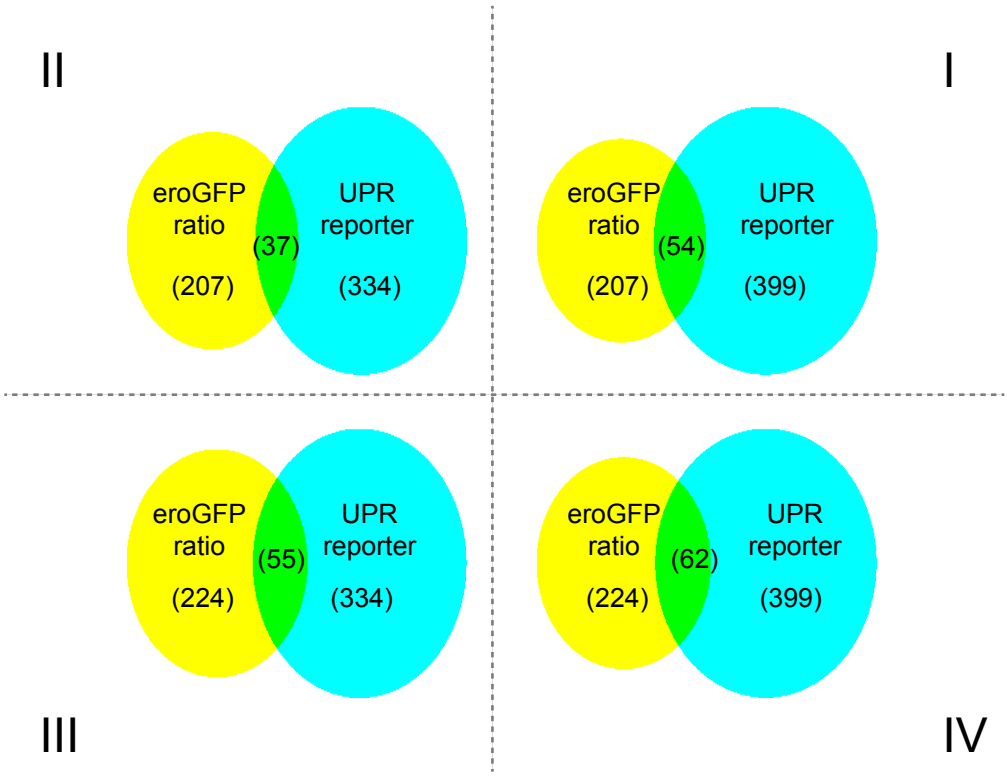

Merksamer et al Figure S3

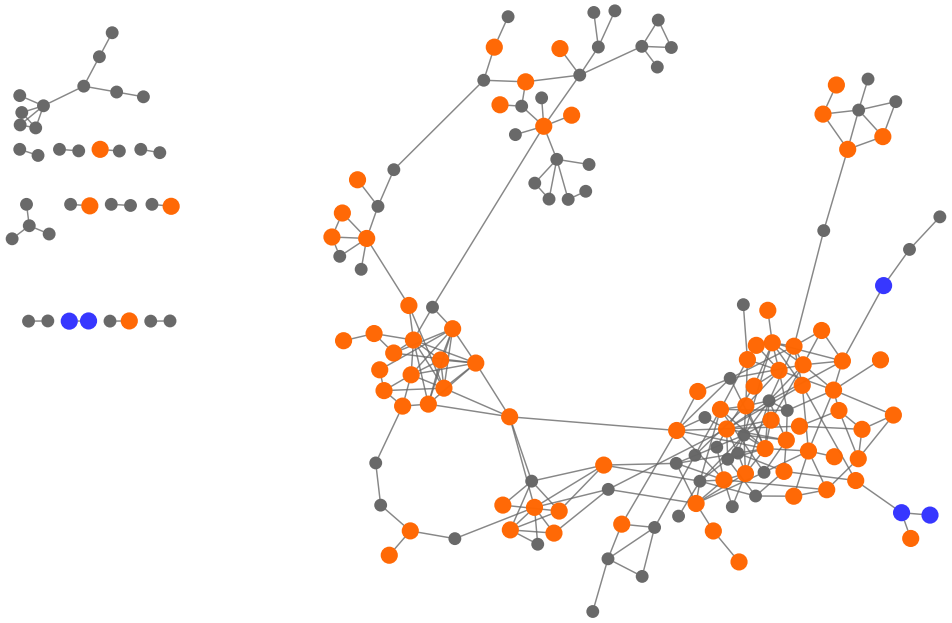

Merksamer Figure S4

Table S1 Strains that perturb eroGFP oxidation during normal growth conditions

UT indicates untreated
UT Rep indicates individual replicates
UT ave indicates the average of 2 replicates

ORF	UT Rep 1	UT Rep 2	UT ave
ATS1	0.032	0.042	0.037
CHA4	0.024	0.022	0.023
UBR2	0.031	0.022	0.027
ERG2	0.033	0.032	0.032
MMM1	0.024	0.032	0.028
MRE11	0.023	0.033	0.028
IRC25	0.059	0.083	0.071
GEM1	0.028	0.033	0.031
YML081W	0.042	0.038	0.040
NUP60	0.036	0.032	0.034
TRM9	0.060	0.112	0.086
SPT21	0.036	0.050	0.043
RAD52	0.022	0.024	0.023
SIC1	0.026	0.026	0.026
BUD28	0.028	0.053	0.041
RPL36A	0.029	0.039	0.034
TSA1	0.024	0.051	0.037
CNE1	0.024	0.050	0.037
PMT2	0.027	0.036	0.032
IRC19	0.027	0.022	0.025
ALT1	0.067	0.068	0.068
CIK1	0.028	0.034	0.031
CSF1	0.025	0.039	0.032
RTT109	0.059	0.063	0.061
UBC7	0.058	0.065	0.062
CUE1	0.039	0.048	0.043
RPS10A	0.054	0.058	0.056
CKA2	0.022	0.024	0.023
IFM1	0.044	0.040	0.042
RPL20B	0.046	0.070	0.058
MRPL33	0.029	0.057	0.043
CAF40	0.039	0.034	0.037
SPE2	0.037	0.030	0.033
DIA2	0.043	0.046	0.044
RPA49	0.030	0.044	0.037
MET22	0.056	0.061	0.058
PET111	0.052	0.053	0.052
RTS1	0.022	0.028	0.025
PHO80	0.031	0.046	0.038
GAS1	0.040	0.039	0.039
PFA4	0.044	0.042	0.043

YOR305W	0.029	0.053	0.041
SIN3	0.047	0.039	0.043
THP1	0.033	0.060	0.047
YPL102C	0.046	0.063	0.055
DFM1	0.046	0.056	0.051
YBR238C	0.052	0.042	0.047
RPL12A	0.043	0.027	0.035
YDR348C	0.023	0.024	0.024
RPP2B	0.050	0.045	0.048
ARX1	0.033	0.033	0.033
FZO1	0.055	0.050	0.052
HPT1	0.069	0.074	0.072
NPL3	0.037	0.029	0.033
YEL043W	0.041	0.033	0.037
POC4	0.075	0.079	0.077
XRS2	0.047	0.060	0.053
MGR2	0.029	0.031	0.030
RPL12B	0.037	0.044	0.040
MSY1	0.034	0.024	0.029
SPF1	1.126	1.093	1.109
TGS1	0.051	0.054	0.052
CIN8	0.035	0.047	0.041
DPB4	0.030	0.033	0.032
SSE1	0.072	0.081	0.077
ROT2	0.025	0.023	0.024
RAD23	0.027	0.032	0.030
SLM6	0.035	0.035	0.035
PET100	0.030	0.026	0.028
INO2	0.080	0.057	0.069
ATP17	0.031	0.037	0.034
SWD3	0.044	0.030	0.037
ELP4	0.055	0.046	0.050
OCA6	0.032	0.036	0.034
RRM3	0.024	0.027	0.026
PIH1	0.023	0.022	0.022
YHR100C	0.049	0.041	0.045
CHO2	0.137	0.132	0.135
RPN10	0.073	0.080	0.076
YCL060C	0.021	0.024	0.023
FCY2	0.059	0.057	0.058
MRC1	0.027	0.033	0.030
OCA5	0.024	0.025	0.025
MOT2	0.073	0.074	0.074
MSH1	0.024	0.036	0.030
ARG5,6	0.050	0.028	0.039
PRE9	0.118	0.113	0.115
YER087C-A	0.021	0.027	0.024
RNR4	0.073	0.055	0.064
UBA4	0.032	0.022	0.027

BUD3	0.021	0.020	0.021
ELP2	0.050	0.049	0.050
CDC10	0.033	0.037	0.035
RER1	0.023	0.024	0.024
SPE1	0.027	0.032	0.029
RSC1	0.037	0.046	0.042
PCP1	0.050	0.058	0.054
KTI12	0.041	0.043	0.042
MMR1	0.042	0.032	0.037
PAC10	0.046	0.067	0.056
PUS7	0.023	0.029	0.026
ATP7	0.025	0.027	0.026
YKL053W	0.025	0.037	0.031
UPS1	0.053	0.047	0.050
OAR1	0.027	0.042	0.035
SWI6	0.024	0.070	0.047
YKE2	0.048	0.069	0.059
ART5	0.040	0.041	0.041
NUP120	0.029	0.039	0.034
CAX4	0.040	0.081	0.060
YLR184W	0.054	0.028	0.041
MUD2	0.035	0.033	0.034
RTF1	0.029	0.040	0.034
SUR4	0.036	0.033	0.035
RAI1	0.041	0.037	0.039
RCY1	0.034	0.034	0.034
VID22	0.059	0.066	0.063
BUD19	0.033	0.028	0.030
RSC2	0.036	0.043	0.039
VIP1	0.034	0.031	0.033
MRPL7	0.036	0.027	0.032
MMS22	0.030	0.070	0.050
NGG1	0.042	0.087	0.065
ELP3	0.050	0.052	0.051
IKI3	0.057	0.052	0.055
YLR402W	0.035	0.026	0.031
ARV1	0.036	0.049	0.042
SAC3	0.048	0.050	0.049
RPN13	0.028	0.024	0.026
MSS18	0.027	0.038	0.033
SEM1	0.075	0.071	0.073
YNL226W	0.022	0.025	0.023
YBL081W	0.025	0.033	0.029
KAP122	0.032	0.044	0.038
YPL062W	0.049	0.035	0.042
LDB7	0.330	0.044	0.187
CDC50	0.038	0.039	0.039
SGF73	0.022	0.024	0.023
GUP1	0.026	0.046	0.036

ERV14	0.022	0.029	0.025
SHP1	0.071	0.021	0.046
YGL072C	0.021	0.022	0.022
YGL042C	0.034	0.022	0.028
ERJ5	0.043	0.039	0.041
DST1	0.037	0.038	0.037
PEP7	0.040	0.041	0.040
NUP133	0.032	0.022	0.027
COS10	0.051	0.059	0.055
ERV29	0.037	0.038	0.038
YNL170W	0.058	0.041	0.050
RPL42B	0.026	0.021	0.024
ZUO1	0.034	0.021	0.027
PSD1	0.066	0.039	0.052
IPK1	0.031	0.047	0.039
ALF1	0.078	0.051	0.065
SNL1	0.041	0.026	0.033
HAC1	0.037	0.040	0.039
YTA7	0.030	0.041	0.035
YFL032W	0.034	0.041	0.037
SWA2	0.035	0.041	0.038
SNT309	0.076	0.063	0.069
ASF1	0.056	0.037	0.046
RAD5	0.035	0.024	0.029
?ML095C-A	0.049	0.055	0.052
SPT10	0.057	0.027	0.042
MED1	0.050	0.056	0.053
LSM1	0.027	0.036	0.031
ARG3	0.042	0.041	0.041
TKL1	0.031	0.033	0.032
YJL120W	0.037	0.028	0.032
OPI11	0.041	0.039	0.040
MET6	0.081	0.070	0.075
RPE1	0.021	0.024	0.022
RAD50	0.079	0.021	0.050
YPR045C	0.031	0.038	0.035
IKI1	0.061	0.060	0.060
ATP20	0.023	0.027	0.025
ELP6	0.046	0.041	0.044
MUB1	0.039	0.038	0.038
ASC1	0.036	0.026	0.031
GIM5	0.044	0.038	0.041
INO4	0.069	0.075	0.072
YDL118W	0.038	0.042	0.040
YDL119C	0.054	0.054	0.054
REG1	0.042	0.034	0.038
YJR087W	0.029	0.038	0.033
SRB8	0.108	0.080	0.094
YJR018W	0.060	0.050	0.055

POL32	0.041	0.032	0.037
UFD2	0.187	0.190	0.188
CRD1	0.026	0.040	0.033
DPB3	0.027	0.025	0.026
BRE5	0.030	0.034	0.032
RPL6B	0.027	0.046	0.037
MGM101	0.025	0.033	0.029
NUP84	0.052	0.029	0.041
SAM37	0.064	0.047	0.056
FEN1	0.048	0.040	0.044
SIW14	0.025	0.037	0.031
UBP14	0.050	0.043	0.046
MRP7	0.021	0.020	0.021
FYV6	0.079	0.050	0.065
HSM3	0.030	0.029	0.030
SSN8	0.047	0.068	0.058
TOM7	0.023	0.024	0.023
AXL2	0.029	0.020	0.024
NCS2	0.020	0.020	0.020
SCO1	0.028	0.041	0.034
YIL141W	0.028	0.020	0.024
CSE2	0.037	0.034	0.036
NNF2	0.042	0.038	0.040
YDJ1	0.048	0.050	0.049
PHO88	0.127	0.149	0.138
SED4	0.036	0.035	0.035
ADA2	0.093	0.115	0.104
HCR1	0.029	0.035	0.032
SLX5	0.046	0.035	0.040
IWR1	0.049	0.044	0.047
RPL43A	0.053	0.032	0.043
RXT2	0.022	0.023	0.022
TUP1	0.054	0.041	0.048
SSM4	0.021	0.031	0.026
YFL013W-A	0.032	0.040	0.036
RPN4	0.072	0.091	0.082
RPL27B	0.026	0.025	0.025
RPL21A	0.054	0.058	0.056
YLR358C	0.036	0.027	0.031
CBS1	0.032	0.036	0.034
UBC4	0.050	0.046	0.048
PTC1	0.039	0.047	0.043
YDR442W	0.039	0.028	0.034
SEC61	0.443	0.283	0.363
UMP1	0.134	0.129	0.131
DEG1	0.050	0.039	0.045
POB3	0.028	0.030	0.029
OCH1	0.027	0.029	0.028
NRP1	0.029	0.029	0.029

NUT1	0.024	0.032	0.028
SLX8	0.052	0.034	0.043
GIM3	0.042	0.046	0.044
IES1	0.021	0.025	0.023
GLO3	0.026	0.024	0.025
RPC25	0.030	0.044	0.037
RPT1	0.059	0.069	0.064
NDC1	0.064	0.031	0.048
MNN10	0.042	0.033	0.037
KAE1	0.024	0.023	0.023
TEN1	0.043	0.036	0.040
CDC42	0.054	0.039	0.046
COG1	0.037	0.042	0.040
LSM7	0.029	0.024	0.026
GCN5	0.066	0.040	0.053
PRE5	0.104	0.105	0.105
TOM22	0.036	0.040	0.038
ANP1	0.039	0.027	0.033
RNA1	0.061	0.045	0.053
CWC25	0.027	0.026	0.027
PRE6	0.086	0.101	0.094
PFS2	0.031	0.029	0.030
YDR524C-B	0.021	0.022	0.021
SAP30	0.033	0.031	0.032
YER087W	0.042	0.044	0.043
MRPL20	0.040	0.031	0.036
YIF1	0.020	0.026	0.023
SEC12	0.115	0.100	0.107
WRS1	0.053	0.045	0.049
KTI11	0.070	0.068	0.069
IES6	0.030	0.025	0.027
LIP1	0.030	0.031	0.031
TPT1	0.270	0.291	0.281
POR1	0.036	0.024	0.030
YMR242W-A	0.024	0.026	0.025
RPB11	0.032	0.030	0.031
HRT1	0.023	0.034	0.029
RPT5	0.083	0.070	0.076
YCL057C-A	0.034	0.026	0.030
HPR1	0.044	0.028	0.036
CEG1	0.039	0.061	0.050
SMD1	0.038	0.055	0.046
PRE8	0.074	0.089	0.081
SCL1	0.082	0.092	0.087
TAF13	0.048	0.066	0.057
TAF10	0.046	0.049	0.048
RPC11	0.021	0.023	0.022
RPT6	0.103	0.102	0.102
PRI1	0.040	0.041	0.040

CCT2	0.033	0.031	0.032
TIF34	0.023	0.031	0.027
IPP1	0.061	0.053	0.057
RPN6	0.073	0.074	0.073
PRP38	0.040	0.022	0.031
PRE4	0.088	0.101	0.095
PRE1	0.070	0.061	0.066
RPN12	0.065	0.070	0.068
RPT2	0.048	0.055	0.052
SPN1	0.022	0.041	0.031
SEC62	0.100	0.093	0.096
RPN7	0.074	0.076	0.075
YDL163W	0.038	0.029	0.034
YPL238C	0.046	0.056	0.051
TCP1	0.030	0.024	0.027
PUP1	0.065	0.067	0.066
NOC4	0.027	0.024	0.026
SME1	0.036	0.038	0.037
PRE2	0.091	0.095	0.093
RPN3	0.037	0.025	0.031
RPN5	0.052	0.054	0.053

Table S2 Sensitive eroGFP hits during tunicamycin treatment

TM indicates tunicamycin-treated
Rep indicates individual replicates
Ave indicates average of 2 replicates

ORF	TM Rep 1	TM Rep 2	TM Ave
ATS1	0.901	0.934	0.917
CMP2	0.752	0.691	0.722
IRC25	0.800	0.864	0.832
YLR064W	0.679	0.705	0.692
SPT21	0.793	0.834	0.813
UBX2	0.758	0.759	0.758
PUF3	0.737	0.772	0.754
HSP104	0.872	0.816	0.844
DEP1	0.723	0.757	0.740
YLL014W	0.762	0.721	0.741
MFT1	0.725	0.722	0.723
ADD37	0.977	0.748	0.863
ERG3	0.901	1.010	0.955
YAP1	0.711	0.772	0.742
UBC7	1.118	1.044	1.081
CUE1	1.133	1.029	1.081
RPS10A	1.287	1.320	1.303
SGT2	0.883	0.844	0.864
SKI7	0.754	0.804	0.779
VPS21	0.682	0.767	0.724
VTS1	0.720	0.812	0.766
DGK1	0.746	0.775	0.761
RPL20B	1.403	1.308	1.356
CAF40	0.817	0.843	0.830
IRA2	0.688	0.879	0.783
VMA4	0.705	0.713	0.709
RPA49	0.707	0.707	0.707
PET111	1.402	1.525	1.464
HRD1	0.826	0.740	0.783
PHO80	0.968	1.213	1.090
DSK2	0.839	0.811	0.825
ISW2	0.746	0.736	0.741
YPL225W	0.720	0.837	0.779
LDB19	0.817	0.833	0.825
SIN3	0.751	0.703	0.727
YBR194W	0.687	0.742	0.714
DFM1	1.122	1.074	1.098
DOA4	0.703	0.698	0.700
KAP120	0.701	0.682	0.691
YEL043W	0.809	0.706	0.757
POC4	0.912	0.829	0.871

SAN1	0.694	0.716	0.705
BEM1	0.718	0.681	0.699
YEL014C	0.678	0.738	0.708
MRPL40	0.703	0.722	0.713
SPF1	1.574	1.592	1.583
RAD55	0.692	0.690	0.691
UME1	0.755	0.735	0.745
MTC7	0.700	0.685	0.692
YBR174C	0.693	0.699	0.696
RAD23	0.777	0.778	0.777
INO2	1.100	0.938	1.019
REI1	0.739	0.722	0.731
YPL182C	0.714	0.729	0.721
BNA7	0.729	0.721	0.725
MAK10	0.726	0.793	0.760
IRE1	0.846	0.780	0.813
LDB16	0.748	0.766	0.757
CHO2	0.951	1.206	1.079
GOS1	0.797	0.794	0.795
RPN10	1.133	1.065	1.099
KSP1	0.681	0.748	0.714
STP22	0.688	0.758	0.723
YCL045C	0.772	0.815	0.793
SGF29	0.997	0.938	0.968
YCL046W	0.764	0.733	0.748
RIM101	0.709	0.709	0.709
URA4	0.729	0.677	0.703
ARG5,6	1.230	0.899	1.064
PRE9	1.153	1.125	1.139
RMD11	0.760	0.683	0.722
NMD2	0.734	0.695	0.714
STM1	0.921	0.931	0.926
UPF3	0.686	0.679	0.682
YOR139C	0.695	0.677	0.686
RFX1	0.845	0.741	0.793
MDR1	0.689	0.712	0.700
CEX1	0.725	0.686	0.706
SFL1	0.679	0.732	0.705
HNT3	0.879	1.700	1.290
FYV12	0.725	0.687	0.706
KTI12	0.722	0.755	0.738
SSP2	0.780	0.833	0.807
MRPL38	0.738	0.801	0.769
ATP7	0.785	0.731	0.758
BFR1	1.071	0.990	1.030
LTV1	0.744	0.700	0.722
YOR246C	0.871	0.889	0.880
RFM1	0.726	0.695	0.710
DID4	0.699	0.731	0.715

VPS24	0.777	0.747	0.762
TMA19	0.710	0.852	0.781
NUP120	0.749	0.801	0.775
DPH5	0.754	0.698	0.726
CLG1	0.759	0.717	0.738
RTF1	1.017	0.945	0.981
RTN1	0.732	0.760	0.746
YGL231C	0.735	0.722	0.728
SWE1	0.730	0.710	0.720
YDR186C	0.794	0.860	0.827
YJL169W	0.766	0.711	0.738
NIF3	0.792	0.751	0.771
SET2	0.834	0.781	0.807
SKI2	0.810	0.742	0.776
FAR10	0.682	0.702	0.692
NGG1	1.199	1.046	1.122
VAM7	0.737	0.736	0.737
ZRT1	0.729	0.688	0.709
SKI8	0.922	0.800	0.861
YGL214W	0.777	0.736	0.756
NUP170	0.710	0.722	0.716
SKI3	0.847	0.806	0.826
QCR2	0.700	0.749	0.724
SEM1	0.821	0.806	0.813
SFB3	0.912	0.976	0.944
MET16	0.796	0.751	0.774
JJJ1	0.752	0.732	0.742
SGF11	0.815	0.679	0.747
ERV14	0.770	0.854	0.812
RPL23A	0.733	0.714	0.724
YGL072C	0.957	0.915	0.936
YBL071C	0.894	0.819	0.857
HDA3	0.774	0.731	0.753
RPL7A	0.884	0.828	0.856
YGL042C	0.865	0.784	0.824
EGD1	0.801	0.795	0.798
PUF4	0.807	0.764	0.786
URE2	0.799	0.831	0.815
SEC28	1.232	1.111	1.172
CBR1	0.773	0.715	0.744
KRE27	0.811	0.775	0.793
MGA2	0.713	0.694	0.704
COS10	1.369	1.344	1.356
YKL207W	0.828	0.791	0.810
ERV29	0.968	1.043	1.006
SSD1	0.938	0.876	0.907
BST1	0.785	0.783	0.784
YNL171C	0.788	0.727	0.758
YNL155W	0.814	0.712	0.763

HDA2	0.742	0.783	0.763
YDR333C	0.770	0.683	0.727
ICE2	0.737	0.764	0.751
UBX4	0.708	0.794	0.751
DPH2	0.838	0.790	0.814
DOA1	0.873	0.855	0.864
YKR074W	0.781	0.839	0.810
MSN5	0.717	0.800	0.759
HAC1	1.359	1.520	1.439
TED1	0.870	0.880	0.875
YFR012W	0.691	0.690	0.690
YPR084W	0.887	0.811	0.849
ECM17	0.719	0.710	0.714
CAF130	0.806	0.712	0.759
MET6	0.774	0.731	0.752
SSZ1	0.767	0.694	0.730
YOP1	0.726	0.694	0.710
INO4	1.111	1.112	1.112
IKS1	0.822	0.909	0.866
YJR088C	0.761	0.771	0.766
SCH9	0.779	0.849	0.814
YJR087W	1.014	0.948	0.981
YLR426W	0.817	0.743	0.780
ARF1	0.886	0.930	0.908
UBP1	1.003	1.006	1.004
SRB8	0.785	0.751	0.768
YJR018W	0.710	0.686	0.698
UFD2	1.116	1.096	1.106
VPS53	0.831	0.687	0.759
BRE5	0.923	0.947	0.935
JJJ3	0.868	0.819	0.843
SAM37	0.773	0.720	0.746
CYS3	0.714	0.732	0.723
SIW14	0.725	0.722	0.723
OCA2	0.679	0.726	0.703
UBP14	0.960	0.871	0.916
HDA1	0.914	0.762	0.838
RPL16A	0.680	0.731	0.705
VPS27	0.701	0.677	0.689
CTK1	0.784	0.903	0.843
DPH1	0.848	0.806	0.827
MST1	0.805	0.736	0.770
KGD1	0.799	0.798	0.798
YRO2	0.776	0.680	0.728
YDJ1	0.947	0.957	0.952
EAP1	0.789	0.722	0.755
PEX29	0.733	0.723	0.728
EAF3	0.695	0.683	0.689
PHO88	0.734	0.703	0.718

SED4	0.753	0.765	0.759
YDL025C	0.680	0.708	0.694
ADA2	1.223	1.166	1.195
HCR1	0.982	0.893	0.937
SNF4	0.892	0.870	0.881
TUP1	1.060	0.995	1.028
SSM4	0.977	0.898	0.938
YFL013W-A	0.839	0.759	0.799
CYB5	0.942	0.831	0.887
YPR050C	0.711	0.722	0.716
RPN4	1.178	1.180	1.179
UGO1	0.849	0.745	0.797
YBR099C	0.749	0.699	0.724
GPM2	1.564	1.567	1.566
RPL21A	1.073	0.959	1.016
MET13	0.741	0.688	0.715
NHP10	0.765	0.762	0.763
UBC4	0.882	0.814	0.848
SCS3	0.935	0.927	0.931
UMP1	1.581	1.511	1.546
RPL9A	0.818	0.730	0.774
GET1	0.771	0.714	0.742
BRE1	0.763	0.724	0.744
RPS31	0.814	0.702	0.758
FTR1	0.772	0.740	0.756
GRX5	0.771	0.678	0.725
RPB9	0.865	0.771	0.818
SNF1	1.051	0.968	1.009
CHD1	0.717	0.686	0.701
ERG13	0.731	0.679	0.705
GRR1	1.039	0.990	1.014
AEP1	0.812	0.764	0.788
IES1	0.807	0.764	0.786
GLO3	0.920	0.987	0.953
NUP116	0.807	0.681	0.744
DJP1	0.732	0.677	0.705
RPT1	0.817	0.827	0.822
NDC1	1.290	0.748	1.019
YML010W-A	0.699	0.713	0.706
PER1	0.967	0.889	0.928
BUD31	0.956	0.941	0.948
GEF1	0.699	0.682	0.690
PRE5	1.132	1.088	1.110
RNA1	1.265	1.245	1.255
MPT5	0.883	0.912	0.897
PRE6	0.932	0.990	0.961
ISA1	0.803	0.743	0.773
BUR2	0.697	0.722	0.710
YNL296W	1.026	1.045	1.035

YIF1	0.777	0.708	0.742
SEC12	0.981	1.056	1.019
IES6	0.762	0.694	0.728
TFB5	0.874	0.774	0.824
TPT1	1.183	1.108	1.145
PMT4	0.765	0.763	0.764
SEC21	1.009	1.021	1.015
PRE8	1.064	1.030	1.047
SCL1	1.184	0.994	1.089
RET2	0.879	0.842	0.860
PDI1	0.912	0.820	0.866
ARP2	0.761	0.702	0.732
RPC11	0.730	0.679	0.705
RPT6	0.983	0.964	0.973
SEC26	0.821	0.821	0.821
TOM40	0.726	0.685	0.705
IPP1	0.729	0.710	0.720
RPN6	0.896	0.838	0.867
PRE4	1.492	1.412	1.452
EFB1	0.735	0.684	0.709
PRE1	1.089	1.022	1.056
RPN12	0.898	0.815	0.857
RPT2	0.826	0.814	0.820
CCT8	0.711	0.698	0.705
SPN1	0.925	0.899	0.912
RPN7	0.815	0.753	0.784
RPL33A	0.885	0.817	0.851
YPL238C	1.745	1.675	1.710
PUP1	0.812	0.735	0.773
NOC4	0.973	0.898	0.935
TIM50	0.714	0.943	0.828
PRE2	1.103	1.032	1.068
BET2	0.729	0.680	0.705
RPN5	0.797	0.798	0.798

Table S3 Resistant eroGFP hits during tunicamycin treatment

TM indicates tunicamycin-treated
Rep indicates individual replicates
Ave indicates average of 2 replicates

ORF	TM Rep 1	TM Rep 2	TM Ave
UBR2	0.247	0.224	0.236
YHM2	0.433	0.476	0.454
AVL9	0.357	0.245	0.301
HLJ1	-0.096	-0.188	-0.142
YLR111W	0.373	0.368	0.370
HFA1	0.459	0.469	0.464
RPS10B	0.433	0.348	0.391
PDC1	0.461	0.371	0.416
SCJ1	0.188	0.146	0.167
SWC3	0.410	0.375	0.392
BUD20	0.437	0.331	0.384
FPS1	0.446	0.319	0.383
DRS2	0.350	0.305	0.327
RPS17A	0.363	0.455	0.409
RPS16A	0.380	0.450	0.415
YMR221C	0.298	0.284	0.291
ARP6	0.401	0.433	0.417
SPT8	0.215	0.268	0.242
TYE7	0.374	0.412	0.393
CKA2	0.423	0.424	0.424
MDM20	0.420	0.414	0.417
YOL050C	-0.073	0.038	-0.018
BUD21	0.373	0.256	0.314
RPS19B	0.384	0.436	0.410
SHE4	0.117	-0.039	0.039
MET22	0.336	0.402	0.369
UBP15	0.327	0.438	0.383
HTZ1	0.446	0.389	0.417
RTS1	0.452	0.433	0.442
PEX6	0.464	0.365	0.414
ALG5	0.396	0.250	0.323
SNF2	0.355	0.182	0.269
OST3	0.315	0.355	0.335
YPL205C	0.443	0.460	0.452
SXM1	0.463	0.431	0.447
ERD1	0.360	0.284	0.322

GCN4	0.366	0.296	0.331
MTC5	0.400	0.374	0.387
POS5	0.357	0.329	0.343
RPS6B	0.443	0.444	0.444
THI6	0.465	0.475	0.470
TGS1	0.344	0.352	0.348
ARO80	0.450	0.452	0.451
ISW1	0.461	0.446	0.453
SSE1	0.116	0.141	0.128
YPL184C	0.403	0.407	0.405
SWC5	0.351	0.391	0.371
VPS61	0.442	0.416	0.429
LSM6	0.237	0.291	0.264
SPT3	0.449	0.394	0.421
PDB1	0.426	0.368	0.397
YHR078W	0.434	0.438	0.436
RPS24A	0.221	0.236	0.228
MRPL6	0.345	0.338	0.341
YHR100C	0.321	0.325	0.323
NSR1	0.332	0.358	0.345
DIA4	0.408	0.388	0.398
SBH2	0.433	0.476	0.454
YGR160W	0.275	0.294	0.285
TDH3	0.467	0.441	0.454
MOT2	0.359	0.464	0.412
YHR177W	0.311	0.277	0.294
RPS4B	0.346	0.441	0.393
ARO9	0.409	0.377	0.393
YND1	0.454	0.421	0.438
PEX4	0.419	0.447	0.433
CDC10	0.269	0.238	0.254
CEM1	0.364	0.381	0.372
MRPL32	0.424	0.397	0.410
LST7	0.247	0.172	0.210
ELM1	0.398	0.403	0.400
MET7	0.439	0.450	0.444
PCP1	0.453	0.403	0.428
TUL1	0.471	0.425	0.448
MMR1	0.448	0.468	0.458
PAC10	0.403	0.289	0.346
RPS28A	0.466	0.452	0.459
YOR277C	0.458	0.463	0.460
YOR199W	0.349	0.299	0.324
SLX9	0.408	0.439	0.424

LST4	0.397	0.454	0.426
SLP1	0.044	-0.040	0.002
MCT1	0.388	0.283	0.336
IRC13	0.439	0.443	0.441
CAX4	0.127	0.140	0.133
LHS1	0.343	0.284	0.313
ULS1	0.469	0.473	0.471
SWI3	0.278	0.144	0.211
RPS28B	0.453	0.413	0.433
RCY1	0.399	0.343	0.371
RPL39	0.409	0.296	0.352
YDR203W	0.395	0.380	0.387
VID22	0.361	0.411	0.386
RPS29A	0.393	0.430	0.411
BUD19	0.143	0.147	0.145
LYS4	0.406	0.444	0.425
RSC2	0.437	0.456	0.446
VIP1	0.367	0.374	0.370
GLR1	0.099	0.087	0.093
ACO2	0.065	0.100	0.083
MRPL7	0.461	0.445	0.453
BER1	0.450	0.395	0.423
BOP2	0.415	0.437	0.426
UME6	0.402	0.393	0.398
RLM1	0.444	0.434	0.439
BUD26	0.380	0.350	0.365
HXK2	0.334	0.324	0.329
OST5	0.439	0.444	0.442
LIP2	0.347	0.289	0.318
YLR287-A	0.412	0.360	0.386
CHS5	0.432	0.455	0.444
VMA7	0.361	0.332	0.347
CDC73	0.458	0.440	0.449
ARV1	0.162	0.226	0.194
VPS63	0.449	0.356	0.402
LAA1	0.435	0.418	0.426
YDR230W	0.382	0.404	0.393
PIN4	0.236	0.317	0.277
TIF4632	0.451	0.473	0.462
RTT106	0.407	0.475	0.441
ALG3	0.450	0.424	0.437
SLA1	0.186	0.402	0.294
YBL083C	0.372	0.472	0.422
CKB1	0.350	0.424	0.387

CDC50	0.284	0.356	0.320
YPR172W	0.439	0.452	0.445
ALG9	0.444	0.429	0.437
PIB2	0.363	0.418	0.390
YGL024W	0.363	0.369	0.366
PEX17	0.423	0.393	0.408
GCR2	0.110	0.179	0.145
HEK2	0.430	0.408	0.419
CWH41	0.378	0.453	0.416
YNL198C	0.126	0.159	0.143
WHI3	0.259	0.337	0.298
BUD27	0.432	0.426	0.429
PEX3	0.459	0.474	0.466
YNL170W	0.323	0.336	0.330
ZUO1	0.243	0.270	0.256
LOC1	0.326	0.246	0.286
PEX10	0.425	0.372	0.399
PSD1	0.298	0.312	0.305
MEH1	0.314	0.329	0.322
NAP1	0.369	0.348	0.358
ALF1	0.458	0.436	0.447
SWR1	0.318	0.387	0.353
PEX1	0.424	0.408	0.416
PEX5	0.413	0.442	0.428
HIS6	0.426	0.461	0.444
MOT3	0.316	0.425	0.371
APQ12	0.378	0.344	0.361
SNT309	0.311	0.239	0.275
?ML095C-A	0.231	0.307	0.269
SPT10	0.437	0.371	0.404
LSM1	0.365	0.359	0.362
ARG3	0.329	0.231	0.280
MSC1	0.463	0.476	0.470
BRR1	0.457	0.450	0.454
NEM1	0.428	0.401	0.414
RIC1	0.335	0.336	0.336
MUB1	0.376	0.228	0.302
GIM5	0.316	0.365	0.340
ADE3	-0.222	-0.413	-0.318
TSR2	0.407	0.376	0.392
SPC72	0.161	0.216	0.189
YDL172C	0.453	0.449	0.451
ECM30	0.392	0.338	0.365
ATG17	0.424	0.358	0.391

REG1	0.410	0.358	0.384
RAV1	0.473	0.424	0.449
PTC6	0.407	0.299	0.353
YJR015W	0.475	0.297	0.386
LYS9	0.361	0.355	0.358
CRD1	0.471	0.393	0.432
ISY1	0.394	0.412	0.403
OPI6	0.383	0.433	0.408
LYS20	0.401	0.429	0.415
BIO4	0.453	0.466	0.460
IST3	0.374	0.474	0.424
TAT1	0.318	0.349	0.334
RPS9B	0.407	0.421	0.414
YAK1	0.460	0.391	0.425
FLX1	0.409	0.415	0.412
PRM5	0.450	0.457	0.453
RPS11B	0.437	0.400	0.418
FYV6	0.193	0.274	0.233
YAF9	0.427	0.402	0.415
LAT1	0.337	0.393	0.365
SPT4	0.346	0.401	0.373
SLM4	0.475	0.453	0.464
SET3	0.389	0.375	0.382
YJL175W	0.066	0.044	0.055
MET18	0.462	0.332	0.397
ETR1	0.359	0.410	0.385
YKR040C	0.472	0.466	0.469
SNF5	0.184	0.220	0.202
TPS1	0.303	0.368	0.335
YME1	0.462	0.405	0.433
RIM1	0.175	0.408	0.291
RPS29B	0.450	0.450	0.450
CWC21	0.266	0.280	0.273
POP2	0.398	0.311	0.354
RPS18A	0.448	0.409	0.429
CCW12	0.351	0.376	0.363
VPS72	0.417	0.396	0.407
RPL43A	0.429	0.299	0.364
SNT1	0.359	0.387	0.373
PEX19	0.475	0.434	0.455
SEC66	0.373	0.372	0.372
VPS71	0.390	0.407	0.399
YMR160W	0.450	0.470	0.460
RPP1A	0.310	0.310	0.310

BUD23	0.317	0.393	0.355
YDR455C	0.472	0.401	0.437
PSP1	0.411	0.417	0.414
DAL81	0.373	0.350	0.361
RPS16B	0.386	0.382	0.384
SIF2	0.353	0.426	0.390
BDF2	0.395	0.430	0.413
ARC18	0.396	0.414	0.405
PTC1	0.330	0.352	0.341
YDL071C	0.462	0.425	0.444
COX15	0.453	0.435	0.444
TOR1	0.465	0.451	0.458
ARO2	0.430	0.324	0.377
VRP1	-0.077	-0.071	-0.074
OCH1	0.326	0.257	0.292
NRP1	0.313	0.464	0.388
PDA1	0.306	0.235	0.270
OPI9	0.388	0.340	0.364
RPL31A	0.209	0.300	0.255
LPD1	0.338	0.310	0.324
RPS26B	0.449	0.419	0.434
YGL088W	0.445	0.389	0.417
NOP56	0.396	0.354	0.375
GIM3	0.388	0.299	0.344
PMR1	0.225	0.270	0.248
BCK2	0.404	0.351	0.378
CPR7	0.402	0.060	0.231
HUR1	0.240	0.249	0.245
SSK1	0.438	0.470	0.454
CHC1	0.319	0.329	0.324
MNN10	0.406	0.319	0.363
CDC42	0.379	0.393	0.386
RTR1	0.409	0.384	0.397
ANB1	0.444	0.433	0.439
BUD13	0.372	0.413	0.393
YER140W	0.124	0.082	0.103
SUI1	0.450	0.454	0.452
YCR075W-A	0.391	0.373	0.382
GPI15	0.432	0.436	0.434
SWP1	0.391	0.415	0.403
TIF11	0.051	0.327	0.189
YBL039W-A	0.327	0.332	0.329
YER087W	0.364	0.475	0.420
EFG1	0.308	0.348	0.328

YBL071C-B	0.342	0.365	0.353
HAS1	0.354	0.294	0.324
YJR114W	0.465	0.316	0.390
TRM112	0.429	0.421	0.425
YOR293C-A	0.358	0.411	0.385
POR1	0.334	0.343	0.338
YGL188C-A	0.466	0.382	0.424
RNR1	0.132	0.155	0.144
PRE7	0.444	0.422	0.433
SMD1	0.243	0.224	0.233
NOP1	0.306	0.262	0.284
GCD11	0.378	0.288	0.333
SPT14	0.202	0.262	0.232
TAF13	0.327	0.326	0.326
RVB2	0.457	0.371	0.414
SLN1	0.416	0.399	0.407
STT3	0.458	0.454	0.456
GPI17	0.376	0.342	0.359
KAR2	0.200	0.154	0.177
FCF1	0.443	0.389	0.416
WBP1	0.296	0.243	0.269
LSM4	0.402	0.321	0.361
CCT2	0.401	0.321	0.361
SAD1	0.332	0.330	0.331
GPI18	0.366	0.332	0.349
CMD1	0.323	0.349	0.336
SEC11	0.141	0.133	0.137
ARC15	0.415	0.379	0.397
OST1	0.403	0.398	0.400
PRP38	0.316	0.307	0.311
PET9	0.455	0.462	0.459
BIG1	0.323	0.307	0.315
DCP1	0.387	0.389	0.388
SPC29	0.470	0.473	0.471
RIB5	0.267	0.300	0.284
LSM3	0.380	0.366	0.373
YDL163W	0.415	0.360	0.387
YHC1	0.451	0.454	0.453
TCP1	0.337	0.282	0.310
RPB8	0.401	0.284	0.343
DIB1	0.292	0.254	0.273
SME1	0.406	0.435	0.421

Chapter 4

Conclusions and Future Directions

The work described in this thesis details the application of fluorescent protein reporters to measure ER stress in single living cells. Using an ER-targeted redox-sensitive green fluorescent protein (eroGFP) and a UPR-responsive red fluorescent protein (UPR-RFP) I was able to measure changes in protein oxidation and the UPR during ER stress in *S. cerevisiae*. With this reporter system, I found that diverse stressors to ER protein folding cause measureable oxidation changes in eroGFP. Through dynamic monitoring, I identified conditions in which the UPR is capable of promoting adaptation to specific stressors. Finally, using high-throughput screening I identified hundreds of genes that are important for ER function.

Moving forward, the tools and concepts developed here should be easily extended to investigate ER stress and the UPR in mammals. In the following pages, I present a review article of the mammalian UPR and its connection to apoptosis. Elucidating how the UPR triggers apoptosis during instances of ER stress is critical in order to develop effective therapeutics for ER-stress-related diseases. Mammalian versions of the eroGFP-based reporter system should aid our understanding of the complex relationship between the UPR and apoptosis.

The Unfolded Protein Response and Cell Fate at a Glance

Philip I. Merksamer and Feroz R. Papa

Department of Medicine, Diabetes Center, & California Institute for Quantitative Biosciences

University of California, San Francisco

San Francisco, CA 94143-2520. U.S.A.

philip.merksamer@ucsf.edu

frpapa@medicine.ucsf.edu

In eukaryotic cells, secreted and resident proteins of the endomembrane system fold into their native structures within the endoplasmic reticulum (ER). The ER is a network of membranous tubules and sheets whose lumenal environment is crowded with molecular chaperones and protein-modification enzymes that are specialized to fold proteins. In addition, the ER contains stringent quality-control systems that selectively export correctly folded proteins and selectively extract terminally misfolded proteins for ubiquitin-dependent proteolytic degradation in the cytosol, a process known as ER-associated protein degradation (ERAD) (Vembar and Brodsky, 2008). The ER is a dynamic organelle, and its capacity to fold proteins can be adjusted in response to changes in cellular protein folding requirements through several intracellular signaling pathways that are collectively known as the unfolded protein response (UPR) (Ron and Walter, 2007). Dysregulation of the UPR contributes to the pathology of several important human diseases, including diabetes, neurodegeneration and cancer (Kim et al., 2008). In this article and its accompanying poster, we summarize how the mammalian UPR influences cell fate by promoting either cell adaption or apoptosis when protein folding homeostasis is perturbed.

Activation of the proximal UPR sensors

Mammalian UPR signaling is initiated by three ER-resident transmembrane proteins: protein kinase RNA (PKR)-like ER kinase, (PERK), activating transcription factor-6 (ATF6) and inositol-requiring enzyme-1 (IRE1). The presence of unfolded ER proteins is thought to activate each of these three proximal detectors; however, the ‘sensing’

mechanism remains unclear (Kohno, 2007). IRE1 was the first characterized sensor and its mechanism of activation has been the most thoroughly studied. IRE1 is a type-I transmembrane protein containing three domains: an N-terminal lumenal domain, a cytosolic kinase domain and a cytosolic RNase domain (Tirasophon et al., 1998; Wang et al., 1998). IRE1 becomes active when monomers oligomerize into either dimers or higher order structures, causing trans-autophosphorylation of the kinase domains, which in turn activate the RNase domains. Two models have been proposed to explain IRE1 oligomerization. In the first model, the ER-resident chaperone immunoglobulin-binding protein (BiP) functions as a master regulator by binding to IRE1 and inhibiting its oligomerization under basal conditions. In this scheme, when unfolded proteins accumulate BiP dissociates from IRE1 to preferentially interact with them, thus allowing IRE1 oligomerize (Bertolotti et al., 2000). The second model proposes that unfolded proteins bind directly to the lumenal domain of IRE1, which induces its oligomerization (Credle et al., 2005). More work is needed to resolve the relative contributions of BiP dissociation and direct binding of unfolded proteins to IRE1 activation.

PERK is also a type-I transmembrane protein that has a cytosolic kinase domain and an N-terminal lumenal domain that is homologous to that of IRE1. As a consequence, PERK is postulated to be activated by similar mechanisms to that of IRE1 (Bertolotti et al., 2000; Liu et al., 2000).

ATF6 is an ER-resident type-II transmembrane protein that exists as an oxidized monomer, dimer, and/or oligomer associated with BiP under basal conditions. When unfolded proteins accumulate, ATF6 dissociates from BiP and conserved intra- and/or intermolecular disulfide bonds in the lumenal domain of ATF6 are reduced, creating

ATF6 monomers (Nadanaka et al., 2006; Shen et al., 2005). Reduced monomeric ATF6 translocates to the Golgi and becomes a substrate for the Site-1 and Site-2 proteases, which liberate the N-terminal cytosolic fragrament of ATF6 [ATF6(N), a basic leucine zipper (bZiP) transcription factor] via regulated intramembrame proteoslysis (Haze et al., 1999). More work is need to elucidate the mechanisms governing ATF6 disulfide bond reduction, BiP dissociation, and regulation of ATF6 translocation to the Golgi.

Adaptive responses of the UPR

When the proximal UPR sensors become activated, they initiate a response to restore protein folding homeostasis in the ER. This adaptive response involves several outputs and can be conceptualized as two negative feedback loops acting on two different time scales: a fast negative feedback loop that decreases the influx of proteins into the ER, and a slow negative feedback loop that requires de novo mRNA and protein synthesis to increase the folding capacity of the ER (Trusina et al., 2008).

Activated PERK's kinase phosphorylates eukaryotic translation initiation factor 2α (eIF2α, which impedes subsequent rounds of translation initiation (Harding et al., 1999). In addition, IRE1 is responsible for the rapid degradation of several ER-localized mRNAs (Hollien and Weissman, 2006). Transient translation attenuation and mRNA decay constitute the fast negative feedback loop because they rapidly reduce the protein load on the ER. This provides the ER's folding machinery an extended opportunity to fold existing unfolded proteins and the ERAD machinery an extended time to degrade them.

IRE1 also catalyzes the non-conventional splicing of *XBP1u* mRNA into *XBP1s* mRNA, which encodes the bZIP transcription factor X-box-binding protein 1 (XBP1s) (Calfon et al., 2002; Yoshida et al., 2001). The slower phase of the adaptive response is controlled by XBP1s together with ATF6(N). ATF6(N) and XBP1s increase transcription rates of genes encoding ER-resident chaperones, protein-modification enzymes, ERAD components and lipid biosynthetic enzymes to augment ER size and to increase the ER's folding and degradation activities (Yamamoto et al., 2007). Translation of the activating transcription factor-4 (ATF4) also increases when eIF2α is phosphorylated by PERK, causing increased transcription of many genes that promote survival under many types of cellular stress (Harding et al., 2003). Additional transcription factors may also contribute to the transcriptional UPR program in certain cell types; for example, CREBH (cyclic AMP response element–binding protein H) appears to be involved in hepatocytes (Zhang et al., 2006). Together, these negative feedback loops reduce the concentration of unfolded proteins in the ER to maintain cellular homeostasis in the face of changing metabolic and protein-folding requirements. As the concentration of unfolded proteins decreases, the UPR shuts off, although the molecular details of UPR attenuation remain unclear.

ER stress

The term 'ER stress' is often used to describe a condition in which ER homeostasis is lost because of an overload on the ER's protein folding capacity. In practice however, ER stress is often used operationally to describe any condition in which cells have activated the UPR. This operational definition has evolved because it is difficult to directly measure the ER unfolded proteins that are thought to be the activating signals of the

UPR. However, solely monitoring UPR signaling does not necessarily provide information about the functional state of protein folding in the ER. Therefore, it is important to consider additional physiological end-points, such as ER distention, or changes in the secretion, glycosylation or oxidation of ER proteins (Merksamer et al., 2008). In experimental settings, ER stress is generally induced by treating cells with toxic chemicals that severely comprise ER protein folding or trafficking. Under these non-physiological conditions, the adaptive mechanisms of the UPR are insufficient to maintain homeostasis in the ER and cells ultimately die, typically through apoptosis.

Putative links between the UPR and apoptotic responses

Cells experiencing irremediable ER stress commit to apoptosis when the outer mitochondrial membrane (OMM) is permeabilized and cytochrome *c* is released to activate executioner caspases. This intrinsic (mitochondrial) apoptotic pathway, which is typically triggered in response to intracellular stresses including DNA damage and viral infections, is regulated by the Bcl-2 protein family (Youle and Strasser, 2008). The Bcl-2 family can be divided into three groups: multi-domain pro-apoptotic proteins (e.g. Bax, Bak), anti-apoptotic proteins (e.g. Bcl-2, Bcl-XL) and pro-apoptotic BH3-only proteins (e.g. Bid, Bad, Bim, Noxa, Puma) (Brunelle and Letai, 2009). In response to ER stress, the pro-apoptotic BH3-only proteins are transcriptionally or post-translationally activated to stimulate pro-apoptotic Bax and Bak either directly or indirectly through antagonizing anti-apoptotic members. Once activated, Bax and/or Bak form homo-oligomers in the OMM to initiate mitochondrial permeabilization (Wei et al., 2001). At this time, it is unclear if and how UPR signaling components communicate with the Bcl-2 family

members or other apoptotic signaling molecules to initiate apoptosis. In the following section, we summarize some of the more compelling data supporting such a link.

Of the 11 members of the BH3-only family, Puma, Noxa, Bid and Bim have been described to mediate apoptosis triggered by ER stress (Li et al., 2006; Puthalakath et al., 2007; Upton et al., 2008). However it remains possible that other BH3-only proteins serve important roles, with the relative contribution(s) of each BH3-only member varying in different tissues. Recently, the transcription factor C/EBP homologous protein (CHOP) was found to increase the rate of *Bim* transcription during ER stress, marking an important connection between a UPR signaling component and a BH3-only protein (Puthalakath et al., 2007). *CHOP* mRNA levels increase sharply during ER stress, an effect that is mediated primarily through the upstream transcription factor ATF4. In addition to regulating Bim expression, CHOP has been reported to antagonize the expression of anti-apoptotic Bcl-2. Although CHOP is clearly an important mediator between the UPR and the apoptotic machinery, $CHOP^{-/-}$ cells are only partially resistant to ER-stress-induced apoptosis. In addition, $PERK^{-/-}$ cells readily undergo apoptosis despite minimal CHOP expression (Oyadomari and Mori, 2004). Therefore, parallel signaling pathways might compensate for the loss of CHOP and possibly other pro-apoptotic components upstream of Bax and Bak.

Another signaling pathway that operates in parallel with CHOP is mediated by the mitogen-activated protein kinase (MAPK) c-Jun NH2-terminal kinase (JNK). JNK is activated by cytokines and several cellular stresses, and JNK signaling can promote protective or apoptotic responses, depending on cellular context (Weston and Davis, 2007). JNK signaling increases during ER stress in a manner that depends on IRE1 and

the MAPK kinase kinase (MAP3K) apoptosis signal-regulating kinase 1 (ASK1). Activated IRE1 associates with tumour necrosis factor receptor-associated factor 2 (TRAF2), leading to the activation of ASK1, which in turn initiates a phosphorylation cascade resulting in JNK phosphorylation and activation (Nishitoh et al., 2002; Urano et al., 2000). How TRAF2 is recruited to IRE1 and how this complex activates ASK1 remains unclear. JNK is thought to promote apoptosis under these conditions through several interactions with Bcl-2 family members: there is evidence that JNK can phosphorylate and inhibit the anti-apoptotic proteins Bcl-2, Bcl-XL, and Mcl-1. Furthermore, JNK can also phosphorylate and activate several BH-3 only proteins, including Bid and Bim to promote apoptosis (Weston and Davis, 2007).

There are several additional parallel pathways that might contribute to ER-stress-induced apoptosis that will not be reviewed in depth here. They include ER Ca^{2+} release regulated by ER-resident Bcl-2 family members (Kim et al., 2008), as well as interactions between Bcl-2 family members and IRE1 (Hetz and Glimcher, 2009). The vast numbers of factors that can transmit signals from the ER to mitochondria suggests that tight regulation of these signals is crucial for ensuring that only irremediably ER-stressed cells undergo apoptosis.

Speculative model for the UPR-mediated homeostatic-apoptotic switch

The UPR simultaneously transmits survival and apoptotic signals. Understanding the interplay between these competing signals is necessary to elucidate the mechanism by which cells decide whether to continue to attempt adaptation or to initiate apoptosis. This decision could ultimately depend on how Bcl-2 proteins interpret the mix of survival and

apoptotic signals transmitted by the UPR: such interpretation results in cell survival under conditions of remedial stress and cell death when homeostasis cannot be restored following catastrophic ER protein misfolding. To make this decision, cells might incorporate a time factor in which sustained UPR signaling (as could occur during chronic ER stress) increases the likelihood of apoptosis. In support of such a model, the mRNA and protein half-lives of pro-apoptoic CHOP were found to be short lived compared with pro-survival UPR outputs such as the ER chaperone BiP (Rutkowski et al., 2006). Sustained PERK activity (which is primarily responsible for CHOP upregulation) might thus be necessary to build CHOP levels to a required threshold to stimulate Bcl-2 proteins to commit to apoptosis. In addition, sustained PERK activity should result in protracted translation attenuation, which should be incompatible with survival. Similarly, sustained mRNA degradation mediated by IRE1 may deplete ER cargo and protein folding activities (Han et al., 2009). In support of this notion, overexpression of PERK or IRE1, which leads to their spontaneous oligomerization and activation, is typically sufficient to cause apoptosis. This is reminiscent of apoptosis that occurs during the sustained activation of other protein kinases such as JNK (Ventura et al., 2006).

In addition, the severity of ER stress might alter the relative activation level of certain UPR output pathways to influence cell-fate decisions. For example, IRE1 has at least three established outputs: *XBP1* mRNA splicing, non-specific mRNA cleavage and JNK activation (Han et al., 2009; Hollien et al., 2009; Hollien and Weissman, 2006; Urano et al., 2000). It is possible that different degrees of protein misfolding differentially affect

which of these IRE1 outputs are realized by differentially altering its oligomerization state.

Perspectives

Over the past twenty years since the UPR was first described, many of its molecular components have been identified and characterized. To move forward, it will be necessary to investigate how these individual components function as a signaling network to direct cell-fate decisions. To this end, we will need to develop quantitative tools to study various UPR components dynamically in individual living cells as they experience ER stress. In addition, it will be important to challenge cells with physiologically relevant stressors to understand how the UPR contributes to cellular physiology and pathogenesis of protein misfolding diseases. It is likely that the elucidation of key components of the UPR's homeostatic-apoptotic signaling network will reveal pharmacological targets for drug discovery and potential therapeutics for ER-stress-related diseases.

References

Bertolotti, A., Zhang, Y., Hendershot, L. M., Harding, H. P. and Ron, D. (2000). Dynamic interaction of BiP and ER stress transducers in the unfolded-protein response. *Nat Cell Biol* **2**, 326-32.

Brunelle, J. K. and Letai, A. (2009). Control of mitochondrial apoptosis by the Bcl-2 family. *J Cell Sci* **122**, 437-41.

Calfon, M., Zeng, H., Urano, F., Till, J. H., Hubbard, S. R., Harding, H. P., Clark, S. G. and Ron, D. (2002). IRE1 couples endoplasmic reticulum load to secretory capacity by processing the XBP-1 mRNA. *Nature* **415**, 92-6.

Credle, J. J., Finer-Moore, J. S., Papa, F. R., Stroud, R. M. and Walter, P. (2005). On the mechanism of sensing unfolded protein in the endoplasmic reticulum. *Proc Natl Acad Sci U S A* **102**, 18773-84.

Han, D., Lerner, A. G., Vande Walle, L., Upton, J. P., Xu, W., Hagen, A., Backes, B. J., Oakes, S. A. and Papa, F. R. (2009). IRE1alpha kinase activation modes control alternate endoribonuclease outputs to determine divergent cell fates. *Cell* **138**, 562-75.

Harding, H. P., Zhang, Y. and Ron, D. (1999). Protein translation and folding are coupled by an endoplasmic-reticulum-resident kinase. *Nature* **397**, 271-4.

Harding, H. P., Zhang, Y., Zeng, H., Novoa, I., Lu, P. D., Calfon, M., Sadri, N., Yun, C., Popko, B., Paules, R. et al. (2003). An integrated stress response regulates amino acid metabolism and resistance to oxidative stress. *Mol Cell* **11**, 619-33.

Haze, K., Yoshida, H., Yanagi, H., Yura, T. and Mori, K. (1999). Mammalian transcription factor ATF6 is synthesized as a transmembrane protein and activated by proteolysis in response to endoplasmic reticulum stress. *Mol Biol Cell* **10**, 3787-99.

Hetz, C. and Glimcher, L. H. (2009). Fine-tuning of the unfolded protein response: Assembling the IRE1alpha interactome. *Mol Cell* **35**, 551-61.

Hollien, J., Lin, J. H., Li, H., Stevens, N., Walter, P. and Weissman, J. S. (2009). Regulated Ire1-dependent decay of messenger RNAs in mammalian cells. *J Cell Biol* **186**, 323-31.

Hollien, J. and Weissman, J. S. (2006). Decay of endoplasmic reticulum-localized mRNAs during the unfolded protein response. *Science* **313**, 104-7.

Kim, I., Xu, W. and Reed, J. C. (2008). Cell death and endoplasmic reticulum stress: disease relevance and therapeutic opportunities. *Nat Rev Drug Discov* **7**, 1013-30.

Kohno, K. (2007). How transmembrane proteins sense endoplasmic reticulum stress. *Antioxid Redox Signal* **9**, 2295-303.

Li, J., Lee, B. and Lee, A. S. (2006). Endoplasmic reticulum stress-induced apoptosis: multiple pathways and activation of p53-up-regulated modulator of apoptosis (PUMA) and NOXA by p53. *J Biol Chem* **281**, 7260-70.

Liu, C. Y., Schroder, M. and Kaufman, R. J. (2000). Ligand-independent dimerization activates the stress response kinases IRE1 and PERK in the lumen of the endoplasmic reticulum. *J Biol Chem* **275**, 24881-5.

Merksamer, P. I., Trusina, A. and Papa, F. R. (2008). Real-time redox measurements during endoplasmic reticulum stress reveal interlinked protein folding functions. *Cell* **135**, 933-47.

Nadanaka, S., Okada, T., Yoshida, H. and Mori, K. (2006). A Role of Disulfide Bridges Formed in the Lumenal Domain of ATF6 in Sensing Endoplasmic Reticulum Stress. *Mol Cell Biol*.

Nishitoh, H., Matsuzawa, A., Tobiume, K., Saegusa, K., Takeda, K., Inoue, K., Hori, S., Kakizuka, A. and Ichijo, H. (2002). ASK1 is essential for endoplasmic reticulum stress-induced neuronal cell death triggered by expanded polyglutamine repeats. *Genes Dev* **16**, 1345-55.

Oyadomari, S. and Mori, M. (2004). Roles of CHOP/GADD153 in endoplasmic reticulum stress. *Cell Death Differ* **11**, 381-9.

Puthalakath, H., O'Reilly, L. A., Gunn, P., Lee, L., Kelly, P. N., Huntington, N. D., Hughes, P. D., Michalak, E. M., McKimm-Breschkin, J., Motoyama, N. et al. (2007). ER stress triggers apoptosis by activating BH3-only protein Bim. *Cell* **129**, 1337-49.

Ron, D. and Walter, P. (2007). Signal integration in the endoplasmic reticulum unfolded protein response. *Nat Rev Mol Cell Biol* **8**, 519-29.

Rutkowski, D. T., Arnold, S. M., Miller, C. N., Wu, J., Li, J., Gunnison, K. M., Mori, K., Sadighi Akha, A. A., Raden, D. and Kaufman, R. J. (2006). Adaptation to ER stress is mediated by differential stabilities of pro-survival and pro-apoptotic mRNAs and proteins. *PLoS Biol* **4**, e374.

Shen, J., Snapp, E. L., Lippincott-Schwartz, J. and Prywes, R. (2005). Stable binding of ATF6 to BiP in the endoplasmic reticulum stress response. *Mol Cell Biol* **25**, 921-32.

Tirasophon, W., Welihinda, A. A. and Kaufman, R. J. (1998). A stress response pathway from the endoplasmic reticulum to the nucleus requires a novel bifunctional protein kinase/endoribonuclease (Ire1p) in mammalian cells. *Genes Dev* **12**, 1812-24.

Trusina, A., Papa, F. R. and Tang, C. (2008). Rationalizing translation attenuation in the network architecture of the unfolded protein response. *Proc Natl Acad Sci U S A* **105**, 20280-5.

Upton, J. P., Austgen, K., Nishino, M., Coakley, K. M., Hagen, A., Han, D., Papa, F. R. and Oakes, S. A. (2008). Caspase-2 cleavage of BID is a critical apoptotic signal downstream of endoplasmic reticulum stress. *Mol Cell Biol* **28**, 3943-51.

Urano, F., Wang, X., Bertolotti, A., Zhang, Y., Chung, P., Harding, H. P. and Ron, D. (2000). Coupling of stress in the ER to activation of JNK protein kinases by transmembrane protein kinase IRE1. *Science* **287**, 664-6.

Vembar, S. S. and Brodsky, J. L. (2008). One step at a time: endoplasmic reticulum-associated degradation. *Nat Rev Mol Cell Biol* **9**, 944-57.

Ventura, J. J., Hubner, A., Zhang, C., Flavell, R. A., Shokat, K. M. and Davis, R. J. (2006). Chemical genetic analysis of the time course of signal transduction by JNK. *Mol Cell* **21**, 701-10.

Wang, X. Z., Harding, H. P., Zhang, Y., Jolicoeur, E. M., Kuroda, M. and Ron, D. (1998). Cloning of mammalian Ire1 reveals diversity in the ER stress responses. *EMBO J* **17**, 5708-17.

Wei, M. C., Zong, W. X., Cheng, E. H., Lindsten, T., Panoutsakopoulou, V., Ross, A. J., Roth, K. A., MacGregor, G. R., Thompson, C. B. and Korsmeyer, S. J.

(2001). Proapoptotic BAX and BAK: a requisite gateway to mitochondrial dysfunction and death. *Science* **292**, 727-30.

Weston, C. R. and Davis, R. J. (2007). The JNK signal transduction pathway. *Curr Opin Cell Biol* **19**, 142-9.

Yamamoto, K., Sato, T., Matsui, T., Sato, M., Okada, T., Yoshida, H., Harada, A. and Mori, K. (2007). Transcriptional induction of mammalian ER quality control proteins is mediated by single or combined action of ATF6alpha and XBP1. *Dev Cell* **13**, 365-76.

Yoshida, H., Matsui, T., Yamamoto, A., Okada, T. and Mori, K. (2001). XBP1 mRNA is induced by ATF6 and spliced by IRE1 in response to ER stress to produce a highly active transcription factor. *Cell* **107**, 881-91.

Youle, R. J. and Strasser, A. (2008). The BCL-2 protein family: opposing activities that mediate cell death. *Nat Rev Mol Cell Biol* **9**, 47-59.

Zhang, K., Shen, X., Wu, J., Sakaki, K., Saunders, T., Rutkowski, D. T., Back, S. H. and Kaufman, R. J. (2006). Endoplasmic reticulum stress activates cleavage of CREBH to induce a systemic inflammatory response. *Cell* **124**, 587-99.

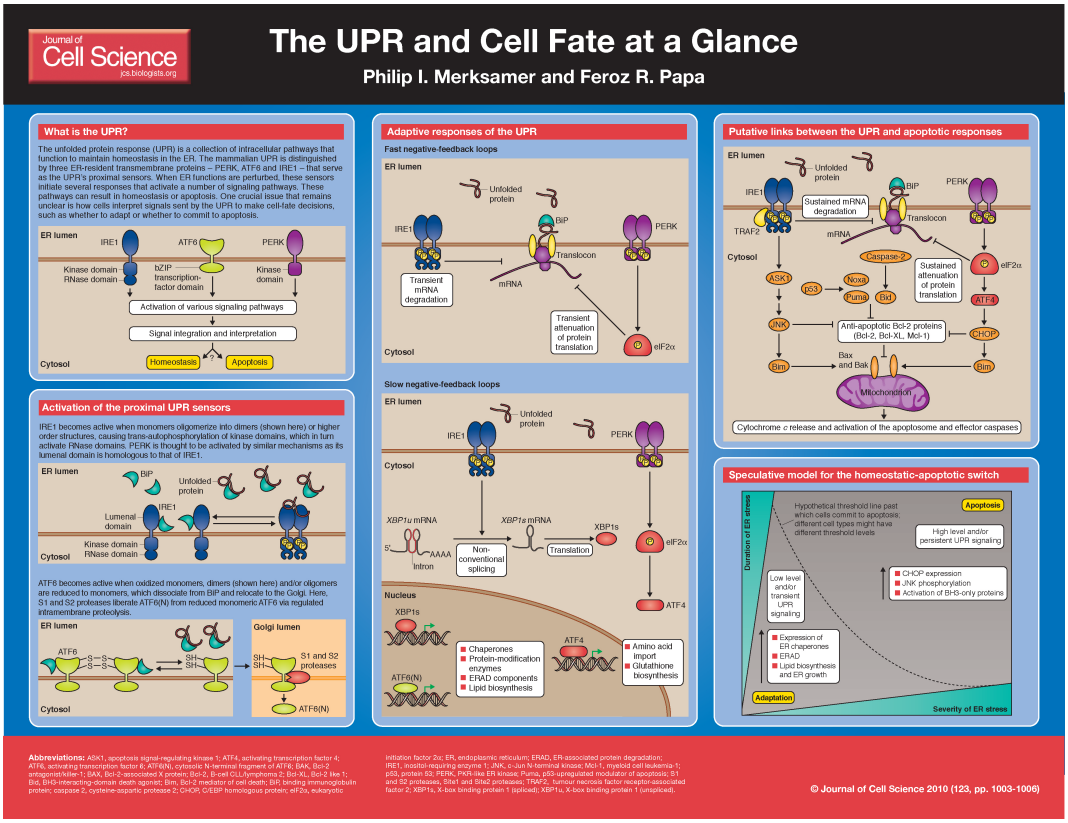

Merksamer et al Figure 1

Publishing Agreement

It is the policy of the University to encourage the distribution of all theses, dissertations, and manuscripts. Copies of all UCSF theses, dissertations, and manuscripts will be routed to the library via the Graduate Division. The library will make all theses, dissertations, and manuscripts accessible to the public and will preserve these to the best of their abilities, in perpetuity.

Please sign the following statement:

I hereby grant permission to the Graduate Division of the University of California, San Francisco to release copies of my thesis, dissertation, or manuscript to the Campus Library to provide access and preservation, in whole or in part, in perpetuity.

Author Signature

12-30-10

Date